

CHAPTER 12

Predicting Future Ozone Changes and Detection of Recovery

Lead Authors:

D.J. Hofmann
J.A. Pyle

Coauthors:

J. Austin
N. Butchart
C.H. Jackman
D.E. Kinnison
F. Lefèvre
G. Pitari
D.T. Shindell
R. Toumi
P. von der Gathen

Contributors:

S. Bekki
C. Brühl
P.S. Connell
M. Dameris
E.L. Fleming
S.M. Hollandsworth
S.J. Oltmans
L.K. Randeniya
M. Rex
B. Rognerud
S. Smyshlyaev
H. Teyssède
G.J.M. Velders
D.K. Weisenstein
J.R. Ziemke

CHAPTER 12

PREDICTING FUTURE OZONE CHANGES AND DETECTION OF RECOVERY

Contents

SCIENTIFIC SUMMARY	12.1
12.1 INTRODUCTION	12.3
12.2 CALCULATION OF FUTURE OZONE CHANGE	12.4
12.2.1 Ozone Change Calculated by 2-D Models	12.4
12.2.1.1 Description of the Model Simulations	12.6
12.2.1.1a Two-Dimensional Model Photochemistry	12.6
12.2.1.1b Scenario Descriptions	12.6
12.2.1.2 Modeling the Observed Trends in Ozone	12.10
12.2.1.3 Ozone Recovery—Model Sensitivity to Key Parameters	12.15
12.2.1.4 Summary	12.20
12.2.2 Chemical Transport Models	12.20
12.2.2.1 Sensitivity to Halogen Loading	12.20
12.2.2.2 Sensitivity to Lower Stratospheric Temperatures	12.21
12.2.3 Three-Dimensional Chemistry-Climate Models	12.23
12.2.3.1 Doubled-CO ₂ Experiments	12.24
12.2.3.1a Temperature and Dynamics Changes	12.26
12.2.3.1b Ozone Changes	12.27
12.2.3.2 Transient Ozone Response	12.27
12.2.3.2a Temperature and Dynamics Changes	12.29
12.2.3.2b Ozone Changes	12.31
12.2.3.3 Conclusions	12.37
12.3 OTHER PERTURBATIONS	12.38
12.3.1 Natural Processes	12.38
12.3.1.1 Solar Cycle Variations	12.38
12.3.1.2 Charged-Particle Precipitation	12.38
12.3.2 Anthropogenic Activities	12.39
12.3.2.1 Shuttle and Rocket Launches	12.39
12.3.2.2 Current Fleet of Subsonic Aircraft	12.40
12.3.2.3 High Speed Civil Transports	12.40
12.3.2.4 Other Effects	12.40
12.4 DETECTION OF THE EXPECTED RECOVERY OF THE OZONE LAYER	12.40
12.4.1 Antarctic Ozone Hole	12.41
12.4.1.1 Area of the 220-Dobson Unit Contour	12.41
12.4.1.2 September Ozone Reduction at 12-20 km from Ozonesonde Profiles	12.42
12.4.1.3 Vertical Extension of the Ozone Hole	12.43
12.4.2 Arctic Springtime Ozone Loss	12.43
12.4.3 Midlatitude Ozone Decline	12.45
12.4.4 Ozone Recovery Scenarios and Expected Dates of Recovery	12.47
12.4.4.1 The Standard Scenario	12.47
12.4.4.2 Perturbations to the Standard Scenario	12.48
REFERENCES	12.50

SCIENTIFIC SUMMARY

A range of models has been used to investigate future changes in ozone in response to changing atmospheric emissions of source gases and greenhouse gases. A significant advance is the use of three-dimensional (3-D) models in these studies. The detection of the beginning of recovery of ozone (where recovery is defined as the response of ozone to reductions in chemical ozone loss due to the halogens) is considered for the first time in this Assessment.

All other things being equal, stratospheric ozone levels should rise as the halogen loading falls in response to regulation. However, the future behavior of ozone will also be affected by the changing atmospheric abundances of methane (CH₄), nitrous oxide (N₂O), sulfate aerosol, and changing climate. Thus, for a given halogen loading in the future, the atmospheric ozone abundance will not be the same as found for that loading in the past. Because of these additional factors, observation of the beginning of ozone recovery is expected to be delayed beyond the time of maximum stratospheric halogen loading.

Model predictions of future ozone

- Ten two-dimensional (2-D) models were used to investigate the response of ozone to past and future changes in halogen loading as well as CH₄, N₂O, and sulfate aerosol. The models provide a reasonable representation of the general structure of recent observed local and column ozone trends, giving credence to their ability to represent future ozone change.
 - In integrations to 2050, excluding the possibility of major volcanic eruptions in the future, the lowest global ozone is predicted to have occurred in the years immediately following the eruption of Mt. Pinatubo in 1991.
 - After 2000, ozone levels are predicted to recover slowly toward their pre-1980 values. The modeled recovery depends sensitively on the emission scenarios for the halogens, and for CH₄, N₂O, and sulfate aerosol density.
 - Increases in future CH₄ will shorten the recovery period. Increases in N₂O and sulfate aerosol surface area density will extend the recovery period. In one model that tested the effects of projected future CO₂ increases, the recovery period was shortened.
 - The methane scenario used here as a baseline had a lower growth rate than in previous Assessments and lengthened the modeled ozone recovery significantly. Understanding the methane trend is an important priority for understanding the future ozone recovery.
 - Model simulations show that future volcanic events at low inorganic chlorine (Cl_y) abundances will not significantly affect the rate of recovery.
- Polar ozone loss in recent Northern Hemisphere winters has demonstrated a large dependence on meteorological conditions, and especially temperature. Those winters with the lowest polar lower stratospheric temperatures have shown largest ozone losses. Recovery of ozone is evidently strongly dependent on meteorological conditions.
- Advances in computing power have allowed the first simulations of future ozone using coupled 3-D models.
 - Three-dimensional models highlight that future Arctic ozone loss is very sensitive to changes in the strength, frequency, and timing of sudden warmings.

PREDICTING THE FUTURE OZONE LAYER

- Three-dimensional models suggest that recovery of Arctic ozone is likely to be delayed past the maximum in stratospheric chlorine abundances and beyond that predicted by 2-D models. For example, coupled chemistry-climate models show greater ozone depletion in the Arctic in 2015 than 1995. The single model that has predicted trends out beyond 2015 shows a recovery of Arctic ozone beginning in the 2020s.
- Model simulations indicate that observations of the onset of ozone recovery from halogen-induced depletion should be possible earlier in the Antarctic than in the Arctic.
- At high latitudes throughout the stratosphere, there are considerable differences in the temperature response of general circulation models (GCMs) to increasing greenhouse gases that are associated with differences in modeled circulation changes.
- Further validation of stratospheric GCMs is necessary for them to reach a consensus on predictions of chemistry-climate interactions in the stratosphere such as that now seen in predictions of surface parameters by climate models.

Detection of recovery

- Observation of the beginning of ozone recovery, defined as the unambiguous detection of an increase toward pre-1980 ozone values, will be possible in the Antarctic before either the Arctic or midlatitudes. This is due to at least two factors: the smaller degree of variability in the Antarctic ozone loss phenomenon and the relatively smaller effect that future climate change will have on ozone loss in Antarctica.
- Antarctic ozone recovery indicators that have been identified include the geographical extent of the ozone hole region as measured by the 220-Dobson unit (DU) ozone contour, the total column ozone during October at South Pole and Halley stations, the amount of ozone depletion at the top of the ozone hole, in the 22-24 km region where the depletion chemistry is not saturated, and the rate of ozone decline during September in the 12-20 km region of maximum polar stratospheric cloud formation.
- Comparison of modeled ozone recovery with observations, and taking into account ozone variability, suggests that the beginning of recovery of the Antarctic ozone hole will likely not be detected before about 2020. The onset of the recovery of the bulk of the global ozone layer may possibly not be unambiguously detected before 2030. Because of the large uncertainties in model predictions associated with changes in CH₄, N₂O, sulfate aerosol, and climate, these estimates are likewise uncertain; however, it is clear that the onset of ozone recovery will be delayed beyond the maximum in stratospheric halogens.
- A pre-recovery period, defined as a cessation of the worsening of global ozone depletion, may be observed during the next decade; however, a major volcanic eruption during this period would cause stratospheric chemical perturbations that would result in a further decline in ozone for several years. Over the longer term, future major volcanic eruptions occurring at decadal intervals would not be expected to alter eventual ozone layer recovery.
- Recovery of ozone from the effects of chlorine may be observed at an earlier time in the 40-km region, where the chemistry affecting ozone is relatively simple and volcanic effects are absent. However, climate change will likewise cause an increase in ozone in this region, possibly masking ozone recovery. In addition, because ozone in this region contributes only a few percent to the total column, observation of recovery at 40 km should not be interpreted as evidence for the recovery of the global ozone layer.

12.1 INTRODUCTION

It is now well established that stratospheric ozone depletion has arisen as a consequence of the emission into the atmosphere of various chlorine- and bromine-containing compounds, whose production and emission are now regulated by the Montreal Protocol and its various Amendments. In consequence, as these compounds are slowly removed from the atmosphere, we should expect the ozone layer to recover. In this chapter we will examine two aspects of the recovery. First, in Sections 12.2 and 12.3, we discuss the range of factors that influence the atmospheric abundance of ozone and investigate how their changes may modify the expected recovery. Second, in Section 12.4 we consider possible measurement strategies that would allow us to make an early detection of the recovery of the ozone layer. Early detection is important because it would allow us to confirm our present understanding of stratospheric ozone and would indicate that the production and emission regulations were having the desired effect.

It is important to establish what is meant by “recovery.” One definition, implicit in earlier studies, is that full recovery occurs when chlorine loading returns to 2 parts per billion by volume (ppbv), considered to be the loading when the Antarctic ozone hole was first apparent. Also implicit in this definition is the assumption that, as chlorine loading grows and then decays, each value of chlorine loading corresponds uniquely to a single ozone value. However, we must recognize that many factors, in addition to halogen loading, influence the ozone distribution. Many of these factors are also changing with time. For example, the atmospheric concentrations of many greenhouse gases are changing, with consequent impacts on transport, temperature, and ozone chemistry. Thus, were the halogen loading to return to 2 ppbv, the atmosphere would differ from that of the late 1970s and, accordingly, the level of ozone may not be the same as then. In reality, “recovery” will be to a different global ozone distribution.

In this chapter, when we consider recovery, and the detection of recovery, we are concerned specifically with the way the atmosphere will respond (“recover”) to the reduction of halogen loading as a result of the Montreal Protocol. In detecting recovery (and especially, in attempting to make an early detection of recovery) we will investigate strategies that will allow the expected impact of reduced halogen loading on ozone to be observed and confirmed.

In the next two sections of this chapter we will present the results of recent modeling studies of future ozone change arising both from changing halogen loading and from other factors. In the final section we will use observational experience combined with these theoretical studies to suggest possible measurement strategies for the detection of recovery and attempt to estimate when the beginning of recovery might be observed.

We now know unequivocally that ozone is destroyed in middle and high latitudes by reactions involving chlorine and bromine radical species, but that the loss depends not just on the abundance of those species but also on a number of other dynamical and chemical factors. In polar latitudes the destruction depends critically on temperature. Temperatures must fall sufficiently to allow heterogeneous reactions to convert the halogens into active forms. A further fall of temperature (as seen every year in the Antarctic but only infrequently in the Arctic) leads to permanent removal of the oxides of nitrogen to lower altitudes, a process that maintains ozone depletion for a longer period. These processes depend in a highly nonlinear fashion on atmospheric temperature: a small fall (rise) in temperature under certain conditions can lead to a large increase (decrease) in the rate of ozone destruction. A downward trend in lower stratospheric temperatures is now established, as discussed in Chapter 5. Below in Section 12.2 we investigate how this could impact future levels of stratospheric ozone.

The changes in stratospheric temperature may have arisen as a result of the increase in greenhouse gas abundance in the atmosphere as well as changes in ozone itself. Several of the greenhouse gases (e.g., nitrous oxide (N_2O), methane (CH_4)) are also important as sources of stratospheric radical species whose changing concentrations will have an impact on stratospheric chemistry. This is also investigated in Section 12.2.

The understanding of the observed ozone decline in middle latitudes has developed significantly in recent years (see Chapter 7). Precise quantification of the contribution of different processes is still controversial, but it is clear that stratospheric aerosol plays an important role, chemically and possibly dynamically. The impact of changing aerosol levels is also considered in Section 12.2.

In addition to changes in those atmospheric properties that can alter the rate of chemical processes (species abundance, surface area of particles, temperature), there is also a fundamental dependence on the

PREDICTING THE FUTURE OZONE LAYER

atmospheric circulation. The amount of ozone in the atmosphere depends on the speed with which ozone is moved from its source to its sink (or from regions with short to long photochemical time constants (see, for example, Brewer and Wilson, 1968)). Thus changes in the circulation, from whatever cause, could lead to changes in ozone abundance, a further point that we discuss in Section 12.2.

Some other anthropogenic influences on ozone are considered very briefly in Section 12.3. These include the increasing emissions from sub- and supersonic aircraft and the possible role of various rocket launchers. We note that the Intergovernmental Panel on Climate Change (IPCC) is assembling a special report on aviation and the environment (IPCC, 1999). That report will provide a detailed assessment. Accordingly the discussion presented here has not attempted to duplicate that major effort.

12.2 CALCULATION OF FUTURE OZONE CHANGE

This section will first present calculations of ozone loss versus time, based on a scenario of future halogen loading. The basic scenario considered is essentially A3 of Chapter 11 of this Assessment, which describes the maximum halogen loading of the atmosphere, following maximum allowed production of ozone-depleting substances under the Montreal Protocol. We will then consider the question of the uncertainty in the calculated ozone layer response to possible feedbacks in the system, e.g., changing temperature or changing levels of source gases (CH_4 , H_2O , N_2O , etc.). The calculations will be based on a range of models, from two-dimensional (2-D) models to fully coupled chemical-radiative-dynamical models that are now becoming available. The uncertainty issue will be considered again later in Section 12.4, where we consider the detection of the ozone layer recovery.

Two-dimensional models have been widely used for assessment studies for many years. Their formulation has continued to advance, and they represent ideal tools for a range of studies of stratospheric change over long time periods. In this Assessment, in Section 12.2.1, the 2-D model calculations of the global, decadal behavior of ozone are emphasized. Three-dimensional (3-D) chemical transport models (CTMs), with circulations forced by meteorological analyses, have been used increasingly in recent years. Here, in Section 12.2.2, they are used to study the sensitivity of Arctic ozone

loss to meteorological conditions. Finally, long-term assessment of the coupled stratospheric system requires 3-D circulation models that include detailed descriptions of chemistry. Such models are now being developed. Generally, they have not yet been run for sufficiently long periods (nor have they been sufficiently validated) to assess the long-term trend in global ozone. However, they have been applied to studies of polar ozone loss, with boundary conditions appropriate to the next decade or so, and these polar studies are discussed in Section 12.2.3.

12.2.1 Ozone Change Calculated by 2-D Models

As reported in the *Scientific Assessment of Ozone Depletion: 1994* (WMO, 1995), nine 2-D models were used to derive the ozone trend from 1980 up to the year 2050. These models generally all predicted maximum ozone depletion between 1995 and 2000, consistent with the imposed surface chlorine source gas abundance. However, during this period, the differences in the magnitudes of the individual model-derived ozone depletions were substantial. This difference was amplified in Northern Hemisphere high latitudes, where ranges in ozone depletion varied by a factor of 2. In addition, one very striking result from that Assessment was the model-derived variations in the rate of ozone recovery. Some models did not recover to the 1980 ozone abundance until 2050, while others reached the 1980 ozone abundance as early as 2020. These 2-D calculations will be reassessed here in models including the latest developments in dynamical formulation and in gas- and heterogeneous-phase chemistry.

The stratosphere is a highly coupled system and, for example, the ozone distribution depends on the distribution of many other species and on the stratospheric temperature and circulation. The sensitivity of halogen-induced ozone perturbations to changes in these other parameters has been considered by many authors in the past (see, for example, WMO, 1986). Recently, Velders (1997) used the Netherlands National Institute of Public Health and the Environment (RIVM) 2-D model to investigate the sensitivity of ozone recovery to assumptions about concurrent changes in halocarbons, CH_4 , N_2O , and temperature trends. The base scenario IS92a (IPCC, 1996), used within the context of the model, recovered to 1980 ozone abundances around the year 2065. This calculation did not include the change in stratospheric temperature caused mainly by increases in

Table 12-1. The 2-D models participating in the Assessment.

Model Name	Institution	Investigators	References
AER	Atmospheric and Environmental Research Inc., <i>U.S.</i>	M. Ko, D. Weisenstein, and C. Scott	Weisenstein <i>et al.</i> , 1998
CAM	University of Cambridge, <i>U.K.</i>	S. Bekki and J. Pyle	Bekki and Pyle, 1994
CSIRO	Commonwealth Scientific and Industrial Research Organization, Telecommunications and Industrial Physics, <i>Australia</i>	K. Ryan, I. Plumb, P. Vohralik, and L. Randeniya	Randeniya <i>et al.</i> , 1997
GSFC	Goddard Space Flight Center, <i>U.S.</i>	C. Jackman, E. Fleming, and D. Considine	Jackman <i>et al.</i> , 1996a
LLNL	Lawrence Livermore National Laboratory, <i>U.S.</i>	P. Connell and D. Kinnison	Kinnison <i>et al.</i> , 1994
MPIC	Max-Planck-Institute for Chemistry, <i>Germany</i>	C. Brühl, J. Groöß, and P. Crutzen	Groöß <i>et al.</i> , 1998
OSLO	University of Oslo, <i>Norway</i>	I. Isaksen and B. Rognerud	Zerefos <i>et al.</i> , 1997
RIVM	National Institute of Public Health and the Environment, <i>Netherlands</i>	G.J.M. Velders	Velders 1995; Law and Pyle, 1993
SUNY_SPB	State University of New York at Stony Brook, <i>U.S.</i> , and Russian State Hydrometeorological Institute, St. Petersburg, <i>Russia</i>	S. Smyshlyaev, V. Dvortsov, V. Yudin, and M. Geller	Smyshlyaev and Yudin, 1995
UNIVAQ	University of L' Aquila, <i>Italy</i>	G. Pitari, B. Grassi, and G. Visconti	Pitari <i>et al.</i> , 1993

CO₂ emissions. When the chemical effect of this temperature change is considered, the recovery of ozone to 1980 levels occurs earlier, in the year 2040. In an extreme case where CH₄ and N₂O abundances and temperature were held constant at 1990 conditions, while allowing CFCs to trend following IS92a, the model-derived ozone recovery occurred in 2080. Results of the model simulation described above highlight the importance of understanding, within the context of multi-dimensional models, the interactions that individual source gases, like CH₄ and N₂O, and temperature change

have on the overall ozone recovery. In general, CH₄ increases tend to mitigate halogen influence on ozone by converting halogen odd-oxygen loss radicals to reservoir species, therefore reducing the ozone recovery time (WMO, 1995; Jackman *et al.*, 1996a; Velders, 1997). Increases in N₂O have the opposite effect on ozone. Here, N₂O increases will increase the abundance of nitrogen oxides (NO_x) in the stratosphere, increasing odd-oxygen loss from NO_x catalytic processes. This increased odd-oxygen (O_x) loss process is more important than the mitigation of chlorine oxide (ClO_x) and bromine oxide

PREDICTING THE FUTURE OZONE LAYER

(BrO_x) abundances by the sequestering of these radicals into reservoir species, like chlorine nitrate (ClONO₂) and bromine nitrate (BrONO₂).

The remaining portion of Section 12.2.1 will show results from two-dimensional models of the global troposphere and stratosphere. Emphasis will be placed on the global behavior of ozone. A particular focus will also be to highlight key uncertainties and sensitivities that can affect model-derived trends in ozone, both past and future.

12.2.1.1 DESCRIPTION OF THE MODEL SIMULATIONS

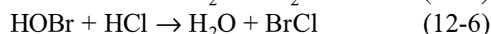
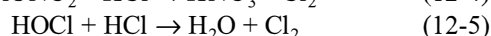
The 10 modeling groups that submitted results for this Assessment are listed in Table 12-1. All of these models have participated in past World Meteorological Organization (WMO), IPCC, and National Aeronautics and Space Administration (NASA) assessments. These assessments range from model evaluation of the effects of trends in trace constituents on ozone to the potential impact on ozone of a fleet of supersonic aircraft. Six out of the 10 models are currently represented in the latest NASA Models and Measurement II Workshop Report (Park *et al.*, 1998). Detailed differences in model engineering are not the focus of this section, however, differences between the models will be highlighted as necessary to help explain differences in model-derived ozone trends. Below is a general description of the chemistry and physics currently employed in the 10 assessment models listed in Table 12-1.

12.2.1.1a Two-Dimensional Model Photochemistry

Current state-of-the-art two-dimensional models are designed to determine the atmospheric distributions of chemically active atmospheric trace constituents in the troposphere and stratosphere. The typical model domain extends from pole to pole, and from the surface to the upper mesosphere. The horizontal resolution is typically 5-10 degrees in latitude and the vertical coordinate is consistent with a resolution of 1-2 km. The photochemistry represents the tropospheric and stratospheric interactions of actinic solar flux and the species families O_x, NO_y, ClO_y, HO_y, BrO_y, and CH₄ and its oxidation products. These models derive the distribution of approximately 40-50 chemical constituents, which is consistent with a chemical mechanism consisting of over 150 thermal and photolytic reactions. Source gases present in the model include NO_x, N₂O, CH₄,

carbon dioxide (CO₂), carbon monoxide (CO), the chlorine-containing compounds (e.g., CFC-11, -12, -113, -114, -115; HCFC-22, -141b, -142b, -123; carbon tetrachloride (CCl₄); methyl chloroform (CH₃CCl₃); methyl chloride (CH₃Cl)), and the bromine-containing compounds methyl bromide (CH₃Br) and the halons H-1211, -1301, and -2402. Most of the thermal and photolytic reaction rate constants were taken from the NASA Panel for Data Evaluation recommendations (DeMore *et al.*, 1997).

Cold aerosol chemistry (i.e., liquid binary sulfate and/or ternary sulfate) is represented to different levels of sophistication within two-dimensional models. Hydrolysis of ClONO₂, dinitrogen pentoxide (N₂O₅), and BrONO₂ on the surface of stratospheric sulfate aerosol is included as the probable dominant heterogeneous process. In addition, most 2-D models also include the reactions of ClONO₂, hypochlorous acid (HOCl), and hypobromous acid (HOBr) with hydrogen chloride (HCl) on sulfate aerosol.



Reactions on nitric acid trihydrate (NAT) and ice particles are also considered in most 2-D models. Representation of the rate constants for the above heterogeneous reactions generally follows the work of Hanson *et al.* (1994, 1996), Hanson and Ravishankara (1994, 1995), and Hanson and Lovejoy (1996). Detailed discussion of these cold aerosol processes is given in Chapter 7 of this report.

12.2.1.1b Scenario Descriptions

The two-dimensional models used in this chapter to explore the scientific issues related to ozone recovery between 1970 and 2050 were forced by supplying time-dependent surface halocarbon, CH₄, N₂O, and CO₂ (in one case) mixing ratios, and time-dependent satellite-derived aerosol surface area density. In Table 12-2, the surface mixing ratios of chlorine- and bromine-containing compounds are given for the base case considered, essentially scenario A/A3 of Chapter 11 of this Assessment. The time-

Table 12-2. Trace-gas boundary conditions (pptv, unless indicated).

Year	CFC-11	CFC-12	CFC-113	CFC-114	CFC-115	CCl ₄	CH ₃ CCl ₃	HCFC-22	HCFC-141b	HCFC-142b	HCFC-123	H-1211	H-1301	H-2402	CH ₃ Br	CH ₃ Cl	N ₂ O (ppbv)	CH ₄ (ppbv)	CO ₂ (ppmv)
1970	50.47	108.88	4.80	6.06	0.00	60.75	13.48	12.29	0.00	0.00	0.00	0.06	0.00	0.01	9.06	550.00	295	1420	325
1975	105.99	198.59	10.04	7.76	0.65	83.75	36.79	23.13	0.00	0.00	0.00	0.29	0.06	0.05	9.06	550.00	298	1495	331
1980	164.46	289.90	20.51	9.81	1.30	100.40	75.92	38.79	0.00	0.00	0.00	0.76	0.30	0.12	9.06	550.00	302	1570	337
1985	206.79	373.37	37.89	12.07	2.84	108.47	103.37	59.91	0.00	0.26	0.00	1.48	0.94	0.23	9.06	550.00	306	1650	345
1990	257.67	467.43	70.96	14.71	4.95	111.07	126.92	84.91	0.00	1.31	0.00	2.77	1.65	0.37	9.06	550.00	310	1700	354
1995	268.90	522.89	89.25	15.52	7.32	106.94	112.40	115.48	2.59	6.82	0.00	3.68	2.22	0.47	9.06	550.00	315	1725	363
2000	264.34	553.71	90.71	15.76	8.63	99.19	57.28	154.26	13.30	14.15	4.80	3.94	2.58	0.47	8.88	550.00	320	1750	372
2005	258.18	570.48	93.12	15.79	8.85	92.50	35.07	226.98	20.37	22.92	5.80	4.09	2.90	0.40	8.31	550.00	325	1775	382
2010	250.64	579.20	93.62	15.67	8.86	85.16	26.87	268.43	22.37	30.32	5.14	4.09	3.17	0.33	7.97	550.00	330	1800	393
2015	239.88	564.22	89.28	15.47	8.84	75.60	23.66	269.64	20.88	34.31	3.33	3.81	3.35	0.26	7.97	550.00	335	1825	405
2020	225.69	538.06	84.18	15.24	8.82	67.11	8.53	228.90	16.86	34.24	1.44	3.31	3.44	0.20	7.34	550.00	340	1850	418
2025	209.90	512.38	79.37	15.01	8.79	59.58	3.07	176.71	12.37	31.23	0.88	2.77	3.46	0.16	7.34	550.00	345	1875	432
2030	193.68	487.87	74.83	14.77	8.77	52.89	1.11	135.47	9.07	27.30	0.88	2.27	3.43	0.12	7.34	550.00	350	1900	446
2035	177.72	464.53	70.56	14.52	8.74	46.96	0.40	107.37	6.96	23.53	0.85	1.83	3.35	0.10	7.34	550.00	355	1925	461
2040	162.43	442.31	66.53	14.29	8.72	41.69	0.14	88.53	5.66	20.28	0.85	1.46	3.25	0.07	7.34	550.00	360	1950	477
2045	148.05	421.15	62.73	14.05	8.69	37.01	0.05	66.65	4.13	17.09	0.02	1.15	3.14	0.06	7.34	550.00	365	1975	493
2050	134.67	401.00	59.14	13.82	8.67	32.86	0.02	44.96	2.56	13.74	0.00	0.91	3.00	0.05	7.34	550.00	370	2000	509

12.7

PREDICTING THE FUTURE OZONE LAYER

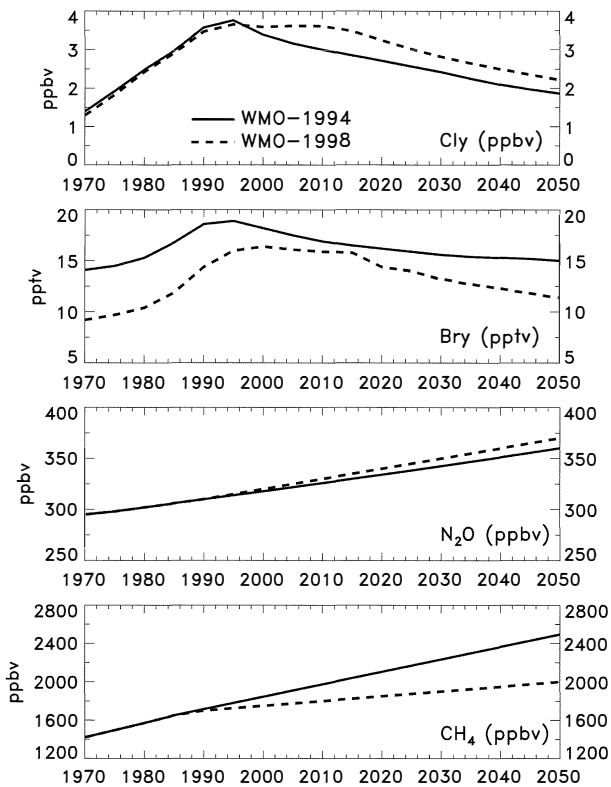


Figure 12-1. Comparison of surface boundary conditions (mixing ratios) between the 1994 WMO ozone Assessment (solid line) and this Assessment (dashed line) for Cl_y , Br_y , N_2O , and CH_4 .

dependent trend in these constituents is obtained from several sources. For the CFCs, HCFCs, and halons, the past and future trend is obtained from Chapter 11, with a very small change in the boundary conditions for HCFC-123 that reflects slightly different assumptions about banking. Note that this difference makes a minuscule difference to integrated halogen loading. The production and consumption data of scenario A3 is based on the Amendments of the Montreal Protocol (Table 11-2). Scenario A3 does not necessarily describe the actual evolution of the future atmospheric concentrations. What it describes is the maximum chlorine and bromine loading of the atmosphere following the maximum allowed production of ozone-depleting substances. We chose to use scenario A3 here as a conservative representation (in terms of the removal from the atmosphere

of ozone-depleting substances) of the Montreal Protocol. See Chapter 11 for a detailed discussion and Table 11-3 for a comparison of various scenarios.

The initial conditions for the scenarios up to 1995 (emissions and amount of substances present in the equipment) are made in agreement with the measured data from the National Oceanic and Atmospheric Administration/Climate Monitoring and Diagnostics Laboratory (NOAA/CMDL) and Atmospheric Lifetime Experiment/Global Atmospheric Gases Experiment/Advanced GAGE (ALE/GAGE/AGAGE) networks. From 1996 onward the Montreal Protocol as amended is applied to the production and consumption for both developed and developing countries. After the phase-out date of CFCs, carbon tetrachloride, methyl chloroform, and halons in the developed countries, these substances are still allowed to be produced by the developed countries for use in developing countries. The amount produced is maximally 15% of the base-level production. This additional production is accounted for in scenario A3 for CFCs, carbon tetrachloride, and methyl chloroform. The emission of carbon tetrachloride is represented well by approximately 8% of the production of CFC-11 and -12. The consumption of HCFCs is based on the revised IS92a data as reported in IPCC (1996). The methyl bromide emissions are based on the data given in Chapter 2. The emissions of the CFCs, halons, and HCFCs are calculated as a fraction of the bank of the species. This fraction is based on an analysis of the quantities in the banks and emitted over the years 1990-1995, and held constant for all future years.

In Figure 12-1, a comparison of the surface total inorganic chlorine and total inorganic bromine (Cl_y and Br_y) forcing for this Assessment and the 1994 Assessment (WMO, 1995) is shown. From 1970 through 1995, the surface Cl_y mixing ratios for the two Assessments are consistent; however, after 1995 Cl_y in this Assessment is significantly higher than that used in the 1994 Assessment. The reassessment of CH_3Br has significantly lowered the Br_y surface forcing relative to the 1994 Assessment (see Chapter 2). CH_4 and N_2O surface values used are given in Figure 12-1 and in Table 12-2 and are consistent with the 1994 Assessment up to 1990. After 1990, N_2O values are prescribed to increase at 1 ppbv/yr through 2050. This is essentially identical to scenario IS92a (IPCC, 1996). The CH_4 values are prescribed to increase at 5 parts per billion by volume per year (ppbv/yr), significantly less than that which the IS92a scenario would suggest or than that used in the

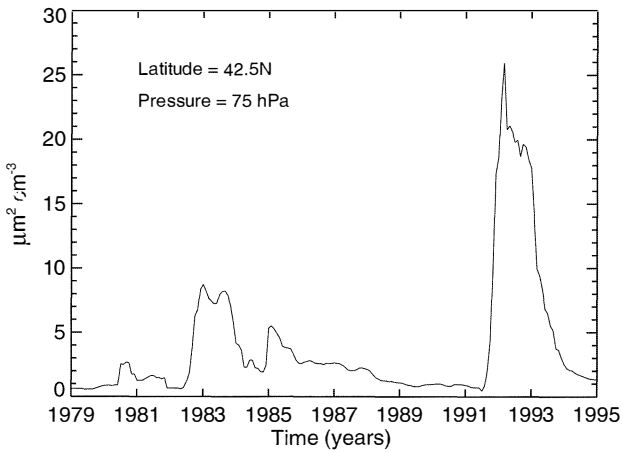


Figure 12-2. Time-dependent sulfate aerosol surface area density ($\mu\text{m}^2 \text{cm}^{-3}$) derived from SAGE I and II, SAM II, and SME data at 42.5°N and 75 hPa.

1994 WMO Assessment. This trend is believed to be more consistent with present changes in CH_4 (see Chapter 2). The sensitivity of the calculated ozone to these changes will be addressed in one set of model integrations and described in Section 12.2.1.3.

In all but one of the participating models listed in Table 12-1, the seasonally varying circulations were not modified between 1970 and 2050. However, the CAM 2-D model is a fully interactive model, meaning that the temperature and circulation are consistent with the model-derived heating rates. If CO_2 is varied in this model, the net heating rates will change and modify both the model-derived temperature and circulation in a consistent manner. For the scenarios examined here, CO_2 was fixed at its 1995 value. To examine the sensitivity to changing CO_2 , a further calculation was performed using a time-dependent CO_2 surface boundary condition. Between 1970 and 1990 the time-dependent CO_2 was taken from the 1991 WMO Assessment (WMO, 1992). After 1990, and up to 2050, the IS92a scenario for CO_2 change was used (IPCC, 1996). This scenario increased surface CO_2 from 354 parts per million by volume (ppmv) in 1990 to 509 ppmv in 2050 (see Table 12-2). For this 2-D calculation, the emphasis is on the global behavior of ozone. Results from more sophisticated coupled 3-D models are presented in Section 12.2.3, with particular attention placed on the polar response.

The sulfate aerosol surface area density (SAD) climatology is derived using extinction measurements from Stratospheric Aerosol and Gas Experiment I (SAGE

I), SAGE II, Stratospheric Aerosol Measurement (SAM II), and Solar Mesosphere Explorer (SME) data (see Rosenfield *et al.*, 1997). The SAM II data consist of monthly zonal-mean $1\text{-}\mu\text{m}$ extinction data taken between 1979 and 1995. The latitudinal coverage is limited to high latitudes for both hemispheres. The SAGE I and SAGE II data also consist of monthly-mean $1\text{-}\mu\text{m}$ aerosol extinction values. The temporal coverage is between 1979-1981 and 1985-1995 for SAGE I and SAGE II, respectively. The SME data are derived from weekly zonal-mean $6.8\text{-}\mu\text{m}$ aerosol extinction values between 1982 and 1984. This SAD was used by Jackman *et al.* (1996a) to study past, present, and future ozone trends. In Figure 12-2 the magnitude of lower stratospheric (75 hPa), middle latitude (42.5°N) SAD is shown. The impact of both the El Chichón (April 1982) and Mt. Pinatubo (June 1991) eruptions can easily be distinguished, as can the smaller eruption of Ruiz (November 1985). The use of the same derived SAD climatology in all the 2-D models is an advance on the last Assessment, in which the models used a range of surface area densities.

The ensemble of time-dependent scenarios is shown in Table 12-3. Scenario A/A3 is taken as the baseline scenario for the sensitivity studies. The modeling groups were asked first to generate a 1970 steady-state atmosphere with the source gas surface boundary conditions for 1970 given in Table 12-2. The 1979 seasonally varying SAD was used for the 1970 spin-up. After ozone steady state was reached, the models were integrated in a time-dependent manner again using the source gas surface boundary values in Table 12-2 (linearly interpolated between supplied temporal points). Between 1970 and 1979 the SAD was kept constant at the volcanically clean 1979 conditions. After 1979, the models were integrated up to 1995 using both the observed source gas boundary condition and the satellite-derived SAD. The 1979-1995 integration is labeled scenario A in Table 12-3. Scenario A3 is the future integration component of scenario A (years 1995 through 2050). Here, the time-dependent source gas boundary conditions are taken from Chapter 11 (see above discussion). The SAD is seasonally fixed using the 1995 data.

Scenarios B-D are an attempt to understand the sensitivity of each assessment model to varying CH_4 and N_2O surface boundary conditions. This sensitivity analysis is built on the 1994 WMO Assessment (see

PREDICTING THE FUTURE OZONE LAYER

Table 12-3. Definitions for the 2-D model scenarios.

Scenario	Period (years)	Aerosol Surface Area Density (SAD)	Halocarbon Boundary Conditions	CH ₄ Boundary Conditions	N ₂ O Boundary Conditions
A	1979-1995	1979-1995	Trend	Trend	Trend
A3	1996-2050	1995	Trend	Trend	Trend
B	1996-2050	1995	Trend	Fixed at 1995	Fixed at 1995
C	1996-2050	1995	Trend	Fixed at 1995	Trend
D	1996-2050	1995	Trend	Trend	Fixed at 1995
E	2000-2050	Repeating 1980-1995 period, starting in 2000, 2016, and 2032	Trend	Trend	Trend
F	1996-2050	2% annual increase*	Trend	Trend	Trend

* The percent increase in SAD is geometric, e.g., SAD (year Y) = SAD (1995) \times (1.02)^(Y -1995)

Chapter 6 of WMO, 1995) and recent work of Velders (1997). In scenario B, the CH₄ and N₂O surface mole fractions are held constant from 31 December 1995 through 31 December 2050. All other surface source gases are allowed to vary as in scenario A3. CH₄ and N₂O are individually held fixed at 31 December 1995 conditions in cases C and D, respectively. For all cases, B-D, the SAD is set to the seasonally varying 1995 values.

To understand better the SAD sensitivity of the ozone recovery, the potential impact of future volcanic eruptions is addressed in scenario E. The 1980 through 1995 period (which includes two major eruptions) was repeated sequentially starting in the years 2000, 2016, and 2032. Under the conditions of this scenario, the future volcanic events will then occur under significantly different Cl_y, Br_y, N₂O, and CH₄ abundances.

In addition to trying to understand the potential impact of large volcanic events on the stratospheric SAD, this Assessment also examines the sensitivity of the ozone recovery to a potential annual, monotonic increase in background sulfate (for example, from dimethyl sulfide (DMS), carbonyl sulfide (OCS), or sulfur dioxide (SO₂) tropospheric sources or possible increased aircraft emissions). Here, in scenario F, the SAD was assumed to increase at a geometric rate of 2% per year starting from 1995.

12.2.1.2 MODELING THE OBSERVED TRENDS IN OZONE

Recently, two model studies have investigated the ozone trend between 1980 and 1995 (Solomon *et al.*, 1996; Jackman *et al.*, 1996a). These studies forced the 2-D models with observed sulfate aerosol SAD, solar-cycle-varying ultraviolet (UV) flux, and source gas boundary conditions. Both studies stressed the importance of using SAD derived from satellite measurements. Without inclusion of volcanically enhanced SAD from El Chichón and Mt. Pinatubo, it was impossible to match the temporal shape and magnitude of the observed ozone trend. In Jackman *et al.* (1996a), with inclusion of the above processes, the GSFC 2-D model derivation of global (65°S to 65°N) column ozone changes was in reasonable agreement with changes observed by the Total Ozone Mapping Spectrometer (TOMS). However, local ozone change was larger in the model at 45 km. This is consistent with the known excess abundance of model-derived ClO relative to Upper Atmosphere Research Satellite (UARS) Microwave Limb Sounder (MLS) data (Waters *et al.*, 1996). In this model integration, there was no allowance for the possible ClO + OH → HCl + O₂ reaction. In the study of Solomon *et al.* (1996) the shape of the ozone trends is matched well but the model underestimates the observed middle-latitude temporal ozone variation by a factor of 1.5. Recent calculations (Solomon *et al.*, 1998) with an improved version of the model, including observed temperatures and their variability, now also

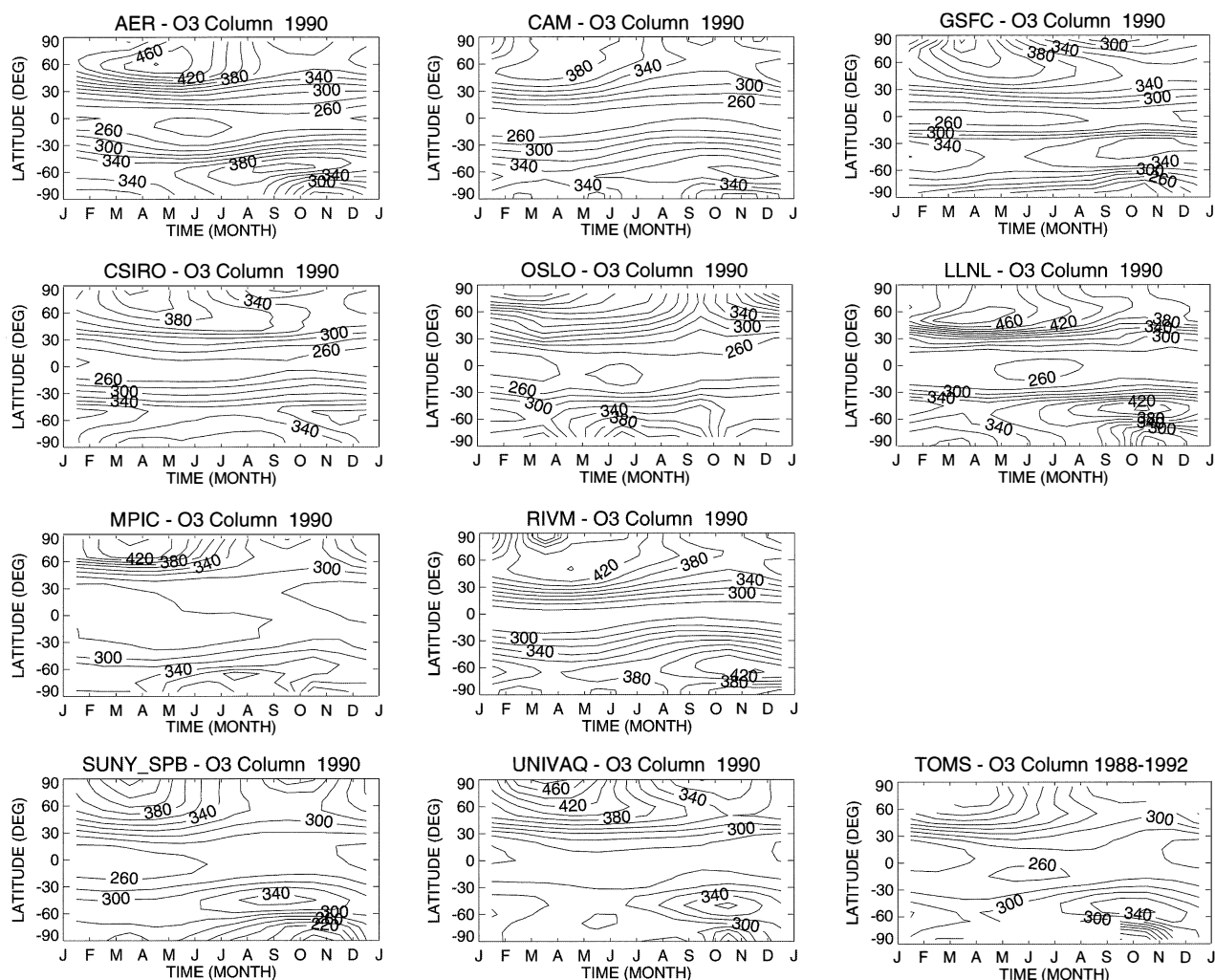


Figure 12-3. Model-derived total column ozone (DU) as a function of latitude and month of the year for 10 models for the year 1990. Observed data, given in last frame, are from TOMS Version 7, 1988-1992 average.

reproduce the magnitudes of the trend rather well (see Chapter 7).

In Figure 12-3, calculated column abundance of ozone for 1990 is shown along with the 1988-1992 column ozone derived from TOMS Version 7. In general the models represent the TOMS column ozone seasonality, with column ozone peaks occurring at high latitudes in the spring hemispheres and a minimum in the tropics. However, it is evident that stratospheric circulations within these 10 assessment models are strikingly different. The depth of the Southern Hemisphere “ozone hole” is also quite different among these 10 models, which suggests that the sensitivity to Cl_y , Br_y , and aerosol odd-oxygen loss processes may

be quite different. All but two of the participating assessment models (CSIRO and RIVM) have detailed representation of spring high-latitude cold aerosol chemistry. However, both the CSIRO and RIVM models do have reactions that represent heterogeneous processes on liquid binary sulfate.

The trend in local ozone between 1979 and 1993 from scenario A is shown in Figure 12-4. Here the model results are compared with data from the Solar Backscatter Ultraviolet spectrometer (SBUV) and SBUV/2 measurements using a linear regression model to derive local ozone trends (see also SAGE I/II ozone trends in Chapter 4, Figure 4-32, which indicate slightly larger trends in the upper stratosphere). The linear regression

PREDICTING THE FUTURE OZONE LAYER

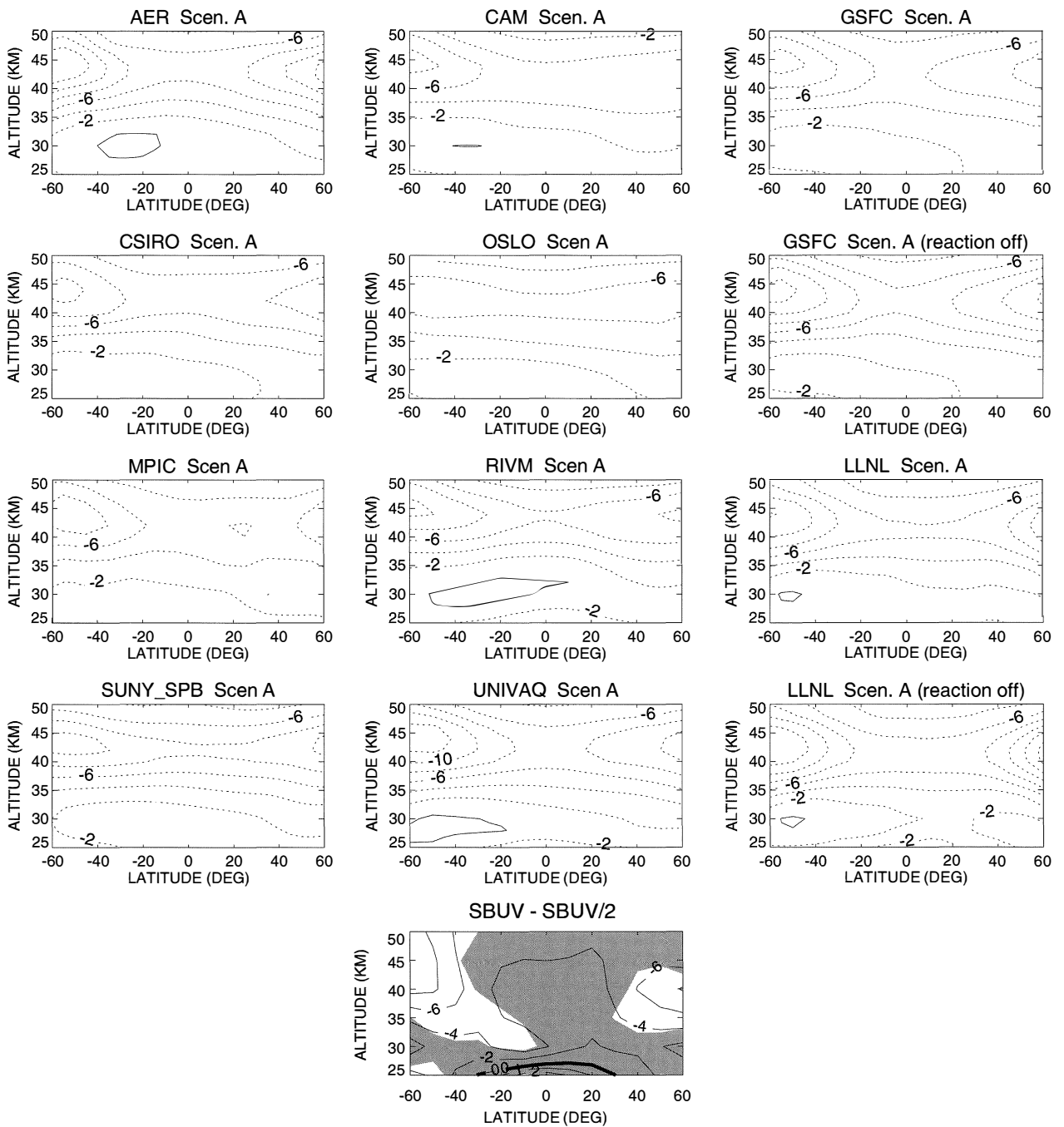


Figure 12-4. Model-derived local ozone trend (% per decade) for the period 1979 through 1993 as a function of altitude and latitude for scenario A using linear regression analyses for 10 models, and for the GSFC and LLNL models with the reaction $\text{ClO} + \text{OH} \rightarrow \text{HCl} + \text{O}_2$ omitted. The observed trends (last frame) are from SBUV and SBUV/2 measurements. The shaded area in the observed trend indicates regions where there is no statistically significant trend.

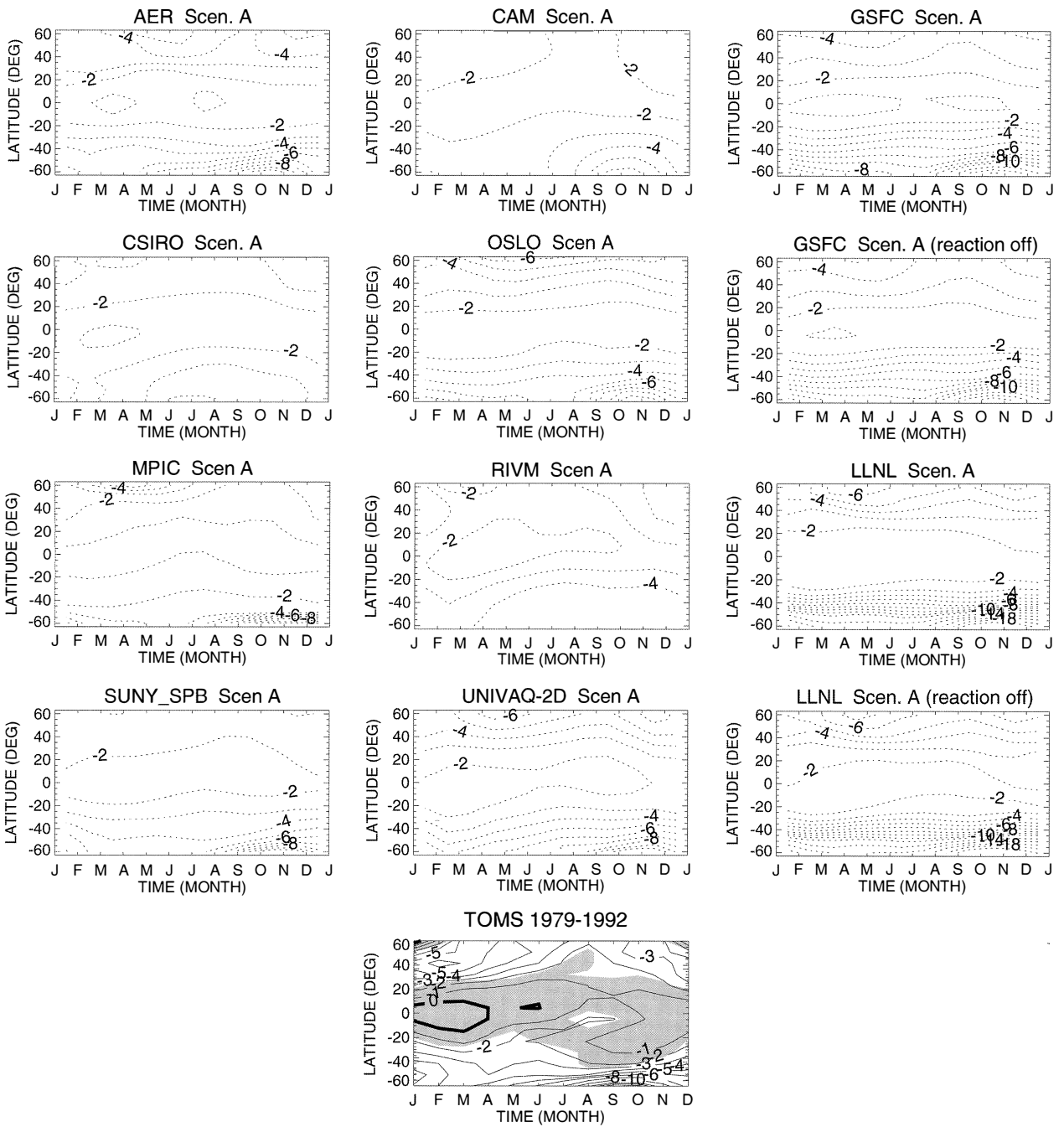


Figure 12-5. Model-derived column ozone trends (% per decade) for the period 1979-1992 as a function of latitude and month of the year for scenario A using linear regression analyses (see text) for 10 models, and for the GSFC and LLNL models with the reaction $\text{ClO} + \text{OH} \rightarrow \text{HCl} + \text{O}_2$ omitted. The observed trends (last frame) are derived from TOMS Version 7 data. The shaded area in the observed trend indicates regions where there is no statistically significant trend.

PREDICTING THE FUTURE OZONE LAYER

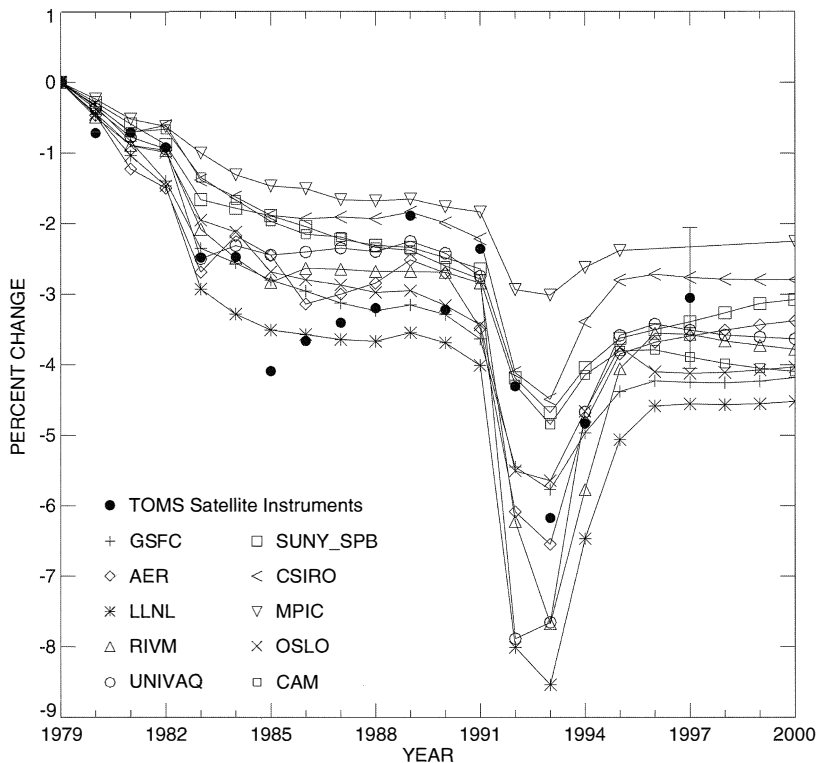


Figure 12-6. Percentage change in global (65°S-65°N) annual-average total column ozone, relative to year 1979, for 10 models for scenario A/A3 compared to observations using TOMS Version 7 data.

model consisted of a seasonal cycle, quasi-biennial oscillations, the 11-year solar cycle, and a linear trend (Hollandsworth *et al.*, 1995). The similarities between the model-derived local ozone trends and the data provide reassurance of satisfactory model performance. The shaded areas in the SBUV-SBUV/2 trends indicate regions where there is no statistically significant trend. All of the model-derived trends peak at about the correct altitude and most have magnitudes similar to the SBUV-SBUV/2 trends. In addition, the LLNL and GSFC 2-D models were used to test the sensitivity of the calculated trend to exclusion of the reaction channel $\text{ClO} + \text{OH} \rightarrow \text{HCl} + \text{O}_2$. For the past trends, both models' estimates exceed the observed trend when this reaction is omitted.

Figure 12-5 shows the TOMS Version 7 column ozone trend based on 14 years of data taken from January 1979 through December 1992 along with the derived trends from the 10 assessment models during the same period. Both the models and data were again analyzed using a linear regression model (Hollandsworth *et al.*, 1995). In general, the assessment models reproduce the gross characteristics of the TOMS ozone trend. They show the large decrease in the Southern Hemisphere spring, consistent with Antarctic "ozone hole" chemical processes. From this column trend analysis, it is evident

that the RIVM and CSIRO models do not include a polar cold aerosol representation. For northern midlatitude (approximately 40-50 degrees) winter, in the Northern Hemisphere, most of the models underestimate the ozone trend, as described in Solomon *et al.* (1996).

The percentage change in global (65°S-65°N) annual average total column ozone, relative to 1979, is shown for the 10 models and compared with TOMS observations (primarily Nimbus-7 and Meteor-3 TOMS data, except for the 1997 data point taken from Earth Probe TOMS) in Figure 12-6. The shape of the ozone trend with time is similar for all the models but there is a significant spread of magnitudes (for example, by approximately 2% about a mean of 2.5% between 1984 and 1990 and by over 5% immediately after the Mt. Pinatubo eruption in 1991). This spread is not surprising. Figures 12-3 and 12-5 have already demonstrated the differences between the models, arising in part from differences in modeled circulation. Furthermore, there are model differences in the formulation of gas-phase and, especially, heterogeneous chemistry. Note also that none of the models include radiative feedback after the volcanic eruptions, which could have changed the circulation (see, for example, Kinne *et al.*, 1992; Michelangeli *et al.*, 1989; Pitari, 1993; Hadjinicolaou *et*

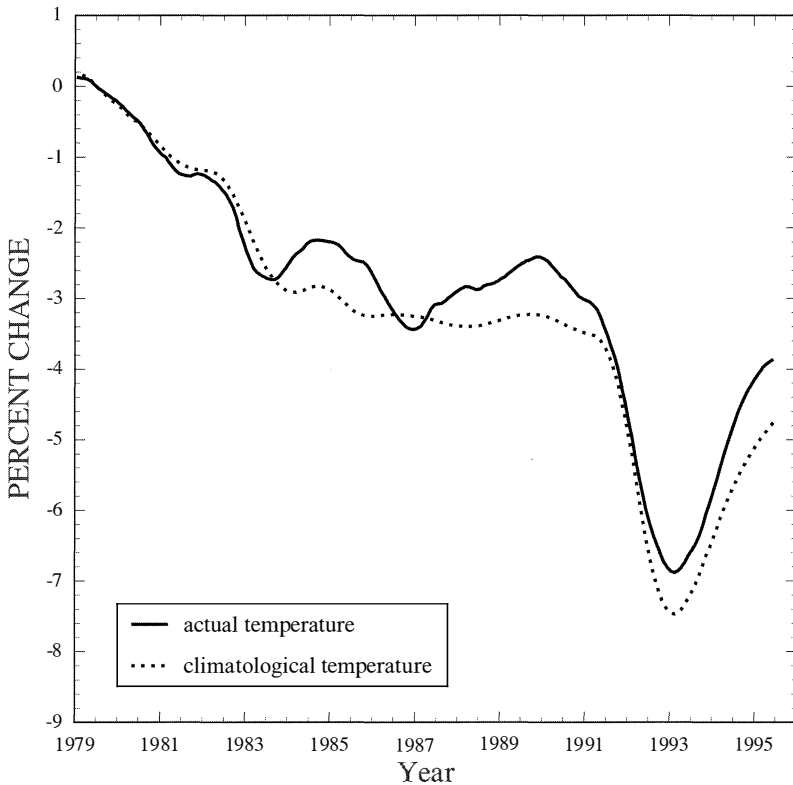


Figure 12-7. Percentage change in global (65°S-65°N) column ozone using a 24-month running mean for the AER model. The solid line represents an integration that includes the use of the mean temperature and temperature probability distribution about the zonal mean taken for each year between 1979 and 1995. The dashed line uses an 8-year average of both mean temperature and temperature probability distributions.

al., 1997). For this reason, comparison between the models and the TOMS data must be treated with caution. With these caveats, several models tend to represent the trend in ozone during the 1980s reasonably well but overestimate the Mt. Pinatubo period. Other models underestimate the trend in the 1980s but seem to be in good agreement during and after the Mt. Pinatubo period.

The formulation of heterogeneous reactions is one reason why the models have different responses to aerosol-induced ozone depletion. For example, the AER 2-D model incorporates a method in which the kinetic rate constants are calculated using both zonal monthly-mean temperatures and temperature probability distributions to account for longitudinal deviations from the monthly zonal mean (see also Solomon *et al.*, 1998). To determine the sensitivity of the result, a second calculation was performed using a temperature climatology averaged over the years 1979-1995. Figure 12-7 shows the global-average ozone column changes calculated by the AER model with climatological temperatures and with year-by-year temperatures. The calculation with year-by-year temperatures shows more structure and year-to-year variability than the climatological case. The trends are similar until 1984; however, from 1984 to 1986, from 1988 to 1991, and

from 1992 to 1995, the calculation with year-by-year temperatures shows less ozone depletion than the climatological calculation. Most of this difference relates to temperature variability at high latitudes in winter, which broadens the climatological distributions. The LLNL model shows a large sensitivity to Pinatubo-aerosol-induced ozone depletion because it used a single year (1996) to derive its temperature probability distribution. This year was colder than the climatological average, and therefore derived ozone trends in the LLNL model are overestimated for some years.

12.2.1.3 OZONE RECOVERY—MODEL SENSITIVITY TO KEY PARAMETERS

There are many factors that can affect the decadal time span of ozone recovery in model-derived trend studies and potentially within the present and future atmosphere. As mentioned in the introduction, the future abundances of Cl_y , Br_y , CH_4 , N_2O , stratospheric sulfate aerosol, and climate conditions can significantly modify model-derived ozone recovery. Figure 12-8 shows the time variation of calculated Cl_y and Br_y for 50°N at 20 km for the 10 models. As previously discussed in the 1994 Assessment (WMO, 1995), there is a very large

PREDICTING THE FUTURE OZONE LAYER

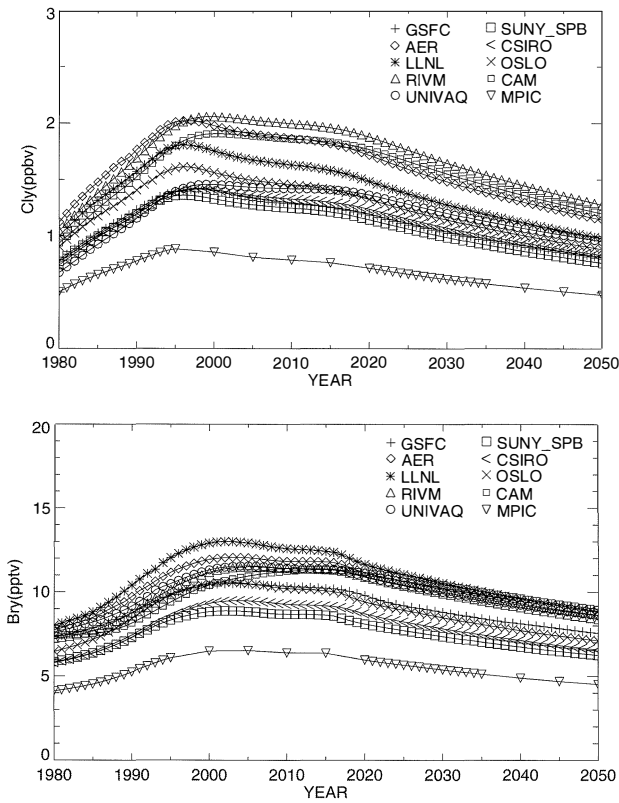


Figure 12-8. Time variation in Cl_y (top panel) and Br_y (bottom panel) mixing ratios at 20 km, 50°N latitude, as determined from 10 models.

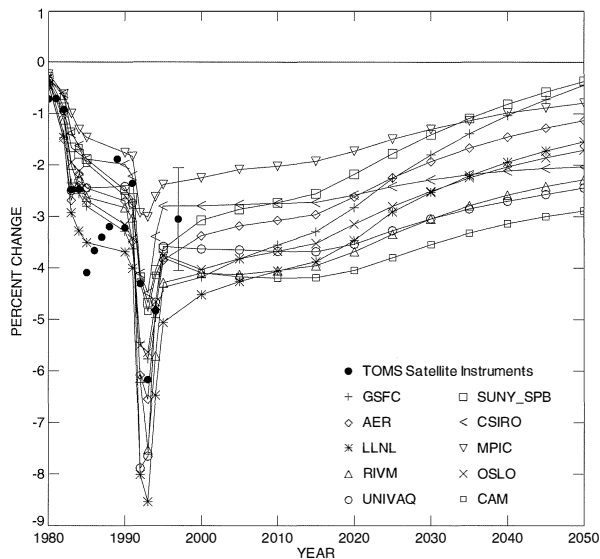


Figure 12-9. Percentage change in global (65°S-65°N) annual-average column ozone, relative to year 1979, between 1980 and 2050, as predicted by 10 models for scenario A/A3 compared to observations using TOMS Version 7 data.

spread in the calculations. The lower stratosphere is a critical region, and this spread remains a reason for concern (ameliorated only slightly by the knowledge that vertical gradients are large in the lower stratosphere so that comparisons at a specific altitude are a very stringent test).

In Figure 12-9, the annual average global (65°S-65°N) ozone change relative to 1979 is shown for scenario A/A3 for all participating assessment models. The period before the year 2000 shows the large impact of the volcanic aerosol on column ozone depletion. For all models the minimum global ozone is calculated in the years immediately after the Mt. Pinatubo eruption in 1991. Between the years 2000 and 2020, the modeled ozone recovers more slowly than after 2020. For all assessment models used in this chapter, none reach their pre-1980 ozone abundance before 2050. This is significantly different from the results obtained in the 1994 WMO Assessment. There, out of the seven participating models used in that Assessment, five returned to pre-1980 conditions by 2040 and only two models did not recover before 2050. As mentioned previously and shown in Figure 12-1, the Cl_y loading is greater and the CH_4 loading is much less after the year 2000 in this Assessment. Methane increases tend to reduce the impact of increased chlorine loading by converting radicals to reservoir species. This, coupled with small differences in N_2O and the future sulfate aerosol abundance, can explain the difference between this 1998 Assessment and the 1994 WMO Assessment. This is demonstrated in Figure 12-10, where the GSFC model systematically replaced components of the 1998 WMO Assessment scenario A/A3 with 1994 WMO Assessment components. The CH_4 and Cl_y abundance caused the biggest effect and significantly shortened the ozone recovery in the GSFC model. Thus, for the scenarios used in this Assessment, the ozone recovery is very sensitive to changes in chlorine and methane. In particular, the use of a lower methane emission rate than in the 1994 WMO Assessment significantly reduces the rate of ozone recovery. We should recall that the future halogen scenarios used here are hypothetical. However, the new methane scenario is consistent with recent measurements (see Chapter 2).

The ozone change results for the 10 models, shown in Figure 12-9, have been normalized to the year 2000 in Figure 12-11. This highlights variations in recovery rates among the models in the current Assessment in a relatively volcanically clean atmosphere (1995 SAD used). There is a wide range of recovery rates, with the

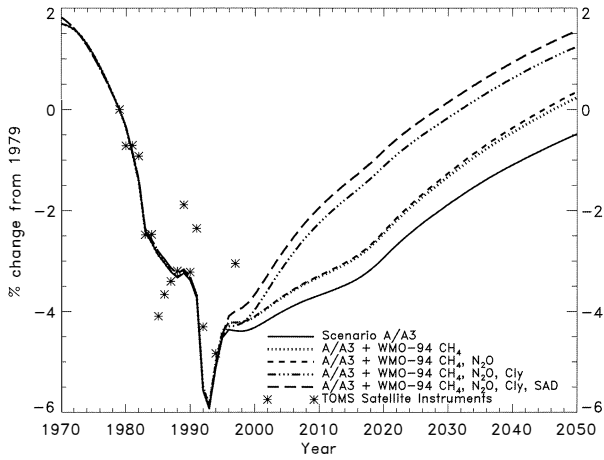


Figure 12-10. Percentage change in global (65°S-65°N) annual-average column ozone, relative to 1979, for the GSFC 2-D model for scenario A/A3 (solid line) compared to TOMS observations, and a comparison of surface boundary conditions of CH₄, N₂O, Cl_y, and sulfate aerosol surface area density (SAD) used in the 1994 WMO Assessment and this Assessment (dashed lines, see legend). The SAD represents volcanically clean conditions (WMO, 1992) between 1995 and 2050.

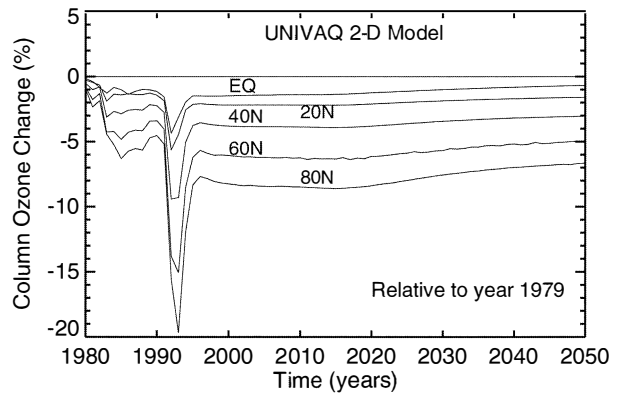
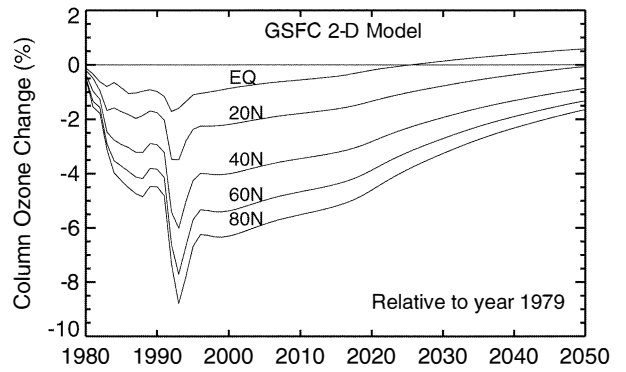


Figure 12-12. Percentage change in annual-average column ozone relative to year 1979 for selected latitudes in the Northern Hemisphere between 1980 and 2050 for scenario A/A3. Results are shown for the GSFC (top panel) and UNIVAQ (bottom panel) models.

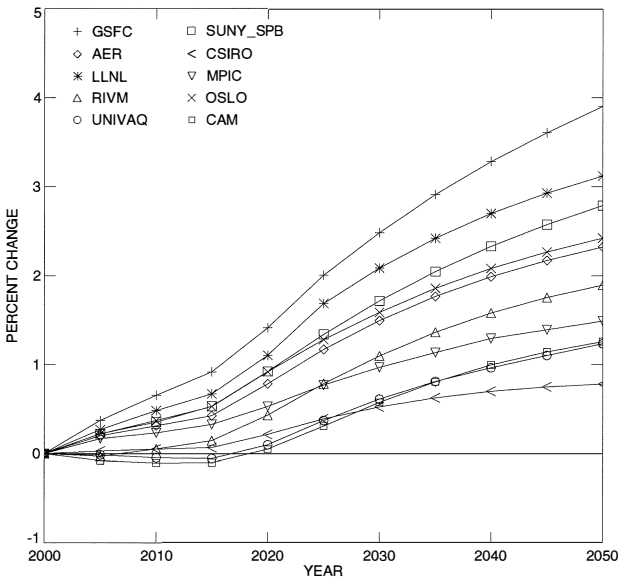


Figure 12-11. Percentage change in global (65°S-65°N) annual-average column ozone relative to the year 2000 for 10 models for scenario A3.

GSFC model recovering most rapidly, followed by the LLNL and SUNY_SPB models. At the other end, the CSIRO, UNIVAQ, and CAM models recover at the slowest rate. Note that, as the chemical conditions in the models change with time, the relative rates of recovery between some of the models vary. Figure 12-12 shows the latitudinal sensitivity for two models that were on the extremes of the total ozone recovery (GSFC and UNIVAQ). The GSFC model recovers to pre-1980 ozone abundances between the equator and 20°N before the year 2050. At high polar latitudes, at 2050 recovery rates, one can estimate that it would take the GSFC model at least 20-30 additional years to recover to pre-1980 ozone levels. For the UNIVAQ model, representative of those models with slow recovery, it is not clear that it will ever reach pre-1980 ozone abundances at any latitude.

PREDICTING THE FUTURE OZONE LAYER

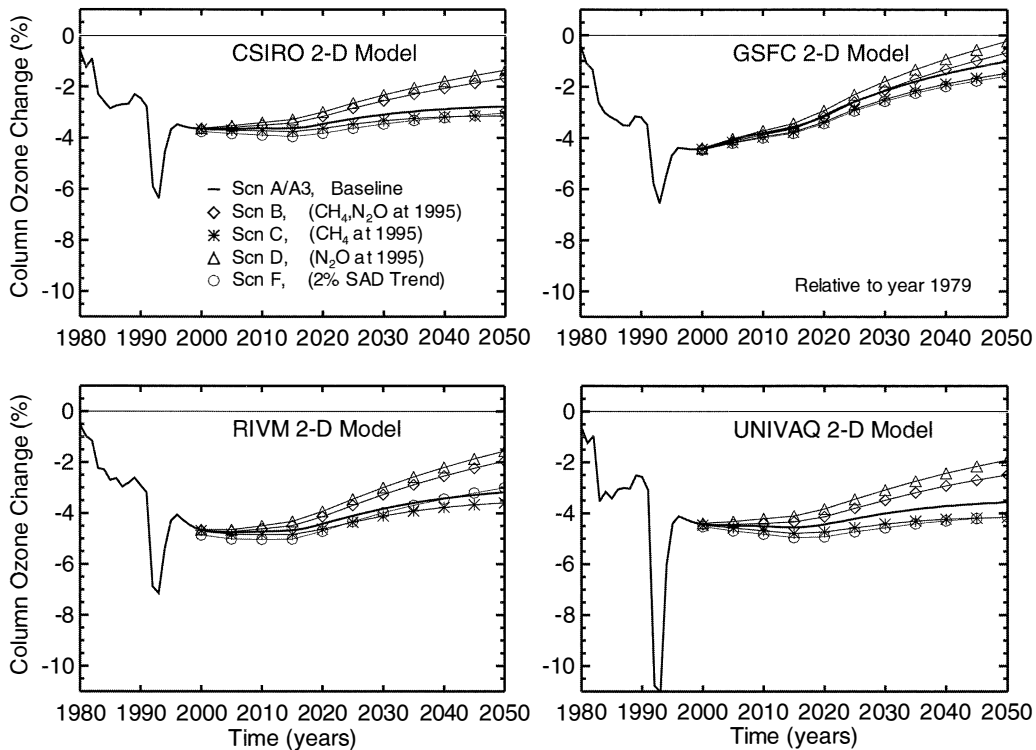


Figure 12-13. Percentage change in annual-average column ozone relative to year 1979 at 45°N latitude between 1980 and 2050 for several emission scenarios to test the model sensitivity to CH₄, N₂O, and SAD. Sensitivity tests for scenarios A through D, and F (see Table 12-3) are shown for the CSIRO, GSFC, RIVM, and UNIVAQ models.

Four modeling groups completed the entire set of sensitivity scenarios A-D and F. In Figure 12-13, the results of these models are shown at 45°N latitude. In all cases the sensitivity to CH₄, N₂O, and sulfate aerosol is consistent between models. When CH₄ is fixed at 1995 conditions (scenario C), the recovery is extended. When N₂O is fixed at 1995 conditions (scenario D), the recovery is shortened. When both N₂O and CH₄ are fixed at 1995 conditions (scenario B), the ozone recovery is shortened, but not to the extent of scenario D. When background stratospheric aerosol is allowed to increase annually by 2% per year (scenario F), the impact is to extend the recovery in three of the four models, with a magnitude similar to the impact of fixing CH₄ at 1995 conditions. The RIVM model initially extends the ozone recovery; however, around year 2040, the additional aerosol SAD hastens the ozone recovery relative to scenario A3.

Recently, laboratory measurements (Lipson *et al.*, 1997) have suggested that there may be a significant branching ratio for the ClO + OH → HCl + O₂ reaction.

As shown earlier, including this reaction improved the past trend comparisons for the LLNL and GSFC models relative to observations. The impact of the reaction on ozone recovery was also investigated in this study. For both models, the reaction changes the absolute magnitude of the ozone depletion by a small amount but does not impact the overall recovery rate. However, it is interesting that during the El Chichón and Mt. Pinatubo periods, including the ClO + OH → HCl + O₂ branch mitigates ozone depletion; at later times there is a crossover where the absolute ozone reduction is greater when the reaction is included. Under lower Cl_y abundance, the additional ClO_x (when the reaction is omitted) is interfering with NO_x odd-oxygen catalytic loss processes, mitigating ozone depletion.

In understanding the time frame over which ozone recovery will occur, one should also consider the impacts of future volcanic eruptions. As mentioned previously, between 1980 and 1995, there were two large volcanic events that significantly affected ozone trends (Solomon

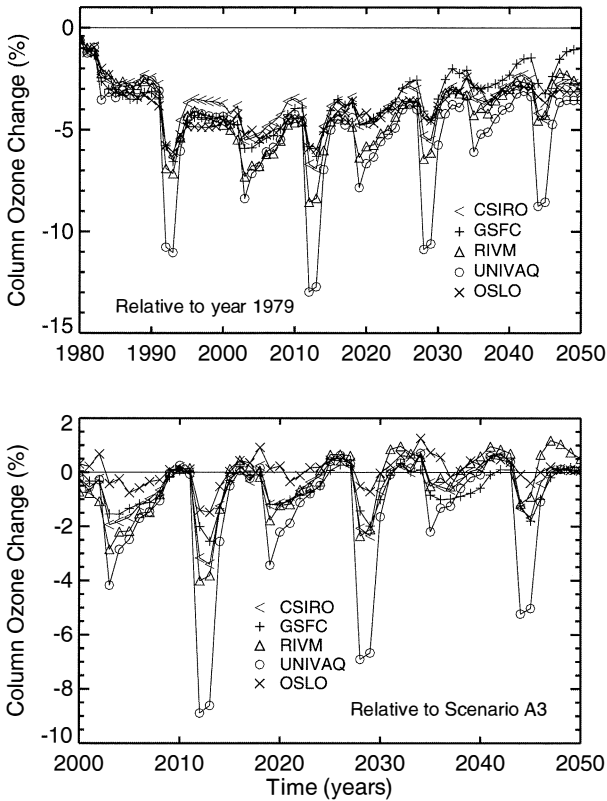


Figure 12-14. Top panel: Percentage change in annual average column ozone relative to year 1979 at 45°N latitude between 1980 and 2050 for five models, for volcanic eruption sensitivity scenario E (see Table 12-3). Bottom panel: The scenario A3 ozone trend has been subtracted to emphasize volcanic effects alone.

et al., 1996; Jackman *et al.*, 1996a). These events occurred during a period of high chlorine abundance. Tie *et al.* (1994) suggest that at lower chlorine abundance the impact of a major volcanic eruption will be less significant and could even increase ozone. In order to study the impact of high SAD in periods when chlorine abundance is much lower than present, scenario E was constructed. During the 1980 through 2050 period, four El Chichón- and Mt. Pinatubo-like eruptions were simulated (see Table 12-3). As indicated in Figure 12-14, the largest ozone reduction from this series of volcanic events occurred around 2010. This is a period of peak Cl_y levels in the stratosphere, before significant reduction has set in (see Figure 12-8). In Figure 12-14, the underlying ozone trend component has also been

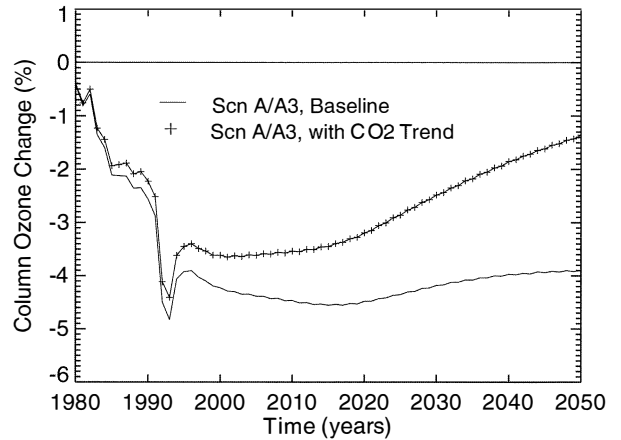


Figure 12-15. Percentage change in annual-average column ozone relative to year 1979 for the CAM 2-D model at 45°N latitude between 1980 and 2050. The solid line represents using CO₂ surface boundary conditions fixed at 1995 levels between 1979 and 2050. The line with crosses represents using a time-dependent trend of CO₂ (see Table 12-2).

subtracted from scenario E. This emphasizes the importance that Cl_y and Br_y abundances will have on the magnitude of the impact of a given volcanic event in the future. During the decade of the 2040s, the magnitude of the ozone reduction following a Mt. Pinatubo-sized eruption is reduced substantially. Thus, while Mt. Pinatubo-sized eruptions will have an effect on the magnitude of ozone depletion as long as halogens are present in the stratosphere, eruptions occurring at decadal intervals, as investigated here, are not expected to substantially alter the eventual ozone layer recovery over the long term.

An important sensitivity to be quantified is the role that future climatic conditions play in extending or mitigating the ozone recovery. In this study, the CAM 2-D model was allowed to respond to changes in CO₂ trends. Results from this sensitivity study are shown in Figure 12-15. For scenario A/A3, without CO₂ trends, the model recovery is very slow. The increases in CO₂ lead to reduced stratospheric temperatures, which then reduce the gas-phase destruction of ozone. In consequence the modeled ozone recovery is significantly accelerated. The model circulation will also change and will impact ozone levels. A more detailed discussion of the impact of changing greenhouse gas concentrations on polar ozone is given in Section 12.2.3.

PREDICTING THE FUTURE OZONE LAYER

Table 12-4. Forcings and/or processes that affect model-derived ozone recovery.

Forcing or Process	Magnitude	Direction
Higher future CO ₂	Large	Shorten*
Higher future Cl _y trends	Moderate	Lengthen
Higher future CH ₄ trends	Moderate	Shorten
Higher future N ₂ O trends	Moderate	Lengthen
Higher future sulfate aerosol loading	Moderate	Lengthen
A series of volcanic eruptions	Small	Lengthen

* Midlatitude result based on one 2-D model. See also the discussion of 3-D models in Section 12.2.3, where increased greenhouse gases delay polar ozone recovery, particularly in the next 10 to 20 years.

12.2.1.4 SUMMARY

There are many factors that influence the ozone recovery as the atmosphere returns to pre-1980 halogen loading. In this section we have specifically considered 2-D model calculations of the global ozone behavior over many decades. We have discussed the model sensitivity to halogen loading, to CH₄ and N₂O emission rates, to variations in aerosol SAD, and to the radiative impact of increasing CO₂. Depending on the model, the recovery of global ozone to pre-1980 conditions is reached at about 2050 on one extreme to potentially never on the other. Reducing the methane increase rate, in line with recent measurements, leads to a significant increase in the time for the ozone layer to recover.

Table 12-4 is a list of “forcings” and/or “processes” that affect the model-derived ozone recovery in the calculations discussed here, in approximate order of significance. “Large” magnitude denotes significant deviation from the baseline recovery—greater than ±30 years or a large (greater than ±2%) absolute difference in column ozone change between the baseline and perturbed forcing in 2050. “Moderate” denotes a significant change, modifying the recovery by less than ±30 years from the baseline, or the absolute difference in column ozone change between the baseline and perturbed forcing in 2050 is greater than ±1%. “Small” signifies that the change will affect the recovery period by less than ±5 years, or the absolute difference in column ozone between the baseline and perturbed forcing in 2050 is less than ±0.5%.

To put the list in context, it needs to be stressed that the magnitude of any effect will depend on the magnitude of the forcing. The classifications given in Table 12-4 relate directly to the different forcing

scenarios considered earlier. These are necessarily uncertain. Thus, larger increases in future halogen loading (or any of the other forcings) than those considered here could lead to a “large” effect.

The sensitivities to forcing as presented in Table 12-4 are consistent between the various 2-D models. The magnitudes must be put into perspective by considering the large inter-model differences predicted for the A3 scenario in 2050 (see Figure 12-9).

12.2.2 Chemical Transport Models

Chemical transport models (CTMs), with circulations and temperatures forced by observations, have been used increasingly in recent years. They have been able to reproduce many observed features of the perturbed lower stratosphere, including the substantial Arctic ozone depletions that have been seen in recent years. These models can now be used for assessment purposes and, especially, for sensitivity studies.

12.2.2.1 SENSITIVITY TO HALOGEN LOADING

The Cambridge CTM has been used to study the sensitivity of ozone depletion within the polar vortex to varying levels of Cl_y and Br_y (Chipperfield and Pyle, 1998). Results are shown in Figure 12-16. The figure shows that within the range of Cl_y and Br_y values tested, the chlorine loading has the strongest influence on ozone loss. For example, at 475 K with Br_y fixed at 30 pptv, increasing Cl_y from 2.0 ppbv to 3.3 ppbv to 4.0 ppbv increases the maximum average ozone depletion from 16% to 35% to 44%, respectively. In contrast, for a fixed Cl_y of 3.3 ppbv, increasing Br_y from 20 pptv to 30 pptv only increases the maximum ozone depletion from 30%

to 35%. This dependence of the ozone loss on Cl_y and Br_y is qualitatively consistent with the results of Danilin *et al.* (1996).

The greater sensitivity of the calculated ozone loss to chlorine reduction is one reason why recovery should be more visible in the Antarctic than the Arctic (since the $ClO + ClO$ cycle is relatively more important there than $ClO + BrO$). Antarctic integrations with the Cambridge CTM (Chipperfield and Pyle, 1998) confirm that a change in chlorine loading from 3 ppbv to 2 ppbv produces a larger absolute reduction in ozone loss than in the Arctic.

12.2.2.2 SENSITIVITY TO LOWER STRATOSPHERIC TEMPERATURES

Although not run in coupled chemistry and climate mode, CTMs have demonstrated that the ozone loss in the Arctic is very sensitive to stratospheric temperatures. Figure 12-17 shows the minimum temperature north of 50°N at 50 hPa from the European Centre for Medium-Range Weather Forecasts (ECMWF) analysis for the Arctic winters of 1991/92 to 1996/97. The differing meteorology of the first four winters has been discussed by Chipperfield *et al.* (1996). Recent winters (1994/95, 1995/96, 1996/97) have all been cold, with periods of record low temperatures. In 1995/96, temperatures fell below the 195K NAT threshold in early December and dipped below the ice point in mid-January. Temperatures remained low until late February. In contrast, in 1994/95 temperatures rose earlier in February followed by a short low-temperature period in mid-March. The winter of 1996/97 started particularly warm, but temperatures dropped below the 195K threshold in mid-January and remained low throughout March, which saw many days with record minima.

Figure 12-18 shows the average ozone depletions calculated in the Arctic lower stratosphere (475K surface) for each year since 1993/94, assuming no change in stratospheric halogen loading. Earlier years were reported in Chipperfield *et al.* (1996). There is a large difference in the calculated ozone loss between the years. In the warm winter of 1993/94 the average depletion calculated is about 15%. Much larger ozone losses are calculated in those years (1994/95, 1995/96 and 1996/97) with lowest stratospheric temperatures. In 1996/97 the calculated depletion began much later but, with low temperatures coinciding with the return of sunlight, ultimately was approximately the same (nearly 25%) as

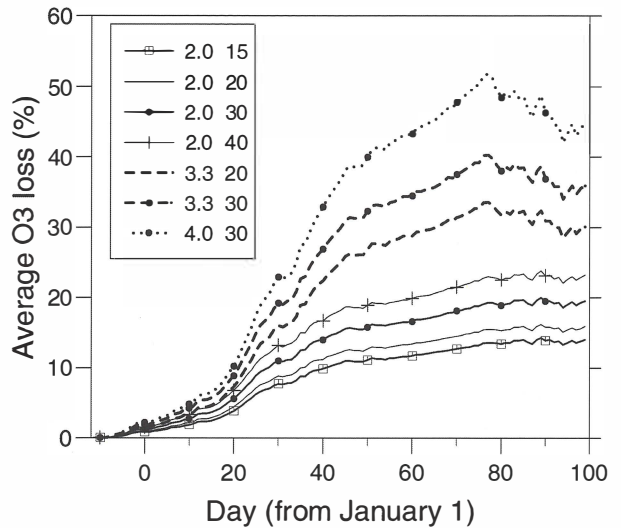


Figure 12-16. Variation of ozone loss (%) calculated within the Arctic polar vortex at 475 K for different values of Cl_y (left in the legend, ppbv) and Br_y (right in the legend, pptv) using the Cambridge CTM (Chipperfield and Pyle, 1998). The edge of the vortex was defined at 36 potential vorticity units (PVU) at 475 K.

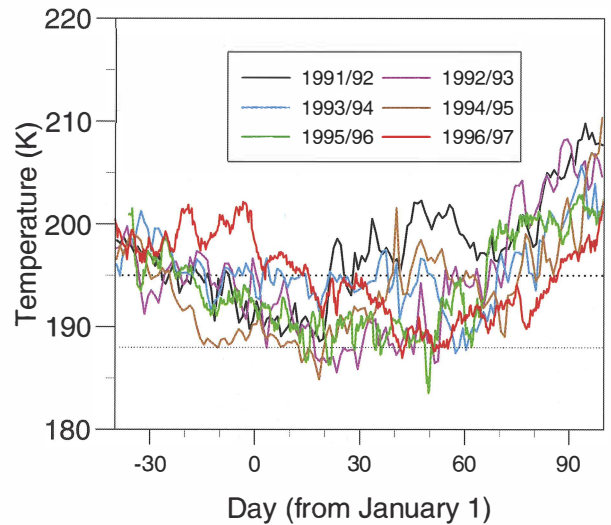


Figure 12-17. Minimum temperature in the ECMWF analysis at 50 hPa poleward of 50°N for the Arctic winters 1991/92 to 1996/97. Also indicated are the approximate formation temperatures of Type-1 (upper line) and Type-2 (lower line) PSCs. Figure updated from Chipperfield *et al.* (1996).

PREDICTING THE FUTURE OZONE LAYER

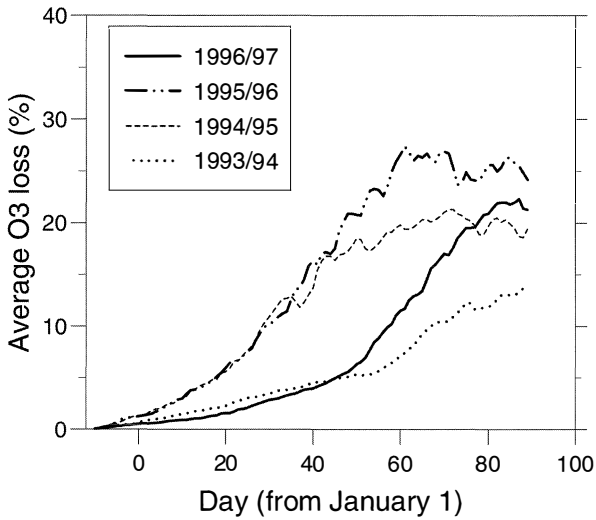


Figure 12-18. Area-weighted average chemical ozone loss (%) poleward of 60°N at 475 K for the Arctic winters 1993/94 to 1996/97, calculated in the Cambridge CTM (Chipperfield and Pyle, 1998).

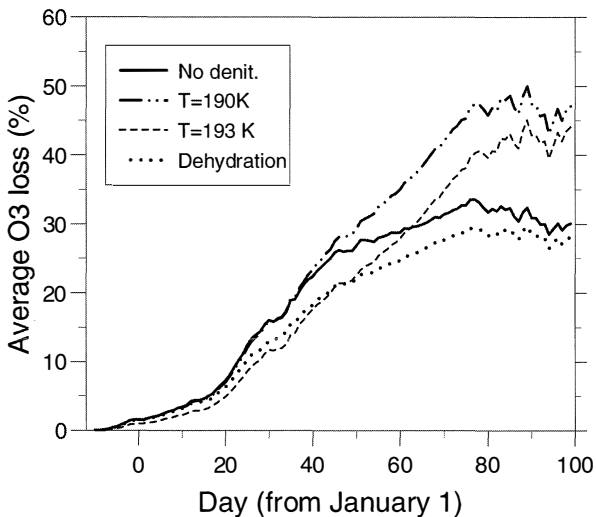


Figure 12-19. Sensitivity of Arctic ozone loss (%) within the polar vortex at 475 K, assuming different temperature thresholds for denitrification (and also dehydration) in the Cambridge CTM (Chipperfield and Pyle, 1998).

in 1995/96. The calculations demonstrate that Arctic ozone loss is very sensitive to lower stratospheric temperatures. Any systematic cooling of the stratosphere (so that, for example, the lower temperatures in recent years might become the norm) would have a very significant impact on stratospheric ozone recovery, a point we consider in more detail in Section 12.2.3 using coupled chemical-radiative-dynamical models.

A related experiment is that of Danilin *et al.* (1998), which used the AER photochemical box model including heterogeneous chemistry to investigate the influence of an imposed stratospheric cooling on Arctic ozone depletion. These results indicate that a 1-K cooling of the lower stratosphere was equivalent to increasing chlorine loading by 0.40-0.95 ppbv for current conditions. The results also imply that continued cooling of the stratosphere over the coming decades, similar to that observed over the past decades, could compensate for decreasing chlorine levels. In a long-term calculation for conditions at 70°N using heterogeneous reactions on NAT surfaces, the model predicts that a cooling trend of -0.05 K yr^{-1} (a conservative estimate based on observations) leads to maximum ozone losses from about 2005 to 2020, with recovery to 1995 levels delayed past 2045. These results suggest the likelihood of a delay in the expected recovery of the ozone layer in the Arctic.

Should extensive denitrification occur in the Arctic polar vortex (similar to that in the Antarctic vortex) then the potential for ozone depletion could be enhanced. The sensitivity of the ozone depletion to the degree of denitrification is shown in Figure 12-19 in a calculation with the Cambridge CTM. One experiment assumed that HNO_3 was permanently removed from the gas phase at temperatures below 190 K. At 475 K this has the effect of delaying chlorine recovery and extending the period of rapid ozone depletion. The maximum average ozone depletion is increased from 30% in the control run (“No denit.,” identical to the 3.3-ppbv Cl_y , 20-pptv Br_y curve shown in Figure 12-16) to 40% when denitrification is included. A further experiment assumed the higher threshold for denitrification of 193 K. At 475 K this causes a reduction in ozone depletion. The removal of NO_y prevents the formation of ClONO_2 as active chlorine decays. With sporadic PSC processing that occurs in the Arctic, the low ClONO_2 inhibits the further rapid activation of the chlorine contained in HCl (reaction (12-4), Section 12.2.1.1a).

12.2.3 Three-Dimensional Chemistry-Climate Models

The most important radiatively active gases in the atmosphere are water vapor, carbon dioxide, and ozone. An increase of these greenhouse gases is expected to produce a warming in the troposphere and a cooling in the stratosphere and a change in the dynamics. The predicted stratospheric cooling is generally expected to reduce homogeneous chemical destruction of ozone, while increasing heterogeneous destruction. Circulation changes will also alter ozone transport and hence its distribution.

In the stratosphere, where the chemical and dynamical transport time scales for ozone are roughly comparable, three-dimensional photochemical models, in which the simulated ozone is used to compute model radiative heating rates, are needed to provide a complete picture of stratospheric ozone and its future behavior. Additionally, the sensitivity to radiative and other perturbations will require simulations of the order of a decade or more to take into account the natural variability of the system. In practice the cost of running such models has, to date, resulted in other simplifications such as restricting the length of integrations to time scales of only a few years or less or simplifying the tropospheric simulation. At the time of the last Assessment (WMO, 1995), 3-D models in the literature included mechanistic models with full chemistry, low-resolution general circulation models (GCMs) with full chemistry, or more complete GCMs with a simplified chemistry. Computer power has only relatively recently reached the stage where comprehensive GCMs can be used with fairly complete stratospheric chemistry schemes. Coupled chemistry-climate models have not yet reached the level of maturity and confidence of climate models.

In mechanistic models, the dynamical situation in the stratosphere is controlled by the forcing at the model lower boundary. Granier and Brasseur (1991) were the first to use such a model to simulate an Antarctic ozone hole in a 3-D model, while Austin and Butchart (1992) demonstrated the importance of interhemispheric differences in polar ozone simulations. Knight *et al.* (1998) investigated the impact of the Mt. Pinatubo eruption on stratospheric ozone and found that the largest effect, a decrease of about 20 DU, occurred at the edge of the ozone hole, broadly in agreement with observations (Randel *et al.*, 1995). Butchart and Austin (1996) investigated the effect of the QBO on the Antarctic ozone

hole to explore the hypothesis of Garcia and Solomon (1987) that deep ozone holes were experienced during westerly phases. The model results (Figure 12-20) suggest that the quasi-biennial oscillation (QBO) does indeed modulate the Antarctic ozone but that this occurs primarily through transport rather than heterogeneous chemistry. The above studies have shown that while mechanistic models reproduce the main characteristics of ozone behavior observed in the atmosphere, they also imply the need for more complete modeling treatments of the atmospheric system.

Short integrations of a low-resolution GCM with stratospheric chemistry have been performed by Pitari and Rizi (1993) in investigating the impact of aerosols from the Mt. Pinatubo eruption. Further short integrations using fairly comprehensive stratospheric chemistry in much more extensive GCMs have also been completed by Rasch *et al.* (1995) and Austin *et al.* (1997). The latter study demonstrated the need for a large number of vertical levels to simulate stratospheric dynamics sufficiently accurately, thereby increasing the computational cost further. Multi-year integrations with GCMs with comprehensive chemistry have been or currently are being run with the European Centre Hamburg model (ECHAM3/CHEM) (Steil *et al.*, 1998; Dameris *et al.*, 1998), the Météo-France Centre National de Recherches Météorologiques ARPROBUS model (Lefèvre *et al.*, 1994), and the UKMO chemistry-climate model (Austin *et al.*, 1997).

Experiments with fairly complete representation of climate processes but with limited chemistry have also been run for longer periods. Of those GCMs that include proper representations of the middle atmosphere (Table 1 of Hamilton (1996) lists many of these), there are comparatively few published predictions of possible changes of the stratospheric climate (Fels *et al.*, 1980; Boville, 1986; Rind *et al.*, 1990).

The Goddard Institute for Space Studies (GISS) climate model (Shindell *et al.*, 1997, 1998a,b; Rind *et al.*, 1998) and the EMÉRAUDE climate model used formerly at Météo-France (Cariolle and Deque, 1986; Cariolle *et al.*, 1990; Mahfouf *et al.*, 1993) have been run with a simple representation of stratospheric chemistry. However, because the chemical and dynamical transport time scales for ozone are roughly comparable in the stratosphere, using such simplified chemistry will have its limitations.

A brief description of the various 3-D models that have been used for ozone predictions is presented in

PREDICTING THE FUTURE OZONE LAYER

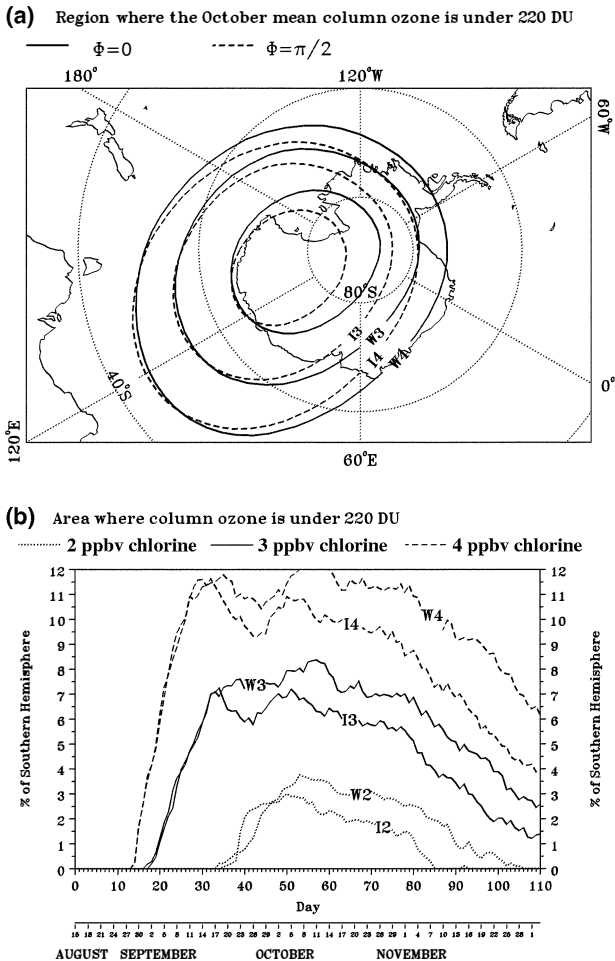


Figure 12-20. (a) Area enclosed by the 220-DU total ozone contour for the UKMO model investigating the impact of the QBO on the Antarctic ozone hole for varying levels of chlorine (from Butchart and Austin, 1996). The curves are labeled with the total chlorine amount in ppbv (2, 3 or 4) and the QBO phase (W denotes westerly; I denotes seven months later). Φ in the figure is the phase of the quasi-biennial oscillation at 24 km, where $\Phi = 0$ corresponds to the westerly phase and $\Phi = \pi/2$ is intermediate between the westerly and easterly phase ($\Phi = \pi$). (b) Time history of the 220-DU contour area; labeling is the same as in (a).

Table 12-5. These models have a number of significant differences, including the region(s) of the atmosphere covered (i.e., troposphere, stratosphere, mesosphere), the resolution, the physics included, and the parameterization of ozone chemistry, both homogeneous and heterogeneous. These differences complicate a comparison of model results, but can be used to suggest which issues may be most important in influencing the future ozone distribution.

In the rest of this section we discuss in more detail the calculations of ozone change that have been performed with coupled chemistry-climate models. In Section 12.2.3.1, published results of doubled- CO_2 experiments are discussed, while results of new experiments to consider the transient ozone response to greenhouse gas forcing over the next two decades are presented in Section 12.2.3.2. For the transient experiments, emphasis is placed on the results in polar latitudes, where the largest response is expected. We recall the earlier caveat that these coupled models are relatively new and, for example, most have not yet been run for decadal time scales. By considering several models, our aim in this Assessment has been to emphasize those results that are most robust. The development of coupled models is an important advance; they will play an increasingly important role in future assessments of the state of the ozone layer.

12.2.3.1 DOUBLED- CO_2 EXPERIMENTS

Doubled- CO_2 experiments can be grouped into two main types: transient and equilibrium. Since the coupled atmosphere-ocean system has considerable inertia, its response to increasing greenhouse gas concentrations can take considerable time. Similar to tropospheric models (IPCC, 1996), the result is that a transient experiment should show a muted atmospheric and oceanic response to doubled CO_2 as compared with an equilibrium experiment with the same model. In the GCM experiments that modeled the ozone response to doubled CO_2 , two were equilibrium (UNIVAQ and GISS), while the EMÉRAUDE simulation was transient. A more recent experiment with the UNIVAQ model examined the ozone response to an increase of CO_2 up to 500 ppmv (Pitari and Visconti, 1994), as predicted for the year 2050 (see WMO, 1992). The GISS stratospheric model gives a response ratio (transient/equilibrium) of 63% at the surface, 60% in the upper troposphere at 150 hPa, 47% in the lower stratosphere at 68 hPa, and 67% in the upper

Table 12-5. The 3-D (chemistry-climate) models.

Model	References	Horizontal Resolution	Vertical Layers	Vertical Extent	Tropospheric/ Stratospheric Dynamics	Gas-Phase Chemistry	Heterogeneous Chemistry	Greenhouse Gas Forcing	Temperature Response to Greenhouse Gases
UNIVAQ	Golombek and Prinn, 1986; Pitari <i>et al.</i> , 1992	Spectral, rhomboidal 6, ~10° × 20°	25	Surface to 71.6 km	Not properly represented due to spectral truncation	Detailed	Simplified	Equilibrium 2 × CO ₂	On-line, global balance approximation in troposphere
EMÉRAUDE	Mahfouf <i>et al.</i> , 1993	T = 42, ~2.8° × 2.8°	30	Surface to 80 km	Full general circulation model	Linearized scheme	None	Transient 2 × CO ₂	On-line, based on SST changes from Hamburg GCM (Cubash <i>et al.</i> , 1992)
UKMO Mechanistic	Austin <i>et al.</i> , 1992; Austin and Butchart, 1994	5° × 5°	32	316 to 0.0316 hPa (~8 to 72 km)	Planetary waves prescribed at lower boundary*	Detailed	Detailed	Equilibrium 2 × CO ₂	Calculated in separate experiment with similar model, then prescribed for chemistry runs
UKMO Chemistry-Climate	Austin <i>et al.</i> , 1997	2.5° × 3.75°	49	Surface to 65 km	Full general circulation model	Detailed	Detailed	Projected increases, 1990-2015	On-line, based on SST changes from separate atmosphere/ocean coupled simulation
ECHAM3/CHEM	Roeckner <i>et al.</i> , 1992; Steil <i>et al.</i> , 1998	Triangular 21, ~5.6° × 5.6°	19	Surface to 10 hPa	Model top location limits stratospheric dynamics	Detailed	Detailed	Projected increases, 1990-2015	Calculated in separate experiment with related model, then prescribed for chemistry runs
Arpège/REPROBUS (ARPROBUS)	Deque and Piedelievre, 1995; Lefèvre <i>et al.</i> , 1994	T = 21, ~5.6° × 5.6°	41	Surface to 80 km	Full general circulation model	Detailed	Detailed	Projected increases, 1995-2015	On-line, based on SST changes from separate atmosphere/ocean coupled simulation
GISS	Rind <i>et al.</i> , 1998; Shindell <i>et al.</i> , 1998a	8° × 10°	23	Surface to 85 km	Full general circulation model	Simplified [†]	Simplified	Projected increases, 1959-2070, and Equilibrium 2 × CO ₂	On-line, including SSTs

The models described in the bottom four rows are used in Section 12.2.3.2 to assess future ozone changes.

* Various planetary wave amplitudes were prescribed at the model's lower boundary to simulate a variety of atmospheric conditions.

[†] Parameterized ozone chemical responses to temperature and radiative forcings only; ozone transport changes calculated offline (non-interactively) from the doubled-CO₂ experiments.

PREDICTING THE FUTURE OZONE LAYER

stratosphere at 1.5 hPa, all for equatorial areas. This is similar to the range 47-83% seen in tropospheric models (Table 6-3 of IPCC, 1996). This factor can then be used in the comparison of results from the stratospheric models run in transient doubled- CO_2 experiments with those run in equilibrium doubled- CO_2 experiments.

12.2.3.1a Temperature and Dynamics Changes

There is significant model-to-model variation in temperature response. Figure 12-21 gives the annual-average temperature response to CO_2 doubling in the GISS model, including the feedback of ozone changing the absorption of radiation. Comparisons with the tropospheric models included in IPCC (1996) show a similar pattern of warming, notably including the temperature increase in the equatorial upper troposphere. The warming in the upper troposphere is found in various of the models considered here, but its magnitude varies significantly. For example, the UNIVAQ model gives a warming of 2 to 4 K, which is considerably smaller than the GISS model warming of up to 10 K. However, the UNIVAQ model uses a Newtonian cooling approximation in the troposphere and does not calculate heating rates explicitly. The EMÉRAUDE model also gave a smaller warming of about 2.5 K, although some of the discrepancy with the GISS model can be accounted for by the transient nature of the experiment. The EMÉRAUDE model found a transient doubled- CO_2 surface warming of 1.4 K, near the low end of the 1.3-3.8 K range for similar experiments (IPCC, 1996). The GISS model gave a surface warming of 4.2 K in a climate run with no stratosphere (as compared with 5.1 K in the GISS troposphere-stratosphere model (Rind *et al.*, 1998)), toward the high end of the 2.1-4.6 K range seen in similar experiments (IPCC, 1996). The temperature response in these two models may therefore represent the range of results based on the variability in current climate models.

The tropospheric warming in the GISS model is so large that it extends up into the lower stratosphere. This warming, and the associated circulation changes, affects the transport of heat in the stratosphere, as well as directly altering the radiative flux. Therefore, the degree of warming in the upper troposphere must be thought of as one of the largest sources of uncertainty in estimating the ozone response to increasing greenhouse gases.

In the midlatitude and equatorial upper stratosphere, the coupled models discussed here all show a large cooling of between 6 and 12 degrees, as expected

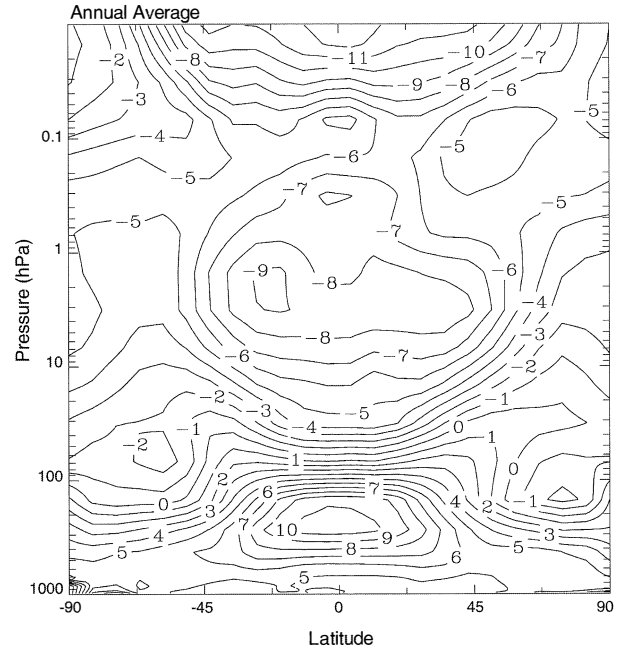


Figure 12-21. Zonal-mean annual-average temperature change (K) induced by doubling CO_2 in the GISS model. The values shown have been averaged over the last 20 years of a 50-year run, after the model had reached equilibrium with the doubled CO_2 .

from greenhouse gas increases (Fels *et al.*, 1980; Boville, 1986; Rind *et al.*, 1990). The magnitude of the cooling is reduced by about 20% by the ozone chemical feedback (see, for example, Rind *et al.*, 1998; Shindell *et al.*, 1998a). In the midlatitude and equatorial lower stratosphere, however, the models disagree, with the GISS model finding a slight warming driven by its tropospheric warming while the other models have a cooling. At high latitudes throughout the stratosphere, there are considerable differences in the temperature response, which are associated with differences in modeled circulation changes.

All the models produce an enhanced residual circulation in response to increasing greenhouse gases, causing an increased transport of ozone to high latitudes, though the magnitude of the increase varies between models. The UNIVAQ experiment with 500 ppmv CO_2 found ozone increases of about 10% of the background values at high latitudes due to circulation changes. Changes in lower stratospheric temperature gradients and consequently zonal winds alter the propagation of planetary waves. This can affect the frequency of sudden

warmings in the models. Again, there is considerable variability between the models. The EMÉRAUDE model finds an increased frequency of Northern Hemisphere sudden stratospheric warmings. On the other hand, the GISS model gives a reduction in the frequency of sudden warmings, leading to a more stable, colder polar vortex, with significant effects on Arctic ozone loss.

12.2.3.1b Ozone Changes

Lower temperatures slow down the rates of the homogeneous chemical reactions that destroy ozone, so that the cooling found in the upper stratosphere in the models results in increased ozone. An increased overhead column reduces the amount of UV reaching the lower stratosphere, decreasing the photochemical production of ozone there, in addition to ozone changes induced by temperature and circulation changes.

Changes in total column ozone amounts are available for the UNIVAQ, EMÉRAUDE, and GISS models. All three models show increases, of up to 4%, in the equatorial region where the temperature responses are similar. However, the UNIVAQ model experiment with 500 ppmv CO₂ showed a decrease in the tropical ozone column, as the additional upwelling outweighs the chemical changes in the middle stratosphere.

At middle latitudes, there was cooling throughout the stratosphere in the UNIVAQ and EMÉRAUDE models, leading to column increases. In the GISS model, the lower stratosphere warmed, leading to a temperature-induced ozone decrease there, which combines with a decrease induced by the larger overhead ozone column. These generally outweigh the upper stratospheric ozone increase, giving a net column decrease.

At high latitudes, the results from the models generally differ more sharply. The EMÉRAUDE model did not include heterogeneous chemistry, while the UNIVAQ model did include a simplified heterogeneous chemistry scheme. The GISS model was run both with and without heterogeneous chemistry. The UNIVAQ model, and GISS model without heterogeneous chemistry, found ozone column changes of -1% to +7% and -2% to +5%, respectively. The seasonal variation also agrees quite well between these models. Both show a slight column loss at high southern latitudes during the austral fall/winter, and column increases before and after. The EMÉRAUDE model found column increases of +4% to +9% at high southern latitudes, however, and showed increases at all times of the year. The differences

likely arise from the inclusion or lack of heterogeneous chemistry and from the varied predictions of the future frequency of sudden warmings.

In the polar spring lower stratosphere, heterogeneous chemistry on PSCs can lead to severe ozone loss, which is particularly sensitive to small changes in temperature. PSC formation is dependent upon local temperatures, therefore adding to the uncertainty of model predictions. Model experiments incorporating parameterized heterogeneous chemistry have been performed with the UNIVAQ and GISS models using constant chlorine abundances. The model response obviously depends critically on both the background temperatures calculated in the model, and the perturbations to those temperatures as greenhouse gases increase. For the Antarctic spring, when a large ozone hole forms with current CO₂ amounts, the doubling of CO₂ has a fairly small impact. In these models, the primary effects are an increase in the areal extent and the duration of the ozone hole.

In the Arctic, the UNIVAQ model finds that the total ozone column decreases by approximately 2% relative to 1 × CO₂. However, only a single fairly warm year was simulated in the experiment. The UKMO mechanistic model was used to simulate the seasonal evolution for several different years (Austin *et al.*, 1992; Austin and Butchart, 1994). During winters in which no stratospheric warmings occurred, total ozone decreased by about 35% (Figure 12-22), similar to, though slightly smaller than, the losses of up to 50% seen in years without warmings in the GISS model (Shindell *et al.*, 1998a). Note that the three models were run with chlorine loadings of 2.5-3.6 ppbv, which are now considered too large for the doubled-CO₂ atmosphere.

12.2.3.2 TRANSIENT OZONE RESPONSE

Three-dimensional experiments using coupled chemistry-climate models with realistic projections of chlorine loading and greenhouse gas emissions are essential for predictions of future ozone. Advances in computing power and our understanding of stratospheric processes have only recently allowed the first such simulations. Results from the GISS model (Shindell *et al.*, 1998b) and the ECHAM3/CHEM model (Dameris *et al.*, 1998) have been published. Two further experiments have recently been completed with the ARPROBUS and the UKMO chemistry-climate models. A preliminary analysis from these two models has also

PREDICTING THE FUTURE OZONE LAYER

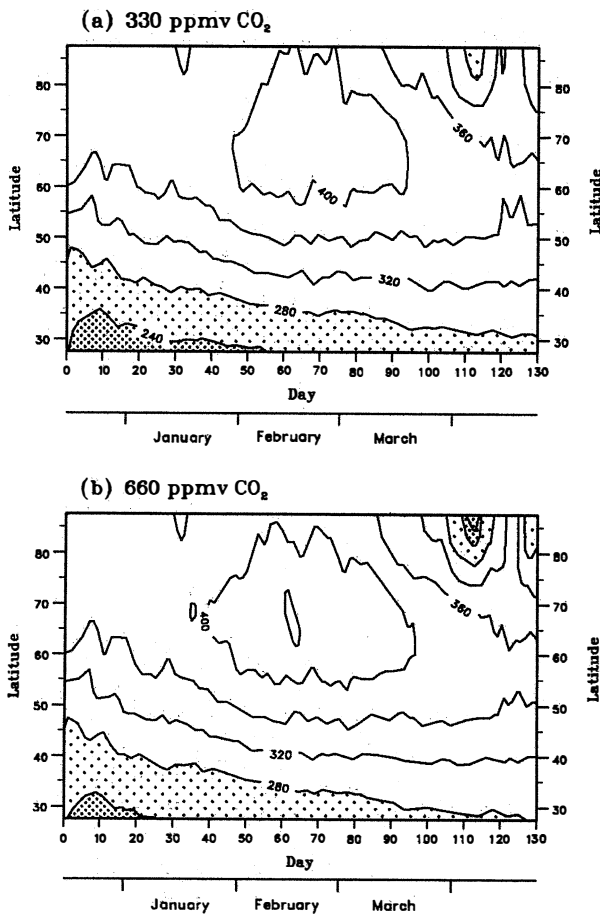


Figure 12-22. Model simulations of the time evolution of total ozone (DU) in mid and high latitudes of the Northern Hemisphere for the winter of 1990 using (a) current levels (330 ppmv) of carbon dioxide and (b) doubled levels (660 ppmv) of carbon dioxide (from Austin and Butchart, 1994). The contours are at 40-DU intervals. Light stippling indicates values between 240 and 280 DU; heavy stippling indicates values below 240 DU. Note in particular the lower values of ozone near 80°N after day 100 for the doubled-CO₂ case.

been performed for this Assessment, providing valuable indications of the robustness of the conclusions of the published work.

The GISS model is a full general circulation model that uses chemistry based upon parameterizations derived in a 2-D model. The chemistry is interactive with the model's radiation, but ozone transport is calculated in a

non-interactive manner. Future chlorine and CFC amounts were based on current emission limits, while greenhouse gas emissions (CO₂, CH₄, and N₂O) were similar to the IS92a (IPCC, 1996) scenario (see Figure 1 of Shindell *et al.*, 1998b). The model simulated conditions from 1959 through 2070. Sea surface temperature (SST) changes were calculated on-line in this model.

The ECHAM3/CHEM general circulation model (Roeckner *et al.*, 1992; Steil *et al.*, 1998) was used in time slice simulations for 1991 and 2015 conditions (Dameris *et al.*, 1998). This model has a detailed treatment of homogeneous and heterogeneous chemistry. However, with a model top located in the middle stratosphere at 10 mb, this model cannot properly reproduce planetary wave propagation in the stratosphere (Austin *et al.*, 1997; Rind *et al.*, 1998). Nevertheless, the model is able to reproduce realistic Northern Hemisphere vortex variability in terms of shape and location (Grewe *et al.*, 1998). The model was run with non-interactive chemistry so that chemical changes did not feed back on the radiation or dynamics. Projected greenhouse gases were included and chlorine amounts went from 3.2 ppbv in 1991 to 2.7 ppbv in 2015 (a faster reduction in chlorine loading than discussed in Chapter 11 of this Assessment). The ECHAM3/CHEM simulations also included changes in tropospheric ozone. The model predicted an increasing trend in tropospheric ozone, driven by emissions of ozone precursors. Because this is the only model described here that included changes in tropospheric ozone, the calculated changes in column ozone should be offset from the models with stratospheric chemistry alone. The model was run for 14 years for each set of conditions (1991 and 2015). Results were averaged over the last 10 years to provide a picture of the average behavior for each set of trace gas loadings with the influence of the initial conditions removed by the 4-year start-up period. SST changes were taken from a transient simulation with a coupled atmosphere-ocean GCM.

The ARPROBUS model is a combination of the Arpège-climat GCM and the REPROBUS CTM. Arpège-climat is the climate version of the Arpège/Integrated Forecast System (IFS) weather prediction model developed jointly by Météo-France and ECMWF. Doubled-CO₂ experiments using Arpège-climat (Timbal *et al.*, 1997; Douville *et al.*, 1998) have shown climate responses close to the projections of previous similar studies performed elsewhere. The REPROBUS CTM

calculates the evolution of 55 species with a detailed treatment of the homogeneous and heterogeneous chemistry. This model has often been used for case studies of polar stratospheric winters, giving results in rather good agreement with experimental data in terms of NO_y, chlorine activation, and ozone loss (e.g., von Clarmann *et al.*, 1997; Lefèvre *et al.*, 1994; Lefèvre *et al.*, 1998; Payan *et al.*, 1998; Renard *et al.*, 1997; Wetzel *et al.*, 1997). For the simulations presented here the ARPROBUS coupled model was integrated at T21 (5.6°) horizontal resolution, on 41 levels from the ground up to 80 km. The ozone field was exchanged every 6 hours between the CTM and the radiative code of the GCM for a fully interactive coupling between chemistry, radiation, and dynamics. Like the ECHAM3/CHEM model, ARPROBUS was run for 6 years for both 1995 and 2015 conditions. IPCC projections of greenhouse gases were used in the model experiments, while chlorine amounts went from 3.7 ppbv in 1995 to 3.3 ppbv in 2015 (again a slightly faster reduction in chlorine loading than assumed in scenario A3 in Chapter 11). SST changes were calculated in a separate transient experiment with the Arpège-climat GCM coupled to an ocean model.

An upgraded version of the troposphere-stratosphere configuration of the UKMO Unified Model (Butchart and Austin, 1998) has been run from 1990 to 2050, assuming greenhouse gas changes specified under scenario IS92a (IPCC, 1996). Sea surface temperature was taken from a coupled ocean-atmosphere version of the Unified Model (Mitchell *et al.*, 1995; Johns *et al.*, 1997). This integration provided dynamical initial conditions for 16-month, fully coupled chemistry integrations at 5-year intervals beginning with 1 March 1994. Appropriate sea surface conditions were obtained from the coupled atmosphere-ocean version of the model. Only the last 12 months of the simulations were used in the analysis presented here, which allowed the model 4 months to come into approximate equilibrium with radiative forcing. Chlorine trends were taken from Chapter 11 of this Assessment, while bromine trends were assumed to increase through 2010. The treatment of chemistry is of similar complexity to the ARPROBUS model. While only 1-year snapshots were performed, the fact that the results are representative can be assessed qualitatively by noting that changes occur steadily throughout the period. The dynamical climatology of the model is in reasonable agreement with observations (Butchart and Austin, 1998), while the trends predicted in the troposphere agree with previous studies (see, for

example, Mitchell *et al.*, 1995). In the upper stratosphere the model response to increasing greenhouse gases is consistent with past temperature trends (Chapter 5). The chemical performance of the model was investigated in Austin *et al.* (1997) and found to be satisfactory for the current atmosphere. Further calculations with improved versions of the model support these conclusions.

12.2.3.2a Temperature and Dynamics Changes

For the behavior of polar ozone, temperatures in the winter/spring lower stratosphere are most important. Figure 12-23 shows the zonal-mean temperature difference between 2015 and 1995 for February and September for the four models. All the models show a tropospheric warming and a general stratospheric cooling, as expected. The magnitudes of the upper tropospheric warmings are fairly similar in the four models, though the ECHAM3/CHEM model shows a larger warming in September and the ARPROBUS model shows a smaller warming in February. A distinct maximum in the tropics appears in the GISS, ECHAM3/CHEM, and UKMO models. In the lower stratosphere, the ECHAM3/CHEM model shows a larger cooling than the other three models, except in the Arctic during February, when the GISS and UKMO models show a cooling of more than 4 K. The GISS and ARPROBUS models include ozone radiative feedback, while the ECHAM3/CHEM and UKMO model results do not, which may partially account for some of the differences.

Analysis of the GISS model results showed that the Arctic winter/spring cooling in that model results from both greenhouse-gas-induced radiative cooling and dynamical changes. The changes in the temperature structure of the atmosphere, especially the increase in the upper troposphere/lower stratosphere latitudinal temperature gradient, increase the lower stratospheric zonal winds, altering the propagation of planetary waves so as to reduce the frequency of Northern Hemisphere sudden stratospheric warmings in the model. The ECHAM3/CHEM model also predicts a colder Arctic vortex but, with a top at 10 hPa, is unable to simulate stratospheric dynamics completely, so that it may not have been able to predict the frequency of sudden warmings properly. The UKMO model also shows its strongest stratospheric cooling in the Arctic region. The ARPROBUS model simulated a colder vortex on average for 2015 conditions, although the magnitude of changes within the vortex can be distorted in the zonal-mean

PREDICTING THE FUTURE OZONE LAYER

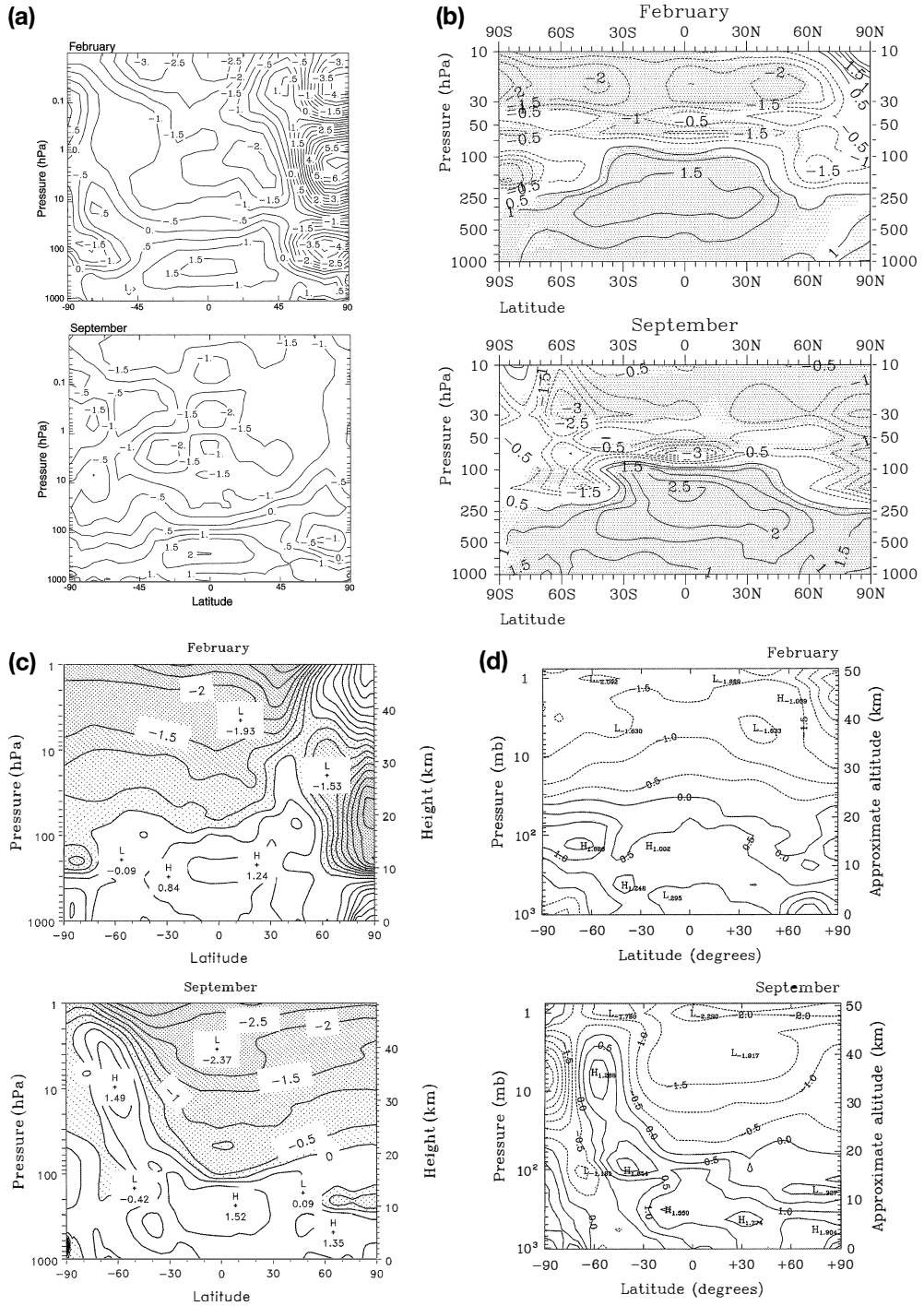


Figure 12-23. Zonal mean temperature changes forced by projected greenhouse gas and halogen emissions during February and September between 2015 and 1995 for four models. (a) GISS model. Note the large cooling in the Arctic lower stratosphere during February. (b) ECHAM3/CHEM model. Shaded areas indicate regions of significant changes. (c) UKMO model. Shaded areas indicate areas with a temperature decrease. (d) ARPROBUS model. Contours of reduced temperature are represented by dashed lines.

averaging of the highly asymmetric Arctic vortex. Given the large variability and that the results for this model are only a 5-year average, it is difficult to draw conclusions about the frequency of sudden warmings.

Another factor linked to the strength of the Arctic cooling is the positive feedback of increased ozone depletion included in the GISS and ARPROBUS simulations, but not in the UKMO dynamical and ECHAM3/CHEM simulations. The lower temperatures in the Arctic vortex found in all four models are consistent with the observed temperature trends. The wintertime Arctic vortex area with temperatures below 195 K has increased considerably over the past three decades (Pawson and Naujokat, 1997), in accordance with an overall stratospheric cooling trend (see Chapter 5 of this Assessment). Wintertime lower stratospheric zonal winds have increased over the last decades as well (Kodera and Koide, 1997), as takes place in the GISS model. Recent Arctic winters have also shown large ozone losses and an increasingly stable and persistent polar vortex (see, for example, Manney *et al.*, 1996; Zurek *et al.*, 1996; Müller *et al.*, 1997a,b; Rex *et al.*, 1997; Newman *et al.*, 1997). In the first 8 years of the 1990s, there has been only one Arctic major warming during December-February, as compared with five that occurred during the 1980s. Increasing greenhouse gases, coupled with the reduction in ozone in the lower stratosphere (see Chapter 5), may be responsible for this abrupt decrease in warmings, and hence for the very large Arctic ozone destruction measured in recent winters.

In the Antarctic lower stratosphere during September there is a noticeable difference between the results of the GISS and ECHAM3/CHEM models, and the more recent results of the ARPROBUS and UKMO models. The first two models show a significant cooling over the polar region, although the changes are typically much smaller than those predicted for the Arctic winter/spring. In contrast the other two models show a warming in the midlatitude stratosphere with the cooling over the pole only occurring above about 20 km. For the UKMO results, which include no ozone-radiative feedback, the most likely cause of the warming is an increase in planetary wave propagation; it is also possible that this occurred in the ARPROBUS model. Therefore the preliminary results from these two models appear to indicate the opposite response, in terms of planetary wave propagation, for the Southern Hemisphere winter to that found by all the models for the late northern winter. Note again that the ECHAM3/CHEM model, with a top at 10

hPa, may not have been able to accurately predict the changes in planetary waves.

In summary, all four GCMs that ran transient chemistry-climate experiments show a general cooling trend in the polar lower stratosphere in the Arctic in February and above 20 km in the Antarctic spring. The degree of cooling varies from model to model, with the largest uncertainties arising from varied dynamical responses and whether the radiative feedback of ozone changes was included in the calculations. In the Arctic, sudden stratospheric warmings are extremely important in determining the polar springtime lower stratospheric temperatures. Changes in the frequency of sudden stratospheric warmings can best be assessed in the models with long-term simulations and an upper boundary above the stratopause, such as employed in the UKMO (dynamical simulation) and GISS models. Both experiments produced a reduction in the frequency of stratospheric warmings over the next several decades, leading to a more stable, colder polar vortex in the Arctic, although for the UKMO results, the frequency of warmings increased again during subsequent decades.

12.2.3.2b Ozone Changes

Minimum column ozone predictions are shown in Figure 12-24 for the Arctic and the Antarctic along with observations. The GISS model predicts maximum Arctic ozone losses during the period 2005-2020, roughly a decade after the peak stratospheric chlorine loading, clearly showing the influence in the model of increasing greenhouse gases. Without this greenhouse gas forcing, maximum losses would of course occur when the maximum chlorine amount is present. Although a decrease in the abundance of lower tropospheric halogens has recently been observed (Elkins *et al.*, 1993; Montzka *et al.*, 1996), implying that stratospheric loading should begin to decrease in several years, the recovery of polar stratospheric ozone will, according to the GISS model, likely be delayed beyond the forthcoming stratospheric maximum halogen loading by climate forcing. In the ECHAM3/CHEM model, there is also a delay in the recovery of polar ozone relative to that seen without climate forcing (Dameris *et al.*, 1998). These results do not show a significant recovery of stratospheric ozone in the Arctic or Antarctic by 2015 relative to 1990, despite the 0.5-ppbv reduction in chlorine loading assumed over this period. Again, that model has a 10-hPa top, limiting its simulation of the dynamical response to greenhouse gas increases.

PREDICTING THE FUTURE OZONE LAYER

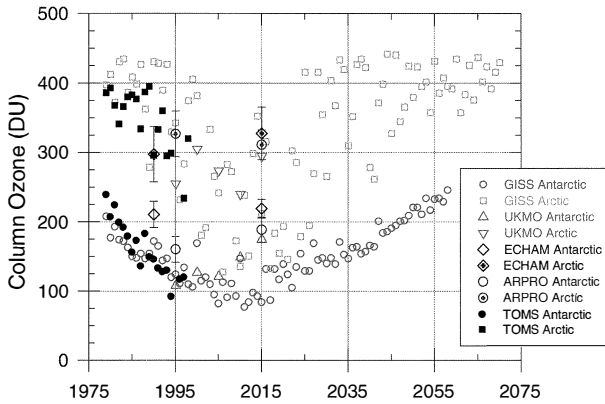


Figure 12-24. Minimum total column ozone south of 65 degrees averaged over the last 3 days of September, except for 1993 for which 23-25 September was used (Antarctic), and north of 65 degrees averaged over the last 3 days of March (Arctic), as seen in TOMS Version 7 data (filled circles and squares), and in the models (GISS—open circles and squares; UKMO—triangles; ARPROBUS—circles with error bars giving the range; ECHAM3/CHEM—diamonds with error bars giving the standard deviation). Note that the four models used somewhat different projections of chlorine loading (see text). Additionally, the ECHAM3/CHEM model included a tropospheric ozone increase with time, which has been subtracted.

The minimum Arctic ozone column amounts from the UKMO results shown in Figure 12-24 are higher than the GISS model results but also show continued low ozone until at least 2010. For the Antarctic, the ozone hole appears slightly later than observed; thus the UKMO results shown here are for the first week of October. Minimum ozone occurs in 1994 but an ozone increase does not become significant until 2009. The ARPROBUS results are similar to the UKMO values, showing an increase in ozone in the Antarctic but no significant change in the Arctic. It is important to note that the models used different assumptions regarding the change in chlorine loading between 2015 and 1995. The UKMO and GISS models used projections with a slow chlorine decrease during this period, 0.2 and 0.1 ppbv, respectively, similar to that used by the 2-D models (scenario A3 of Chapter 11). In contrast, the chlorine in the ARPROBUS and ECHAM3/CHEM models decreased by 0.4 and 0.5 ppbv, respectively (2015 relative

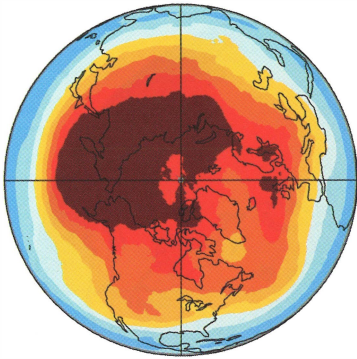
to 1990 for the ECHAM3/CHEM model), a decline somewhere between the WMO 1994 Assessment (WMO, 1995) and the present Assessment baseline cases (see Figure 12-1). This may at least partially account for the differences between the model results.

Although the overall frequency of sudden warmings has decreased, variability in the Arctic is still large during the late 1990s and early 2000s in the GISS model, as shown in Figure 12-25. For example, the model year 1998 was fairly warm, leading to relatively weak ozone depletion in that year as compared with years just before and after. The GCM does not represent the particular meteorological conditions found in any given year, but rather gives representative conditions based on the input trends that drive the simulation. The onset of severe Arctic ozone depletion in the model during the 1990s is well represented, as seen in the comparison between modeled and observed ozone shown in Figure 12-24. Ozone depletion is significantly deeper in the model years 2001 and 2002, which show the most ozone loss during the 2000-2005 period. Note that these figures show model results including only climatological zonal mean ozone transport, illustrating how temperature variations with longitude lead to asymmetric chemical ozone destruction. As discussed in Shindell *et al.* (1998b), changes in transport in the GISS model have little effect on polar ozone through 2015 relative to chemical losses, though the inclusion of longitudinally varying transport would reduce the symmetry about the pole seen at middle and low latitudes.

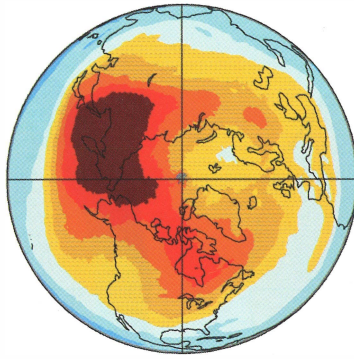
A comparison between 1995 and 2015 total ozone during the spring in both hemispheres is shown in Figure 12-26 for the GISS model. These years are representative of typical conditions for the 1990s and 2010s, respectively, as values for these single years are quite similar to the 1990s and 2010s decadal averaged values. The impact of the increasing greenhouse gases on Antarctic losses is fairly small, as depletion is already so extreme. The ozone hole persists for a longer time as temperatures stay low progressively longer with greenhouse forcing. Variability is much less in the Antarctic than in the Arctic, indicating that the Antarctic will likely be a better location for observations of recovery, as discussed in Section 12.4. Arctic losses increase significantly by 2015, as was seen in Figure 12-24.

The ECHAM3/CHEM model predicts an Antarctic ozone hole in 2015 that is fairly similar to that predicted for 1990, as shown in Figure 12-27. In the Arctic, the model shows a small, non-significant recovery in column

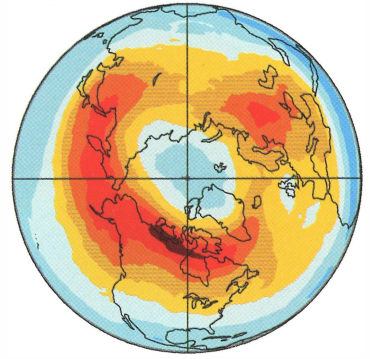
March 1980 Nimbus 7 TOMS



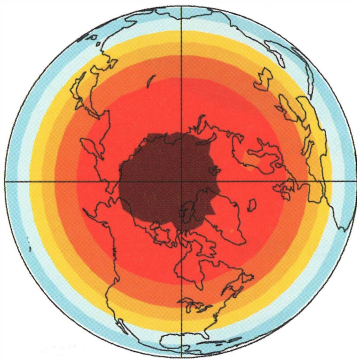
March 1994 Meteor 3 TOMS



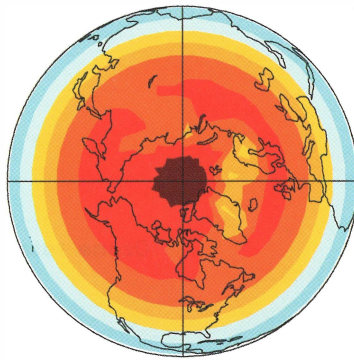
March 1997 ADEOS 1 TOMS



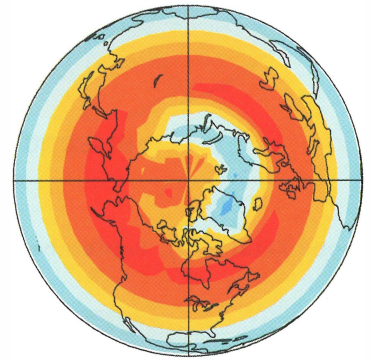
March '1980'



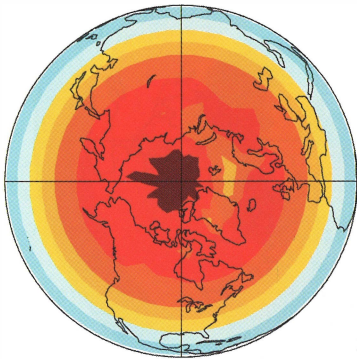
March '1995'



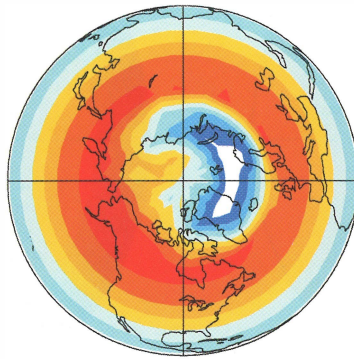
March '1996'



March '1998'



March '2001'



March '2002'

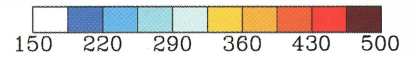
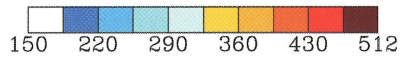
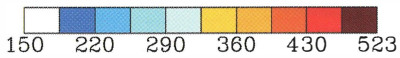
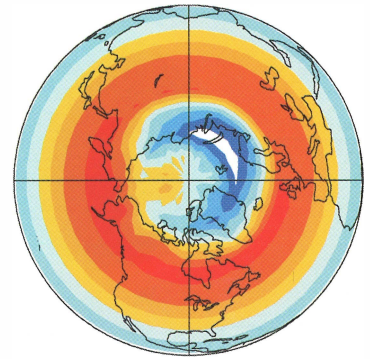
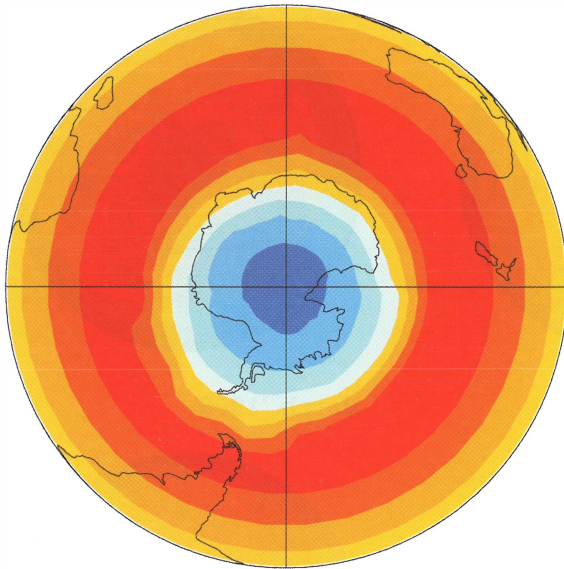


Figure 12-25. Observed and modeled ozone column (DU) averaged over the last week of March. The first three panels are TOMS observations, while the last six are GISS model output. Values are given for the indicated years, with model years in quotes to indicate that they do not represent actual years. The largest scale division represents all values over 465 DU.

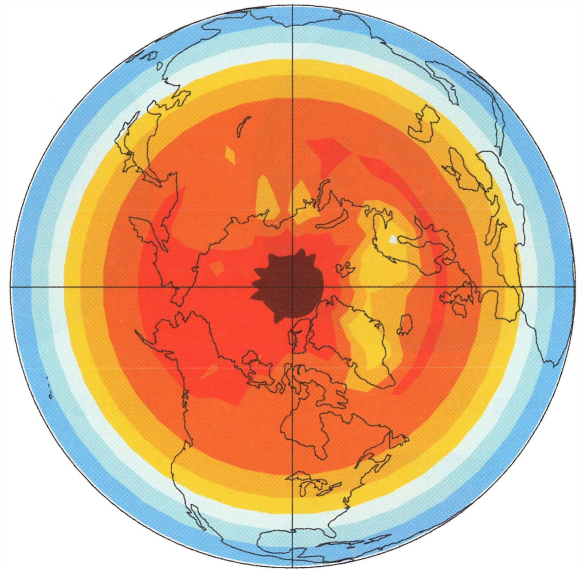
PREDICTING THE FUTURE OZONE LAYER

Ozone total (DU), September 1995



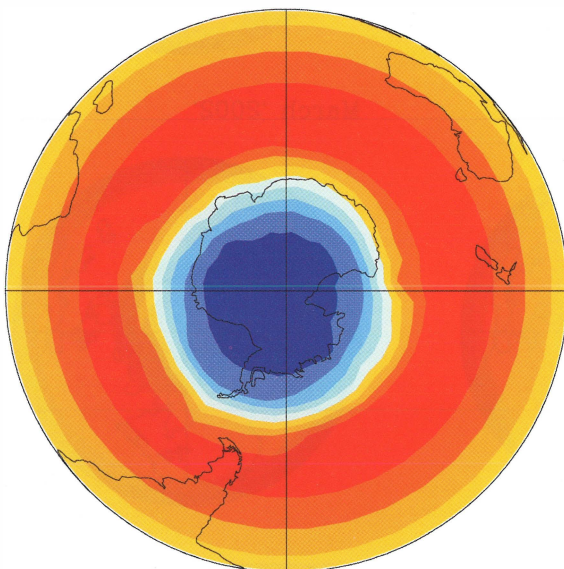
ANTARCTIC

Ozone total (DU), March 1995



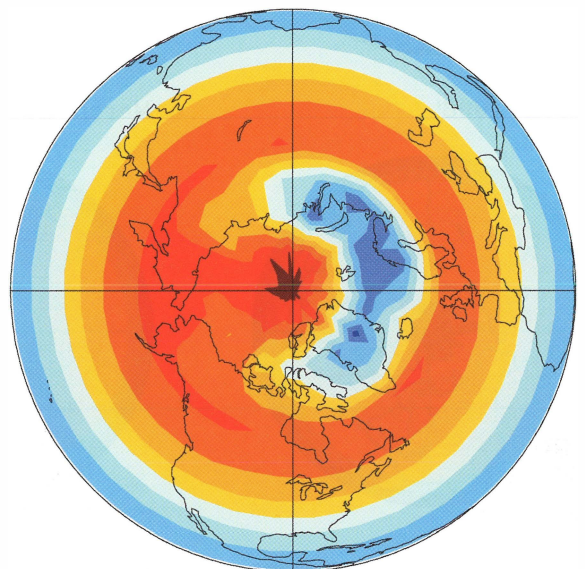
ARCTIC

Ozone total (DU), September 2015



ANTARCTIC

Ozone total (DU), March 2015



ARCTIC

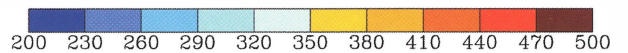
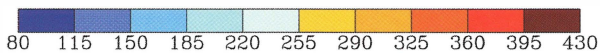


Figure 12-26. Total column ozone amounts (DU) in the GISS model for September and March 1995 and 2015. The results are each from a single year, though these values do not differ significantly from 10-year averages around each time period.

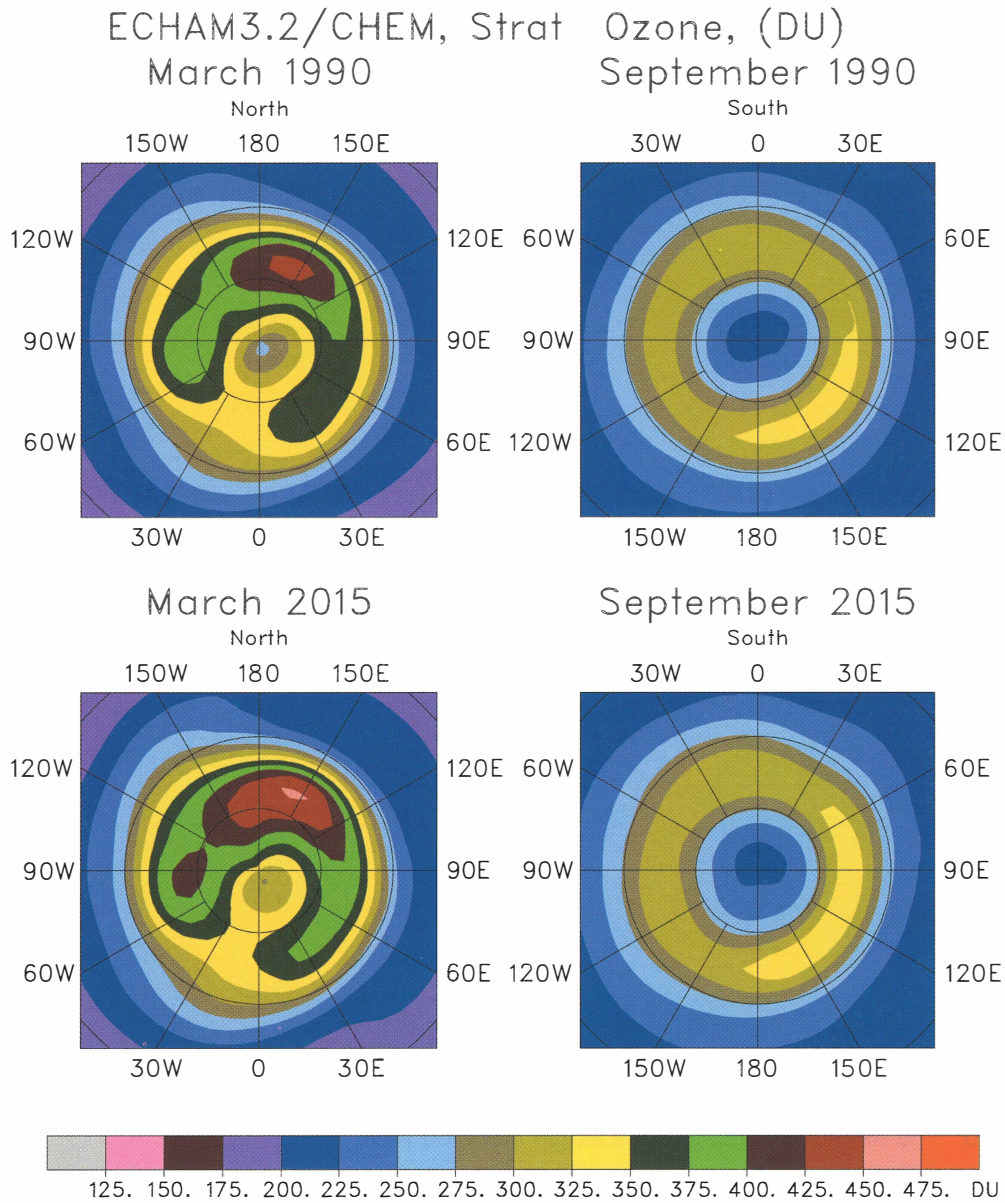


Figure 12-27. Total column ozone amounts (DU) in the ECHAM3/CHEM model for March and September 1990 and 2015. Tropospheric ozone has been removed for consistency with the other models, which did not include tropospheric ozone changes. All results have been averaged over 10 years of model simulations.

ozone by 2015. Stratospheric ozone loss remained roughly constant, indicating that the large decrease in chlorine loading was compensated for by the influence of reduced lower stratospheric temperatures in the model. We note again that the simulation assumed a decrease in chlorine loading of 0.5 ppbv (16%) by 2015 relative to

1990, which is much larger than the base case considered by the 2-D models in this chapter.

The UKMO model results (Figure 12-28) show a maximum in the depth of the Antarctic ozone hole in 1994, and as greenhouse gases increased, the depth of the hole did not initially change significantly. By 2009,

PREDICTING THE FUTURE OZONE LAYER

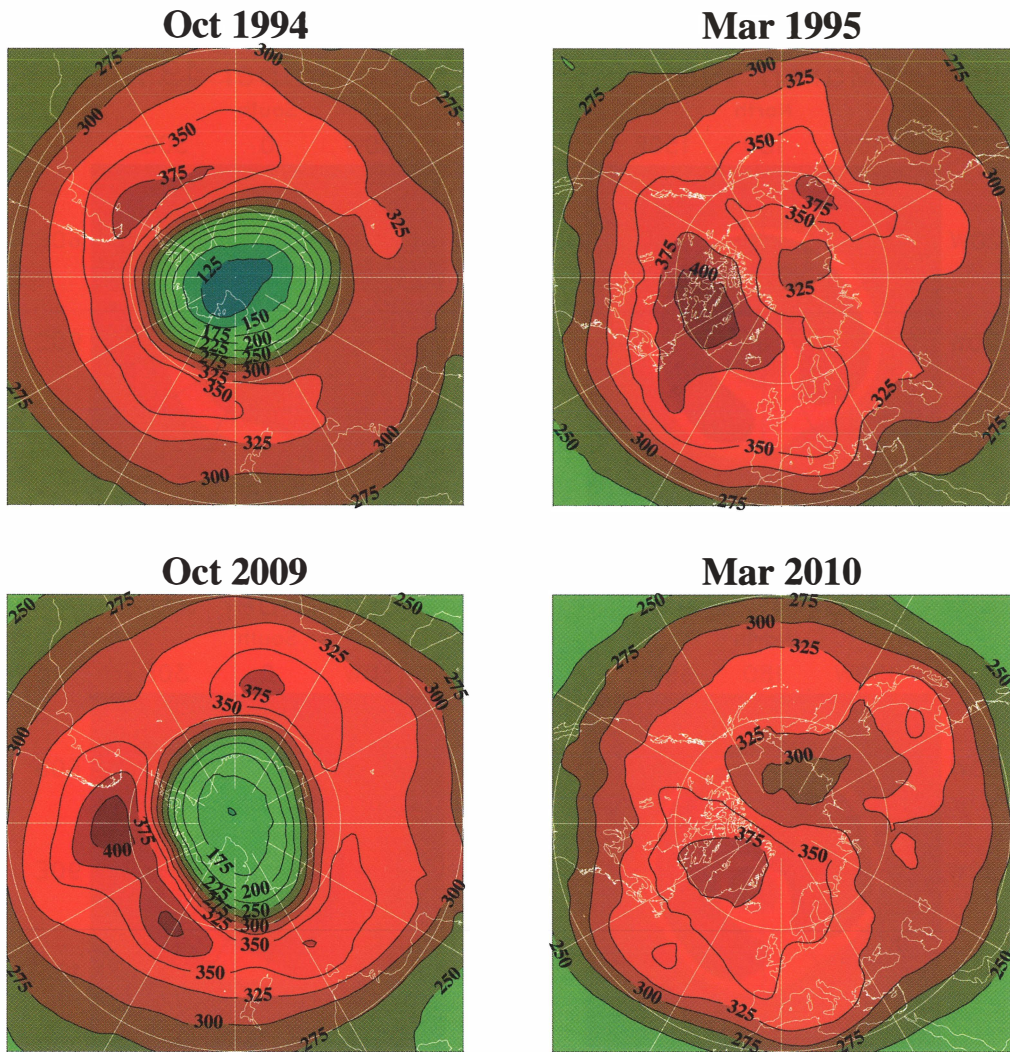


Figure 12-28. Total column ozone amounts (DU) in the UKMO model for October and March 1994/1995 and 2009/2010. The results are each from a single modeled year.

in the ozone hole, total ozone increased by some 40 DU due to a reduction in homogeneous ozone destruction and an increase in ozone transport. For the Arctic, the UKMO model results showed a generally decreasing ozone amount until 2010. Thereafter ozone recovered, indicating a delayed recovery of ozone in the Arctic relative to the Antarctic. Note that the results shown in Figure 12-28 are for 2009/2010, which is the time when the largest contrast with 1995 was simulated in the Northern Hemisphere (although it must be emphasized that the results are only available at 5-year intervals).

The ARPROBUS model shows a significant increase in column ozone over Antarctica during the

spring of 2015 relative to 1995 (Figure 12-29). This is due to the decrease in the amount of chlorine projected in the 2015 atmosphere, which outweighs in the model the effect of the increase in greenhouse gas concentrations. Over the Arctic, the cooling predicted by the model led to a larger number of polar stratospheric clouds (PSCs). Compared to the 1995 simulation, this caused a March-average loss of about 30 DU in the vortex.

In summary, three of the models show increased ozone losses within the Arctic vortex, while the ECHAM3/CHEM model shows no significant changes. An additional effect of the Arctic springtime ozone losses

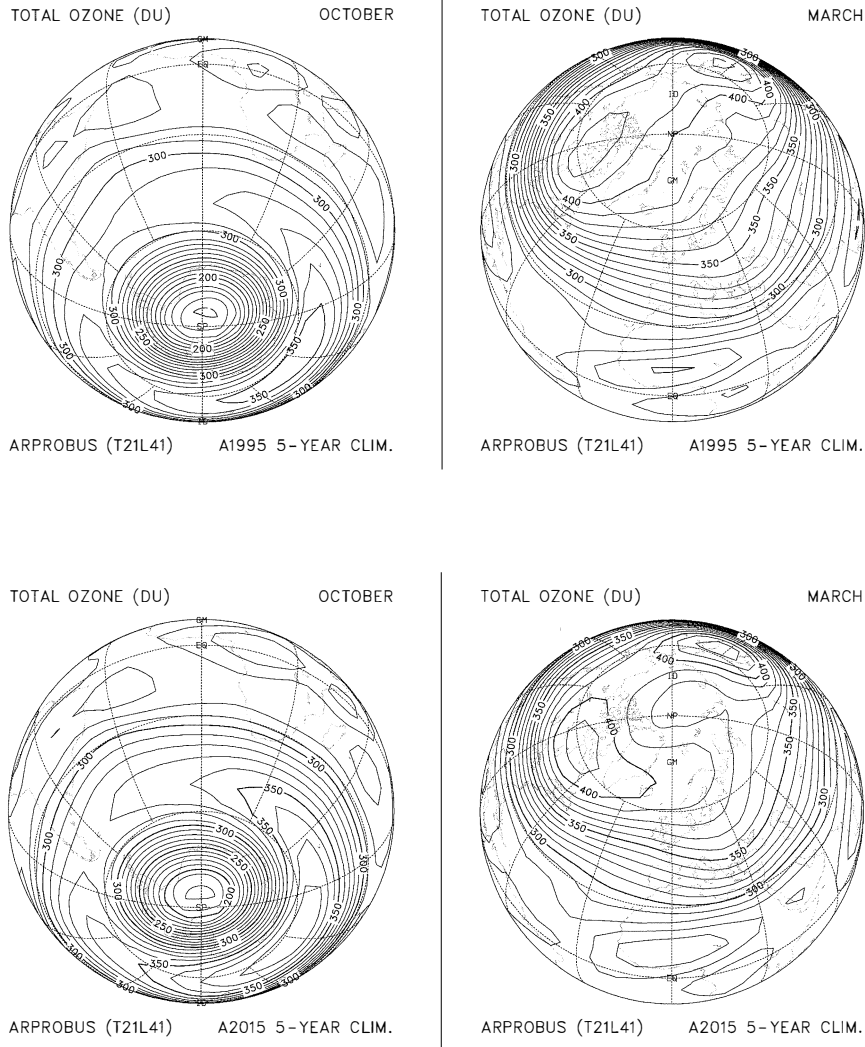


Figure 12-29. Total column ozone amounts (DU) in the ARPROBUS model for October and March 1995 (top) and 2015 (bottom). All results have been averaged over 5 years of model simulations.

has been to reduce the annual cycle in high-latitude total ozone in all four models. We note that in the simulations discussed here (doubled CO_2 and transient), the ECHAM3/CHEM and ARPROBUS models include chemical changes in species other than ozone that are expected to occur with increasing greenhouse gases. These include the production of additional water from the oxidation of increasing methane, additional odd nitrogen from the increasing emissions of nitrous oxide (N_2O), and indirect effects such as changes in stratospheric water vapor due to changes in tropospheric temperatures and dynamics. Also, the UKMO model includes additional odd nitrogen from N_2O increases.

12.2.3.3 CONCLUSIONS

Advances in computing power have allowed the first simulations of future ozone using coupled 3-D models. Despite these improvements, there are considerable differences between the results of individual models. For example, at high latitudes throughout the stratosphere, the temperature response of models to increasing greenhouse gases, which is associated with differences in modeled circulation changes, varies significantly. Further development of stratospheric GCMs is necessary for them to reach a consensus regarding predictions of chemistry-climate interactions

PREDICTING THE FUTURE OZONE LAYER

in the stratosphere such as that now seen in predictions of surface parameters by climate models.

Models highlight that future Arctic ozone loss is very sensitive to changes in the frequency of sudden stratospheric warmings. As greenhouse gases increase, the transient simulations described here predict a strong cooling of the Arctic vortex, consistent with recent observed trends that show a cooling and a reduced frequency of sudden warmings. This cooling trend has a significant impact on Arctic ozone loss through the extremely temperature-sensitive chemistry in this region. All four coupled chemistry-climate models show the same or greater ozone depletion in the Arctic in 2015 as in 1995, despite assumed reductions in chlorine loading ranging from 3% to 16%. Two models give trends through the coming two decades (rather than snapshots at just two times). Both showed steadily increasing ozone loss through 2010, with recovery beginning roughly 1 to 10 years later. All the models indicate that the onset of Arctic ozone recovery is likely to be delayed past the maximum in stratospheric chlorine abundances.

The UKMO and ARPROBUS simulations show the onset of ozone recovery from halogen-induced depletion occurring earlier by 5 years or more in the Antarctic than in the Arctic, while the GISS and ECHAM models show similar timing in the two hemispheres. All the models show a larger degree of variability in the Arctic than in the Antarctic, however, suggesting that observations of Antarctic ozone will likely provide a better indicator of ozone recovery than Arctic observations.

12.3 OTHER PERTURBATIONS

Several factors, other than those discussed in Section 12.2, are important in regulating the levels of stratospheric ozone. Natural processes such as solar cycle ultraviolet flux variations and charged-particle precipitation can serve to either mitigate or enhance ozone changes. Anthropogenic activities such as rocket or shuttle launches, nuclear explosions, and aircraft can also have an influence.

12.3.1 Natural Processes

Solar cycle ultraviolet flux variations, charged-particle precipitation, and interannual and quasi-biennial dynamical changes can all have an influence on ozone. These processes are discussed in the following sections.

12.3.1.1 SOLAR CYCLE VARIATIONS

Solar cycle variations in ultraviolet (UV) flux have been observed and simulated to vary with the 11-year solar cycle and 27-day solar rotation periods (e.g., Brasseur and Simon, 1981; Garcia *et al.*, 1984; Callis *et al.*, 1985; Hood *et al.*, 1993; Huang and Brasseur, 1993; Chandra and McPeters, 1994; Fleming *et al.*, 1995). Brasseur (1993) showed a latitudinal dependence in the total ozone response, with 1% larger levels in the tropics and 1.5% in high latitudes at solar maximum compared to solar minimum. Jackman *et al.* (1996a) used solar UV flux variations measured by the Solar-Stellar Irradiance Comparison Experiment (SOLSTICE) instrument aboard UARS along with F10.7-cm flux variations as a transfer standard for non-UARS observing years (prior to September 1991) to derive solar UV changes beginning from 1947. These computations predicted variations in global total ozone of 1.2% from solar maximum to minimum. Both Brasseur (1993) and Jackman *et al.* (1996a) predictions are in reasonable agreement with the value of 1.2% derived by Reinsel *et al.* (1987), using a statistical analysis of the Dobson data on ozone and the F10.7-cm flux, and the 1-2% values cited in Chapter 7 of WMO (1992). The solar UV flux does have a significant effect on total ozone and will need to be considered when studying future ozone changes.

While the total ozone variation predicted in various models agrees fairly well with the observations, the vertical profile of the observed change greatly underestimates the ozone response to solar variations in the upper stratosphere (McCormack and Hood, 1996). Given that variations in heating rates in the upper stratosphere induced by solar irradiance variations can exert a considerable influence on dynamics (see, for example, Balachandran and Rind, 1995), this deficiency in the models will limit their ability to accurately reproduce the total atmospheric response to the solar cycle. Results from current models should therefore be interpreted with caution. Finally, the impact of the solar cycle on climate, which probably occurs through changing stratospheric ozone (Haigh, 1996), should be considered.

12.3.1.2 CHARGED-PARTICLE PRECIPITATION

Charged particles in the form of galactic cosmic rays, solar flare particles, relativistic electron precipitations, and auroral electrons and photoelectrons have all been predicted to have an effect on ozone (see

references in Jackman (1993) and Chapter 2 of WMO (1992)). Charged-particle effects are largest at polar latitudes, although the magnitude of the effects on ozone is still open to a great deal of discussion and uncertainty. The largest predicted decreases in total ozone from charged particles are a few percent at polar northern latitudes as a result of very large and energetic solar flare particle events (see, for example, Crutzen *et al.*, 1975; Jackman *et al.*, 1995).

The effects of charged particles on ozone are much reduced at lower latitudes, with solar flare particle events and galactic cosmic rays predicted to cause small changes in annually integrated total ozone between 65°N and 65°S by a maximum of 0.22% and 0.02%, respectively (Jackman *et al.*, 1996a). Although the magnitude and frequency of relativistic electron precipitations are still quite uncertain, Callis *et al.* (1997) have computed changes in global total ozone of 0.5% from these events over the 1979 to 1990 time period. Auroral electrons and photoelectrons produce NO_y in the thermosphere with subsequent transport to the stratosphere and may also have an impact on stratospheric ozone. Although Siskind *et al.* (1997) have recently shown evidence of significant transport of this thermospheric NO_y to the upper stratosphere, the effects on total ozone are not well quantified.

12.3.2 Anthropogenic Activities

Other anthropogenic activities besides halogen production and release may have caused or will cause ozone change. These activities include rocket launches, aircraft emissions in the lower stratosphere from the current fleet of aircraft, and a possible future fleet of supersonic aircraft.

12.3.2.1 SHUTTLE AND ROCKET LAUNCHES

Summaries of the effects of exhaust products from rockets are given in Chapter 10 of WMO (1992), the American Institute of Aeronautics and Astronautics report (AIAA, 1991), and by Jackman (1994). Since these publications there has been further substantial research activity regarding the impact of rockets on stratospheric ozone. Significant research on the chemistry in rocket plumes has been undertaken in the past several years. Ross (1996) has simulated total ozone loss of greater than 8% in areas of approximately 100 km² under a Space Shuttle plume about 1 hour after

launch. Such small areas of significant total ozone loss would be difficult for the TOMS instrument to measure with its field of view of about 1600 km² (Syage and Ross, 1996). Instruments aboard a WB-57F aircraft have measured molecular chlorine (Cl₂), ozone (O₃), and particles in Titan IV, Space Shuttle, and Delta exhaust plumes (Ross *et al.*, 1997a,b), showing enhanced Cl₂ and reduced ozone.

Jones *et al.* (1995) have computed the atmospheric impact of the Ariane 5 rocket. Emissions of inorganic chlorine, water vapor, and aluminum oxide were all considered. The steady-state 2-D model calculation, assuming the chlorine and water vapor emissions for 10 Ariane 5 launches per year, shows small losses of ozone (<0.1%). These losses appear to be independent of the form in which chlorine was released. The aluminum oxide emissions are calculated to add modest increases (~1%) to the stratospheric aerosol mass with the same launch scenario. Jackman *et al.* (1996b) investigated the impact of the chlorine emission on the stratosphere using a launch scenario of nine Space Shuttles and three Titan IV rockets per year and found maximum decreases in ozone of 0.14% in the middle to upper stratosphere. Although the calculated impact on profile and total ozone is computed to be quite small, inclusion of heterogeneous chemistry was found to increase the total ozone loss by a factor of 2.5.

Molina *et al.* (1997) have measured relatively high reaction probabilities (~0.02%) for the reaction ClONO₂ + HCl → HNO₃ + Cl₂ on aluminum oxide (alumina) particles. These measurements have been considered in a recent global modeling study (Jackman *et al.*, 1998), which indicated that the alumina particles could be responsible for about one-third of the total ozone depletion from solid fuel rockets. Jackman *et al.* (1998) used historical U.S. launch rates of solid fuel rockets and computed annually averaged global total ozone losses of 0.025% by the year 1997.

It is expected that there will be a higher rate of launches in the future, given the upcoming construction of the International Space Station and proposed launches of the Ariane 5. The computed, relatively minuscule effects on stratospheric ozone are, therefore, expected to increase. Future studies of possible stratospheric ozone effects from rockets should focus on the global launch rates, including not only NASA and European Space Agency (ESA) launches but also launches by other space agencies around the world.

PREDICTING THE FUTURE OZONE LAYER

12.3.2.2 CURRENT FLEET OF SUBSONIC AIRCRAFT

The fleet of subsonic aircraft, operating primarily in the upper troposphere and lower stratosphere, has increased substantially over the past few decades and is expected to increase significantly in the next century. Airplane engines emit CO₂, H₂O, NO_x, CO, hydrocarbons, carbon soot, and sulfur oxides (SO_x), which can all have an influence on the background atmosphere. A number of studies have been completed in recent years on the effects of subsonic aircraft on the atmosphere. Recent assessments of the atmospheric effects of subsonic aircraft emissions were completed by NASA (Friedl *et al.*, 1997) and the European Commission (Brasseur *et al.*, 1998), and included new model computations as well as summaries of the past work on this subject. The Intergovernmental Panel on Climate Change (IPCC) is also examining the impact of aircraft on the atmosphere and is presently enabling the production of a special report on aviation and the global atmosphere (IPCC, 1999), in collaboration with the Ozone Scientific Assessment Panel of UNEP and in conjunction with the International Civil Aviation Organization (ICAO). Changes in lower stratospheric and upper tropospheric ozone caused by increases in subsonic traffic in the future could be a factor when considering future anthropogenic influences on ozone.

12.3.2.3 HIGH SPEED CIVIL TRANSPORTS

The aviation community is investigating the possibility of developing, marketing, and producing a fleet of High Speed Civil Transports (HSCTs) that would operate in the stratosphere. Another component of the IPCC aviation report is the influence of HSCTs on the background atmosphere. Of primary interest are the potential effects on ozone from a fleet of HSCTs. These aircraft could cruise at Mach 2.4 with a range of 5000 to 6500 nautical miles. The primary market for this new fleet of supersonic passenger aircraft will be the Atlantic and Pacific flight corridors, decreasing the average subsonic travel time by over a factor of 2. This HSCT fleet will cruise primarily in the lower stratosphere, within an ozone-rich region. Emissions from this proposed fleet will predominantly occur at Northern Hemisphere midlatitudes. Trace constituents from HSCT engines are produced from (1) direct combustion of the kerosene-based fuel components forming H₂O, CO₂, CO, CH₄, nonmethane hydrocarbons, and soot; (2)

impurities in the fuel (e.g., sulfur, forming SO₂); and (3) high-temperature processes, breaking down atmospheric nitrogen to form NO_x (NO + NO₂). The IPCC special report (IPCC, 1999) will include an assessment of the impacts of a possible HSCT fleet. This information will also be important to understanding future anthropogenic influences on atmospheric ozone.

12.3.2.4 OTHER EFFECTS

In addition to those processes responsible for changing stratospheric ozone, there are others that may affect the troposphere, including surface emissions of NO_x, SO_x, CO, and hydrocarbons. Some of these emissions may increase in the future, leading to ozone production in the troposphere and adding slightly to the ozone column. Convective lifting of these emissions could also affect the tropopause region. No modeling of these processes has been included in this chapter but their effects are discussed in more detail in Chapter 7.

12.4 DETECTION OF THE EXPECTED RECOVERY OF THE OZONE LAYER

One of the scientific highlights of the first decades of the 21st century will likely be the uncovering of evidence for the turnaround in stratospheric ozone depletion owing to the reduction in the emission of ozone-depleting chemicals. Observation of this recovery is important because it will show that the formulation and enforcement of regulations associated with the Montreal Protocol and its Amendments was an effective course to follow. However, as already indicated in this chapter, there are many uncertainties associated with ozone recovery, for example, the possibility of future volcanic eruptions, and they will all impact our ability to actually observe the recovery.

It is the purpose of this section to identify those indicators that might be used for the earliest possible evidence of the beginning of ozone layer recovery. For this purpose, we define the beginning of recovery as a measurable increase in ozone toward pre-1980 values. Clearly, another important observation will be a pre-recovery period, i.e., a cessation of a worsening of ozone depletion. It might be argued that the pre-recovery stage has already begun in Antarctica, where the springtime ozone hole has remained very severe but relatively unchanged since about 1992; however, this observation is mainly due to saturation in which nearly all the ozone

is lost in certain regions of the stratosphere each spring. Thus the cessation of the downward trend in total ozone in the Antarctic spring is not an indication of the pre-recovery stage. As indicated in Chapter 4, there has been a lessening of the downward trend in ozone at mid-latitudes when compared to a linear extrapolation of trends observed in the 1980s (see Figure 4-12). While the cause of this trend diminution is unknown, it should not yet be considered an observation of pre-recovery as the length of the period of reduced trends is inadequate at this time. Confirmation of the pre-recovery of global ozone, a cessation of a downward trend, will require additional observations into the next decade. Obviously, a volcanic event the size of Mt. Pinatubo would further delay this confirmation.

12.4.1 Antarctic Ozone Hole

The phenomenon of chemical ozone depletion was first unequivocally observed in Antarctica because of its magnitude there, with about two-thirds of the overlying ozone destroyed during the month of September at the present time (Hofmann *et al.*, 1994) (about one-third when it was uncovered from data at Halley Bay in 1983 (Farman *et al.*, 1985)). Although springtime Antarctic chemical ozone depletion in recent years appears to be saturated (total ozone destruction) in the 14-19 km altitude region (Hofmann *et al.*, 1997), at the boundaries of the ozone hole the chemical processes are not saturated. These regions, because they have relatively small interannual variability, may provide useful indicators of ozone recovery. It is likely that the earliest evidence for recovery of chemical ozone depletion will be obtained in Antarctica for several reasons:

- The signal-to-noise ratio of the depletion phenomenon is large.
- The natural variability of ozone in the polar vortex during the springtime depletion event is small relative to that observed at midlatitudes or in the Arctic.
- As indicated in Section 12.2, the effects of climate change on ozone depletion, for example, cooling of the stratosphere, will be less than at midlatitudes or the Arctic because any additional cooling in the winter Antarctic stratosphere will be relatively smaller.

- As indicated in Section 12.2, chlorine, as opposed to bromine, dominates the ozone loss process to a greater extent in the Antarctic; thus a lag in bromine reduction will have a smaller effect on recovery there.

It is the purpose of this section to explore observations of the springtime Antarctic ozone hole to identify characteristic features that may be useful in observing the beginning of ozone recovery early in the 21st century.

We consider both satellite and balloonborne measurements. The latter have the advantage that they can observe the vertical profile of ozone depletion during the September period when rapid ozone destruction occurs. Satellite measurements utilizing solar ultraviolet radiation are generally capable of observing only the total column in sunlit regions and thus cannot examine the September rate of ozone decline in the interior of the continent, where perturbations related to transport effects near the continental periphery are absent. Surface-based Dobson instruments have the same disadvantage. In addition, total-ozone measuring devices are subject to variations above and below the ozone hole region, which cause considerable variability not present in the vertical profile of ozone (Hofmann, 1996). However, a distinct advantage of satellite measurements is their ability to map out the horizontal size of the ozone depletion region.

12.4.1.1 AREA OF THE 220-DOBSON UNIT CONTOUR

Although satellite instruments of the backscatter ultraviolet type cannot observe the entire Antarctic continental interior during September, they can map out a particular ozone contour in sunlight, and by late September to early October, when the depletion phenomenon reaches its maximum extent, can define the maximum geographical size of the ozone hole. The 220-DU contour has been used for this purpose in the past. At this ozone level, the depletion phenomenon is not saturated and thus is sensitive to halogen changes. For this exercise we use the TOMS series of instruments, which is able to define the contours accurately with its scanning mode of operation. The TOMS instruments have a continuous record from 1979 to the present, with 1995 missing. These include instruments on board Nimbus-7 from 1979 to 1993, Meteor-3 in 1994, and Earth Probe from mid-1996 to the present.

PREDICTING THE FUTURE OZONE LAYER

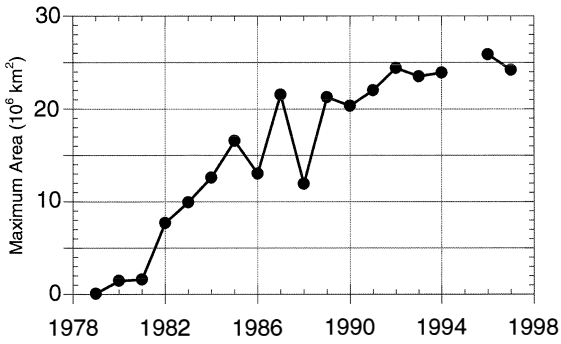


Figure 12-30. The maximum area interior to the 220-DU total ozone contour over Antarctica during springtime ozone depletion as measured by TOMS instruments since 1979.

Figure 12-30 shows the maximum area of the 220-DU contour since 1979, as determined from TOMS data. The time variation of the maximum area of the 220-DU contour has been relatively smooth, except for the year 1988, when the polar vortex broke up unusually early and the ozone hole never fully developed. The maximum area appears to have reached a peak value of about 25 million square kilometers in recent years. A gradual reduction below this asymptotic value in the future could be used as an indicator of the beginning of recovery.

12.4.1.2 SEPTEMBER OZONE REDUCTION AT 12-20 KM FROM OZONESONDE PROFILES

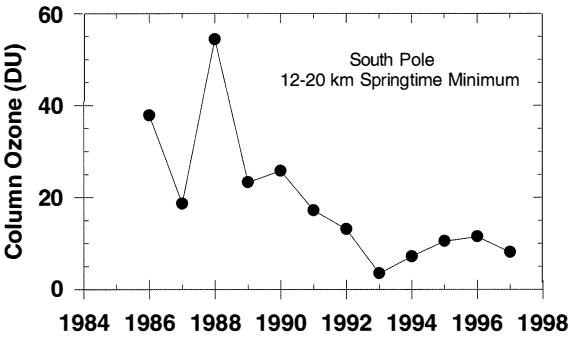


Figure 12-31. The minimum in the 12-20 km ozone column during Antarctic springtime ozone depletion since 1986 as determined from ozonesondes at the South Pole.

In order to avoid complications related to variability in total ozone associated with transport effects above the ozone hole, the vertical profile of ozone loss as determined by ozonesondes in Antarctica has been scrutinized for characteristic features that might be used in the early detection of recovery of the ozone hole (Hofmann *et al.*, 1997). By restricting observations to the 12-20 km region, where springtime Antarctic ozone is primarily affected by polar stratospheric cloud (PSC)-related, chemically induced depletion, one can substantially reduce the variability in observations of the ozone loss phenomenon. Figure 12-31 shows the springtime minimum in the 12-20 km integrated ozone amount since ozonesonde measurements began at the South Pole in 1986. The lowest value of this parameter occurred in 1993, mainly as a result of additional depletion in the 12-18 km region associated with aerosol particles from the Mt. Pinatubo eruption (Hofmann *et al.*, 1994). Since 1995, the minimum amount of ozone in the 12-20 km column has been about 10 DU. Increases to values of 20 DU or above (last seen before 1990) could be used as an indicator of the beginning of ozone recovery.

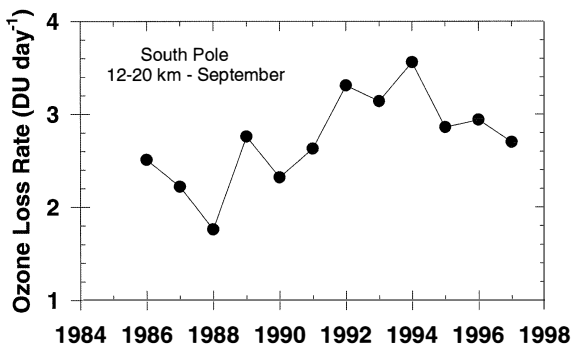


Figure 12-32. The 12-20 km ozone loss rate averaged over the month of September since 1986 as determined from ozonesondes at the South Pole.

Because ozone is totally destroyed over a portion of the 12-20 km altitude range (about 14-19 km), the amount of ozone in this region may not be a sensitive indicator of halogen changes. However, the rate of ozone loss during the development of springtime Antarctic ozone depletion is not subject to saturation but is proportional to halogen amounts, other parameters such as temperature and sunlight remaining the same. The annual rate of ozone decline at the South Pole during September in the 12-20 km region is shown in Figure 12-32. These data were determined from the slope of the ozone versus time curves during September. This parameter is apparently affected by a quasi-biennial

component above 18 km, possibly related to varying transport processes (Hofmann *et al.*, 1997); however, it appears to have reached a pseudo-equilibrium value of about 3 DU per day in recent years. Values as low as 2.5 DU per day have not been seen since before 1990, and thus a return to this value could be used as another indicator of the beginning of recovery.

12.4.1.3 VERTICAL EXTENSION OF THE OZONE HOLE

As indicated earlier, the ozone hole phenomenon is undersaturated at its horizontal boundary (for example the 220-DU contour); similarly saturation is absent at its upper boundary where temperatures are not low enough for substantial formation of polar stratospheric clouds. As halogen levels in the stratosphere have increased, the vertical extension of the Antarctic ozone hole has also increased. Where the top of the ozone depletion region was below 22 km in 1986 (Hofmann *et al.*, 1987), it now extends up to 24 km (Hofmann *et al.*, 1997). Figure 12-33 shows the 15 August to 15 October time development of the 22-24 km ozone column since 1986 as determined by ozonesondes at the South Pole. Considerably lower springtime values have been present at 22-24 km in the 1990s as compared to the 1980s. Figure 12-34 shows the 15 September to 1 October average amount of ozone between 22 and 24 km for each year since 1986. A departure from values near 20 DU began in about 1991, and values appear to be varying around the 15-DU value since 1992. The 1997 value was poorly defined, as a week of soundings was missed in late September owing to balloon problems. It is also likely that this parameter displays a sizable QBO component, possibly related to temperature. Because this region is not affected by volcanic aerosol (Hofmann *et al.*, 1994), a return to values consistently above 15 DU would be a sensitive indicator of ozone hole recovery as halogens decline. Future temperature trends related to greenhouse gas emissions may influence the recovery of the 22-24 km ozone column to some extent; this effect needs to be modeled for the upper reaches of the ozone hole.

12.4.2 Arctic Springtime Ozone Loss

Ozone loss during Arctic spring has been detected since the end of the last decade (Hofmann *et al.*, 1989; Schoeberl *et al.*, 1990; McKenna *et al.*, 1990; Hofmann and Deshler, 1991; Koike *et al.*, 1991; Kyrö *et al.*, 1992; Proffitt *et al.*, 1993; Braathen *et al.*, 1994; Larsen *et al.*, 1994; Manney *et al.*, 1994; Bojkov *et al.*, 1995; von der

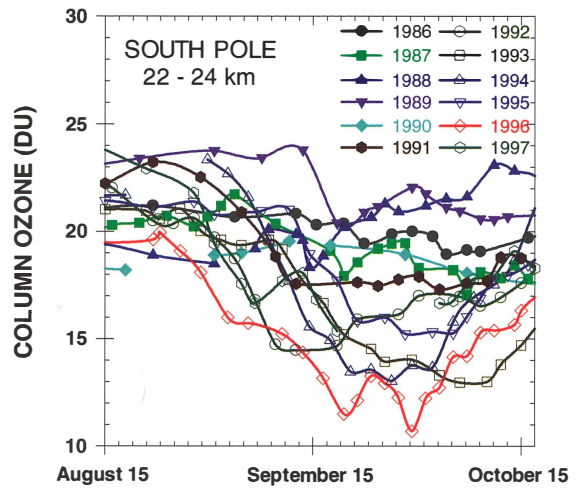


Figure 12-33. The 22-24 km ozone column versus time from 15 August to 15 October since 1986 as determined from ozonesondes at the South Pole.

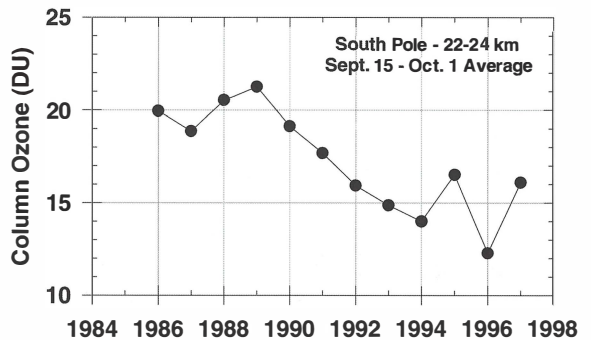


Figure 12-34. The 22-24 km average ozone column for the 15 September to 1 October period since 1986 as determined from ozonesondes at the South Pole.

Gathen *et al.*, 1995; Manney *et al.*, 1995, 1996; Müller *et al.*, 1996; Donovan *et al.*, 1997; Hansen *et al.*, 1997; Manney *et al.*, 1997; Müller *et al.*, 1997a,b; Newman *et al.*, 1997; Rex *et al.*, 1997; Goutail *et al.*, 1998; Knudsen *et al.*, 1998; Rex *et al.*, 1998a,b), mainly during major international campaigns (the Airborne Arctic Stratosphere Expedition (AASE) I & II, the European Arctic Stratospheric Ozone Expedition (EASOE), and the Second European Stratospheric Arctic and Midlatitude Experiment (SESAME)). During the springtime of the years 1995, 1996, and 1997, chemically induced ozone loss in the Arctic reached an extent that

PREDICTING THE FUTURE OZONE LAYER

rivals the springtime loss in the Antarctic, one decade earlier (Müller *et al.*, 1997a,b). These enhanced ozone losses were related to increases in ozone-destroying chemicals and to unusually cold Arctic winters in the stratosphere. It is expected that ozone loss in the Arctic will continue; however, in contrast to the Antarctic this will occur in a largely unpredictable fashion.

It is expected that the detection of recovery in the Arctic springtime ozone loss will be more difficult compared to the Antarctic and the globe in general for two reasons. First of all, quantifying the ozone loss signal itself is more difficult because of the strong meteorological variability within a winter/spring period. An Eulerian view of the ozone loss by measurements at one station alone will in general not be able to cover all aspects due to this variability. Efforts have been undertaken to overcome this problem, and today several independent methods are available that reliably quantify ozone losses. These methods can be classified into satellite-borne measurements such as the Halogen Occultation Experiment (HALOE) and Microwave Limb Sounder (MLS) onboard the Upper Atmospheric Research Satellite (UARS), and measurements made by the Système d'Analyse par Observation Zénithale (SAOZ) and ozonesonde network. However, every method has its advantages and disadvantages and its own way to quantify ozone losses. The output quantities have to be compared with great care because of the intrinsic assumptions of the different methods. Such comparisons will be needed in any trend analysis if certain methods will be available for limited time periods only.

Second, the variability of the ozone loss signal from year to year is strongest in the Arctic. As described in more detail in Chapters 4, 5, and 7 of this Assessment, differences in ozone losses above both polar caps are due to the consequences of deviating meteorological conditions. The Arctic vortex in general is smaller, less stable, and shorter-lived than its Antarctic counterpart. The most important consequence is the temperature, which is roughly 10 K higher in the Arctic compared to the Antarctic stratosphere. The springtime polar ozone loss is directly related to heterogeneous reactions taking place on the surface of polar stratospheric cloud particles. Above Antarctica the temperature remains well below the formation temperature of all known PSC types in major parts of the lower stratosphere during most of the winter. Any meteorological variability from year to year will have only a minor influence on the magnitude of the ozone loss. Above the Arctic, temperatures usually

reach the formation temperature of Type-1 PSCs (the PSC type with the highest formation temperature) in limited space regions and time periods. Therefore the strong meteorological variability above the Arctic from year to year, with temperature around the PSC threshold, leads to considerable variability in PSC existence and consequently in ozone loss.

It is thus clear that the springtime ozone loss above the Arctic is determined not only by the chlorine and bromine content but also by temperature effects. Furthermore, it is to be expected that during the early decades after the maximum in stratospheric chlorine loading, when the chlorine reduction is rather small, any trend in the springtime ozone loss will be mainly dominated by any temperature trend or even by any change in temperature variability, e.g., in the frequency of stratospheric warmings. It must be stated clearly that even if no significant ozone recovery is detectable in the coming decades, or even worse if an ongoing downward trend of Arctic ozone in the coming years continued, depletion of Arctic ozone would likely have been worse without the efforts that have been undertaken in the phase-out of CFCs.

Due to the uncertainties described above, any prediction of Arctic ozone will have a large year-to-year variability. As an example, Figure 12-24 showed the total ozone predictions of a coupled 3-D model (GISS) (Shindell *et al.*, 1998b) for the Arctic case in comparison to the Antarctic case. For these reasons, any indicator for future ozone recovery in the Arctic will not be as reliable as the indicators described earlier for the Antarctic, and should be interpreted with great care, taking into account the variability of the meteorology of the included winter/spring periods.

As stated in the beginning of this chapter, recovery is here defined as the effects expected due to a decrease in anthropogenic chlorine and bromine related to the Montreal Protocol. Therefore those indicators of recovery that are best suited are those that suffer least from meteorological/dynamical influences. An example is the Arctic chemical ozone depletion rate during the time period of total chlorine activation each winter. The depletion rate, given as a change of the ozone mixing ratio per sunlit hour, should be proportional to chlorine/bromine levels. However, even this basic approach is fraught with difficulties. First, the depletion rate is proportional to air pressure. This is due to the fact that the ClO dimer production reaction, which is the time-limiting reaction during the catalytic ozone loss cycle,

depends on a third-body concentration. Therefore the depletion rate is strongly height dependent. Second, the Cl_y content itself is height dependent and the diabatic descent rate of the polar air masses can vary substantially from winter to winter. As a result, the Cl_y content and thus the maximum depletion rates for different winters at a given altitude vary due to this dynamical effect. If used as an indicator for Arctic ozone recovery, these effects have to be taken into account. However, an advantage of this indicator is that it would be insensitive to any future temporal aerosol loading and to especially low temperature events that could lead to denitrification.

A method that is able to determine, as a primary analysis product, the chemical ozone depletion rate in the form of a change of the ozone mixing ratio per sunlit hour is the Match approach (von der Gathen *et al.*, 1995; Rex *et al.*, 1997, 1998a,b) already mentioned in Chapters 4 and 7. This approach provides the depletion rate as a function of time and altitude (see, for example, Figure 7-23) inside the polar vortex. Maximum depletion rates during the time periods and height ranges of total chlorine activation for three winters are shown in Figure 12-35. In future analyses covering additional winters, each altitude level should be compared to a pre-winter altitude level from which an air mass began its descent due to diabatic cooling. These values must be corrected for pressure relevant during the time of maximum ozone depletion.

It should be noted that this type of analysis is not limited to the Match approach. Any technique that is not affected by dynamical processes (e.g., diabatic movements, mixing processes) and that is able to provide ozone depletion rates resolved in time and altitude can be useful (see, for example, Manney *et al.* 1995; Knudsen *et al.*, 1998). If depletion rates are given in changes of ozone mixing ratio per day, they can be converted to changes of the mixing ratio per sunlit hour by including sunlight conditions inside the polar vortex.

Other quantities connected to Arctic ozone loss are less appropriate as indicators of Arctic ozone recovery. Quantities such as ozone loss integrated during the entire winter/spring seasons in total (column density) or at a given altitude (concentration) will be considerably variable from year to year (see, for example, Figure 12-24). It is expected that early ozone recovery will not be detected from such data. However, most of the currently available measurement techniques are able to contribute to this dataset, for example, those discussed in Manney *et al.* (1994), Müller *et al.* (1996), and Goutail *et al.* (1998).

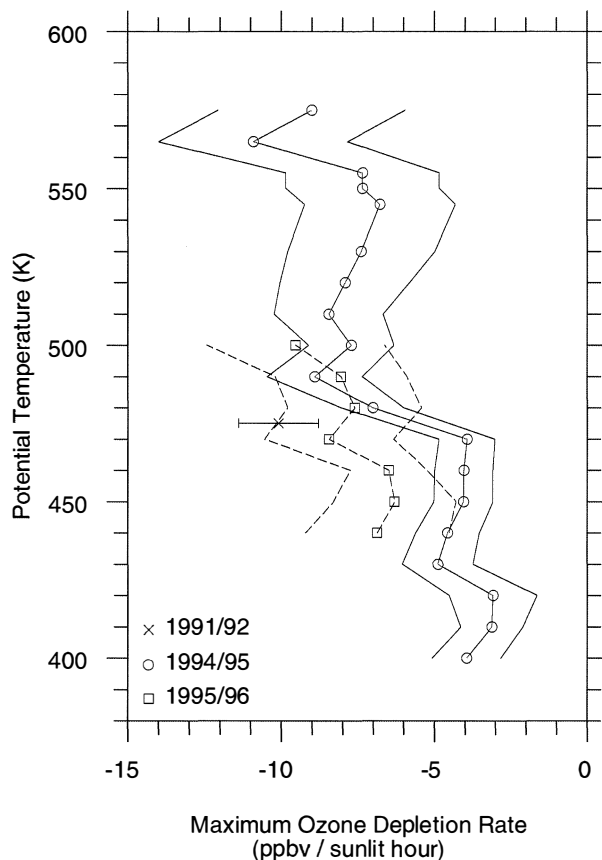


Figure 12-35. Maximum ozone depletion rates, together with the error ranges, during times of total chlorine activation in three Arctic winters as determined by Match campaigns. During the relatively warm winter of 1991/92, total chlorine activation may have occurred only at an altitude of 475 K potential temperature. In 1995/96, reliable rates during the time period of total activation have been determined for a short height interval only.

12.4.3 Midlatitude Ozone Decline

Ozone at midlatitudes is subject to many natural as well as anthropogenic forced variations. Sophisticated linear regression schemes including the seasonal cycle, linear trend, quasi-biennial oscillation, and 11-year solar cycle have been applied to deduce ozone trends (see Chapter 4 of this Assessment). These analyses indicate that the downward trend attributed to chlorine and bromine is about 4% for 65°S to 65°N from 1979 to 1995, or about 2.5% per decade. A relatively large variability, related to dynamic, solar cycle, and volcanic effects, of

PREDICTING THE FUTURE OZONE LAYER

about $\pm 1\%$, exists. Detection of the recovery of a change this small with this large a variability will be a statistical challenge.

Analysis of future changes in middle- and low-latitude ozone (both NH and SH) will primarily require a long-term data record from satellites, with ground-based and balloon measurements for comparisons and cross calibration. At present the Earth Probe-TOMS is making total ozone measurements and NOAA-14 SBUV/2, SAGE II, MLS, and HALOE instruments are measuring profile ozone. Future instruments to measure total ozone include Meteor-3 TOMS (launch in 2000) and ENVISAT (launch in late 1999/early 2000). The Advanced Earth Observing Satellite 2-Improved Limb Atmospheric Sounder 2 (ADEOS 2-ILAS 2) and the Earth Observing System-Chemistry (EOS-CHEM) satellite (launch in 2003) are expected to measure profile ozone.

Because midlatitude ozone is subject to many chemically and dynamically driven variations, it will be difficult to verify its expected recovery. Solar maximum (predicted to occur around the turn of the century) or a particular period of stratospheric dynamics that forces ozone increases could easily be misinterpreted as the beginning of an ozone recovery from the halogen-caused ozone minimum.

Because of possible secondary effects on ozone such as stratospheric temperature reductions related to climate change, as discussed in Section 12.2, changes in total inorganic chlorine amount (Cl_y), while not a direct measure of ozone recovery itself, will be easier to measure than ozone. Combined with a model that deals with the temperature effects on heterogeneous chemistry, it will allow predictions of future trends in ozone to be made. But it must be kept clear that in the end there are no substitutes for the actual observation of recovery of the ozone layer.

As indicated in Chapter 1 of this Assessment, tropospheric chlorine levels peaked in early 1994 (Montzka *et al.*, 1996). Russell *et al.* (1996) have shown with HALOE-measured HCl and hydrogen fluoride (HF) that the time lag for transport of tropospheric gases to 55 km is about 6 ± 2 years. This means that Cl_y should peak at 55 km between 1998 and 2002. Continued monitoring of HCl by HALOE and future monitoring of HCl by EOS-CHEM near 55 km should provide a clear signal of total chlorine reduction in the middle atmosphere, because HCl accounts for 93-95% of the inorganic chlorine family (Russell *et al.*, 1996; Jackman *et al.*, 1996a).

Stratospheric HF has no significant known natural sources; thus it would also be very useful to monitor its peak and subsequent reduction. Although the HF at 55 km should peak about the same time as HCl, a definitive decrease may not be measurable until several years later. The GSFC 2-D model (Jackman *et al.*, 1996a) predicts HCl at 55 km peaking in 1998 and decreasing shortly thereafter. The same model predicts HF at 55 km peaking around the year 2000, but not decreasing substantially until 2010. The reason for this predicted difference in the behavior of HCl and HF lies in the differences among the lifetimes of the CFC source gases. CFC source gas molecules containing more atoms of chlorine generally have shorter atmospheric lifetimes than those containing more atoms of fluorine (see Table 13-1 of WMO, 1995).

Monitoring of ozone in the upper stratosphere (near 40 km), where percentage ozone reductions are more accurately defined than in the lower stratosphere (see Chapter 4), would presumably provide for a more accurate analysis of recovery at midlatitudes. Outside the polar regions, the upper stratosphere is essentially in photochemical equilibrium and should respond rapidly to changes in chlorine (see Chapter 6). The upper stratosphere is also above the aerosol layer, so that temperature trends related to climate change that might affect heterogeneous chemical rates should not have as large an effect. Ozone in this region is affected by the change in seasons and 11-year solar cycle, as well as chlorine amounts, but both of these natural variations can be removed through fairly straightforward analysis techniques. Increases in CO_2 are also expected to reduce stratospheric temperatures and thereby slow gas-phase destruction of ozone. Figure 12-36 shows predicted ozone changes at 40 km, $45^\circ N$ from the CAM 2-D model for integrations with and without the feedback on stratospheric temperature due to CO_2 trends. A slow recovery in ozone is seen beginning about the year 2000 when CO_2 feedback is included, which is not present in the model results without the CO_2 -induced temperature decrease. Interpretation of a measured increase in ozone at 40 km during the first half of the next century will not be simple and will require the use of a model that accurately describes changing halogen loadings and chemistry-climate feedback. Furthermore, the 40-km ozone loss does not represent a very large portion of the total column and realistically would not tell one much about what is happening in the more important lower stratospheric region, where a much larger amount of ozone is lost. Thus, while some measure of ozone

recovery may be extracted from the upper stratospheric data in the future, it will not be conclusive for the total ozone column, which drives increases in surface ultraviolet radiation. However, for scientific purposes, early observation of ozone recovery at 40 km would be reassuring.

12.4.4 Ozone Recovery Scenarios and Expected Dates of Recovery

The goal of this section is to provide the best possible estimate of the expected date of observation of the beginning of ozone recovery through use of the indicators in the previous section and modeled results of expected future variations. Because of the considerable variability in all the indicators of recovery and because of the large uncertainties in model predictions of future ozone levels, this goal is difficult to achieve with much accuracy. However, because regulations were put in place to stop the downward trend in ozone, it is imperative to provide information that can be used to assess the effectiveness of these regulations.

12.4.4.1 THE STANDARD SCENARIO

For the standard scenario we use the equivalent effective stratospheric chlorine (EESC) scenario A/A3 (see Chapter 11 of this Assessment). Scenario A has been determined from the emissions that have occurred up to the present, and scenario A3 consists of the maximum emissions allowed in the future under the Montreal Protocol and reaches 1980 values of about 2 ppb in approximately the year 2052, thus providing a conservative estimate of recovery. As indicated in Table 11-6, except for scenarios A2 and A4 (zero emissions and zero production scenarios), the mean recovery year for the other 16 scenarios is 2047.6 with a standard deviation of 1.9 years. Thus the choice of the maximum emissions scenario does not introduce a large uncertainty in the estimated recovery year. The main difference between scenario A3 and that used in the 1994 Assessment (WMO, 1995) is the relatively flat EESC region between about 2000 and 2020, related to new estimates of the future trends in CFCs, halons, and HCFCs given in Chapter 11.

In Figure 12-37a we assume that ozone will respond directly to EESC, and any perturbations related to greenhouse gas and climate changes, etc., are ignored. The degree of variability in three indicators (the TOMS global total ozone anomaly (Figure 12-37b), the South

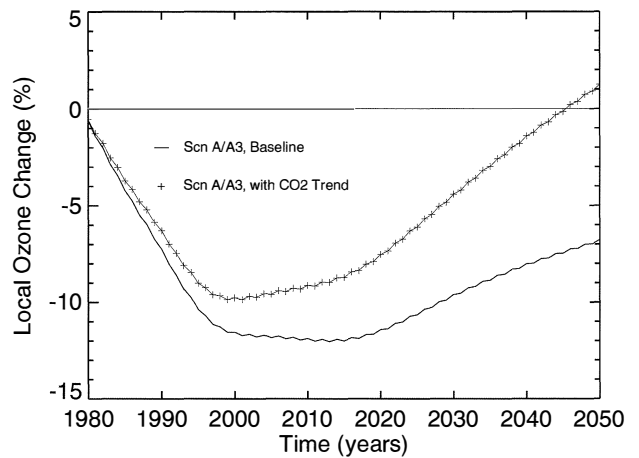


Figure 12-36. Percentage change in annual average ozone concentration at 40 km relative to year 1979 for the CAM model at 45°N latitude between 1980 and 2050. The solid line represents using CO₂ surface boundary conditions fixed at 1995 levels between 1979 and 2050. The line with crosses represents using a time-dependent trend of CO₂ (see Table 12-2).

Pole and Halley October Dobson total ozone values (Figure 12-37c), and the South Pole ozonesonde 12-20 km September ozone loss rates (Figure 12-37d)) is used to construct a recovery curve with bounds for each that include about 90% of the data points prior to 1998. The beginning of recovery is assumed to have been observed when the value of ozone (ozone loss rate) has increased (decreased) to within one unit of the variability above (below) the minimum (maximum) values. The South Pole recovery indicators have been described in detail by Hofmann *et al.* (1997), who investigated detection of ozone hole recovery for EESC levels given in WMO (1995). As indicated earlier, the earliest detection of the beginning of recovery will likely occur in Antarctica, mainly because of the large signal and the lower dynamic variability inside the polar vortex. For EESC recovery considerations alone (scenario A3), the ozonesonde-measured ozone loss rate would document the beginning of recovery as early as 2015 while the beginning of global ozone recovery would not be detectable for an additional 10 or so years. The global ozone pre-recovery period, a cessation of the downward ozone trend, would be apparent during the next decade, based on the predicted EESC trend alone and assuming the absence of major volcanic eruptions.

PREDICTING THE FUTURE OZONE LAYER

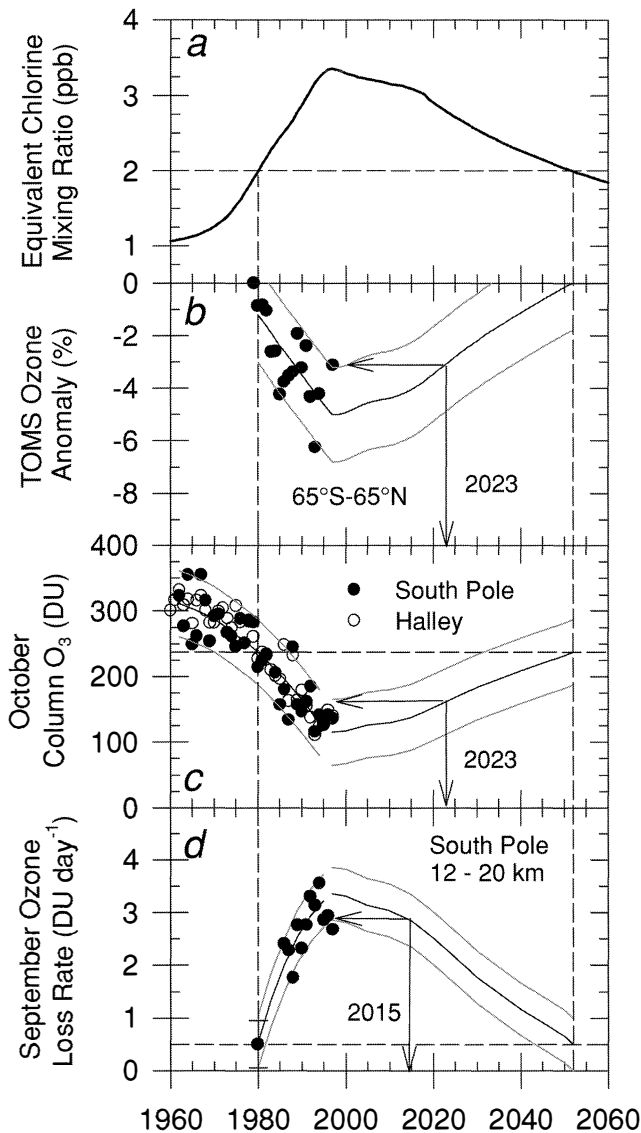


Figure 12-37. (a) Scenario A/A3 equivalent effective stratospheric chlorine (EESC) for 1960 to 2060. The dashed line at 2 ppbv equivalent chlorine is the level believed to have existed when the ozone hole emerged in 1980. (b) Percentage reduction in total ozone from 1979 values for the region 65°S to 65°N as determined from TOMS data (McPeters *et al.*, 1996). The dark smooth curve prior to 1997 is a best fit to the data and the lighter curves are $\pm 1.8\%$, which represents the variability. The extensions of these lines beyond 1997 are based on the projected stratospheric total equivalent chlorine given in (a) with ozone values returning to 1980 levels in 2052. The average non-polar total ozone reduction is estimated to recover to a value one unit of variability (1.8%) above the maximum ozone reduction by the year 2023. (c) Total column ozone from the Dobson spectrophotometers at Halley and the South Pole from 1960 to 1997, averaged over the month of October for Halley and 15-31 October, the earliest period during which adequate sunlight is available for measurements, at South Pole. The dark and lighter curves are as in (b), except for a ± 50 -DU variability interval and the same estimated recovery date of 2023. (d) September ozone loss rate between 12 and 20 km from a linear fit to the September data at South Pole for the period 1986-1997 (adapted from Hofmann *et al.*, 1997). The 1980 value is estimated at 0.5 ± 0.5 DU day⁻¹ from the work of Lait *et al.* (1989). The dark and lighter curves are as in (b), except for a ± 0.5 DU day⁻¹ variability interval and an estimated recovery date of 2015.

12.4.4.2 PERTURBATIONS TO THE STANDARD SCENARIO

As discussed earlier in this chapter, climate change and variations in CH₄ and N₂O could conceivably delay ozone recovery substantially. In order to gauge the extent of this perturbation, a number of comparisons of model predictions of ozone recovery to observations have been made. Figure 12-38 compares the results of 10 2-D models for the 65°S-65°N total ozone anomaly for scenario A/A3 with TOMS measurements. The standard deviation of the model results is under $\pm 1\%$, while the variability in the data is somewhat larger. This figure suggests that observations of the global ozone trend from satellites will not provide strong evidence for the

beginning of ozone recovery prior to about 2030 although the detection of a cessation of the downward trend could occur at a time similar to the standard scenario considered earlier, i.e., during the first decade of the next century, barring volcanic eruptions.

Not all the 2-D models incorporate appropriate PSC chemistry. Those that do, show an ozone hole response about a factor of 2 too small on average. Figure 12-39 compares October total ozone measurements at South Pole and Halley in Antarctica with the LLNL model (scenario A/A3), which does have PSC chemistry and gives the largest depletions in October. However, the LLNL model had to be multiplied by 0.65 to bring October ozone values during the 1990s into the range of

observations. With the adjustment, the LLNL model reproduces the time variation from 1980 to the present very well, including the Mt. Pinatubo volcanic effect in 1992-1993. Except for unusually high ozone observed in October of 1986 and 1988, the variability of the data is reasonably well represented by the dashed curves at ± 25 DU in Figure 12-39 and suggests that total ozone in Antarctica will not be observed to have clearly begun recovery before about 2030. Because of saturation over a portion of the ozone depletion region in Antarctica, the cessation of a downward trend is not a viable indicator of a pre-recovery period as it is mostly due to the fact that almost all of the ozone is already destroyed in the 12-20 km PSC region (see Chapter 4).

Polar ozone 3-D model results were presented earlier (Figure 12-24) for the GISS coupled model compared to TOMS data for the minimum total column ozone north and south of 65° , averaged over the last 3 days of March and September for the Arctic and Antarctic, respectively. As indicated earlier, Figure 12-24 clearly shows why springtime Antarctic ozone, with much less variability than in the Arctic or at midlatitudes, holds the most hope for an early detection of the beginning of ozone recovery. It is of note that the model suggests a continuing decline in this column ozone parameter in Antarctica to values below 100 DU during the first decades of the next century with a following recovery at nearly the same rate as the decline, suggesting a possible detection of the beginning of recovery by about 2020.

The rate of ozone loss in September is not susceptible to saturation and should be proportional to EESC, all else being equal. Similarly, the value of ozone in the PSC region on a particular date in September, prior to the ozone hole reaching a minimum, is a useful indicator. Ozone values on 15 September for the 12-20 km column from South Pole ozonesondes have been used for this purpose in the past and showed the least amount of variability for a number of indicators investigated (Hofmann *et al.*, 1997). In Figure 12-40, the percentage reduction in the 12-20 km ozone column on 15 September as determined from South Pole ozonesondes is compared to the LLNL model for scenario A/A3. The 15 September modeled ozone reduction had to be increased by 50% to bring the values in the 1990s into the range of the observations, again indicating problems with the 2-D models in predicting the magnitude of the ozone hole phenomenon. Also shown in Figure 12-40 is the mean of two models for scenario B (constant 1995 levels of

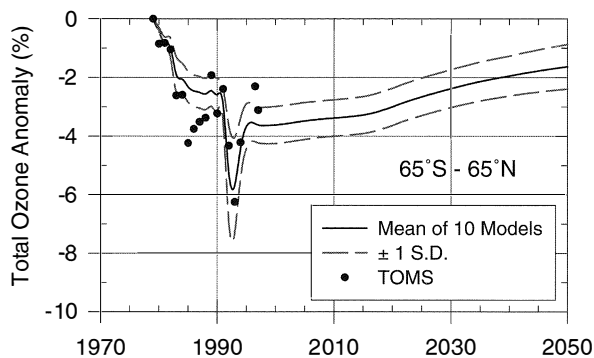


Figure 12-38. The mean of 10 2-D models for the $65^\circ\text{S}-65^\circ\text{N}$ total ozone anomaly for scenario A/A3, compared to TOMS data. The standard deviation of the model results is also shown.

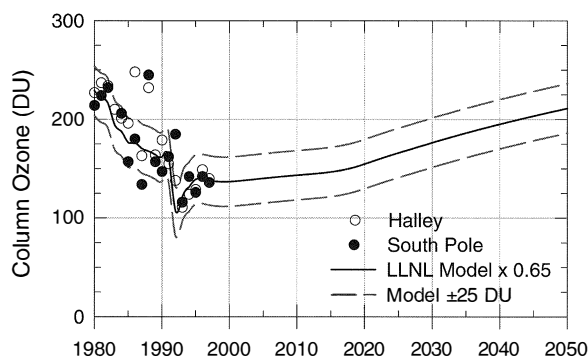


Figure 12-39. Comparison of the LLNL model for scenario A/A3 for October average total ozone at 85°S with observations at South Pole and Halley in Antarctica. The model results were multiplied by 0.65 to bring them into the range of the measurements. A variability range of ± 25 DU, representing the variability in the observations, has been applied to the model results.

CH_4 and N_2O), demonstrating the 10-year or more delay in recovery, mainly due to constant methane levels. Both model representations overestimate the Mt. Pinatubo volcanic effect dramatically. The latter was barely visible in the 12-20 km data, with most of the ozone reduction related to the sulfate aerosol in the 10-14 km region (Hofmann *et al.*, 1994, 1995). The models suggest that the beginning of recovery in this parameter will likewise not be clearly observable until after 2020, but with a

PREDICTING THE FUTURE OZONE LAYER

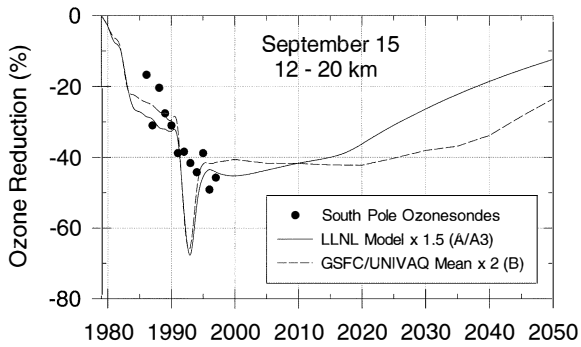


Figure 12-40. The percentage reduction relative to 1979 in the 12-20 km ozone column at the South Pole on 15 September for scenario A/A3 from the LLNL model compared to the ozonesonde measurements from 1986 to 1997. The ozonesonde reference value was obtained from a series of ozonesondes at South Pole in September 1971 (Hofmann *et al.*, 1997). Also shown is the average response for scenario B (CH_4 and N_2O fixed at 1995 levels) for the GSFC and UNIVAQ models. All of the models had to be adjusted to bring them into the range of the measurements.

predicted cessation of the downward trend early in the next century.

In summary, while models indicate that the maximum ozone depletion will occur within the next two decades, uncertainties related to emission scenarios of greenhouse gases and climate change make estimates of the beginning of ozone layer recovery unreliable. Even in Antarctica, where it is believed that the earliest and least ambiguous observation of the beginning of ozone recovery will be possible, the estimated effects of greenhouse gases and climate change indicate that unambiguous detection of the beginning of the recovery of the ozone layer will not occur until well into the next century, beyond the maximum loading of ozone-depleting gases. Barring major volcanic eruptions during the next decade, a cessation of the downward trend in midlatitude ozone should be observed and would be a harbinger of the coming recovery.

REFERENCES

- AIAA (American Institute of Aeronautics and Astronautics), *Atmospheric Effects of Chemical Rocket Propulsion*, Report of an AIAA Workshop, June 28-29, 1991, Sacramento, Calif., 52 pp., Washington, D.C., 1991.
- Austin, J., and N. Butchart, A three-dimensional modeling study of the influence of planetary wave dynamics on polar ozone photochemistry, *J. Geophys. Res.*, *97*, 10165-10186, 1992.
- Austin, J., and N. Butchart, The influence of climate change and the timing of stratospheric warmings on Arctic ozone depletion, *J. Geophys. Res.*, *99*, 1127-1145, 1994.
- Austin, J., N. Butchart, and K. Shine, Possibility of an Arctic ozone hole in a doubled- CO_2 climate, *Nature*, *360*, 221-225, 1992.
- Austin, J., N. Butchart, and R.S. Swinbank, Sensitivity of ozone and temperature to vertical resolution in a GCM with coupled stratospheric chemistry, *Quart. J. Roy. Meteorol. Soc.*, *123*, 1405-1431, 1997.
- Balachandran, N., and D. Rind, Modeling the effects of UV variability and the QBO on the troposphere-stratosphere system: Part I, The middle atmosphere, *J. Clim.*, *8*, 2058-2079, 1995.
- Bekki, S., and J.A. Pyle, A two-dimensional modeling study of the volcanic eruption of Mount Pinatubo, *J. Geophys. Res.*, *99*, 18861-18869, 1994.
- Bojkov, R.D., V.E. Fioletov, D.S. Bais, C.S. Zerefos, T.V. Kadygrova, and A.M. Shalamjansky, Further ozone decline during the Northern Hemisphere winter-spring of 1994-1995 and the new record low ozone, *Geophys. Res. Lett.*, *22*, 2729-2732, 1995.
- Boville, B., Detecting CO_2 -induced temperature changes in the stratosphere, *Adv. Space Res.*, *6*, 45-48, 1986.
- Braathen, G.O., M. Rummukainen, E. Kyrö, U. Schmidt, A. Dahlback, T.S. Jorgensen, R. Fabian, V.V. Rudakov, M. Gil, and R. Borchers, Temporal development of ozone within the Arctic vortex during the winter of 1991/92, *Geophys. Res. Lett.*, *21*, 1407-1410, 1994.
- Brasseur, G., The response of the middle atmosphere to long-term and short-term solar variability: A two-dimensional model, *J. Geophys. Res.*, *98*, 23079-23090, 1993.

- Brasseur, G., and P.C. Simon, Stratospheric chemical and thermal response to long-term variability in solar UV irradiance, *J. Geophys. Res.*, *86*, 7343-7362, 1981.
- Brasseur, G.P., R.A. Cox, D. Hauglustaine, I. Isaksen, J. Lelieveld, D.H. Lister, R. Sausen, U. Schumann, A. Wahner, and P. Wiesen, European Scientific Assessment of the Atmospheric Effects of Aircraft Emissions, *Atmos. Environ.*, *32*, 2329-2422, 1998.
- Brewer, A.W., and A.W. Wilson, The regions of formation of atmospheric ozone, *Quart. J. Roy. Meteorol. Soc.*, *94*, 249-265, 1968.
- Butchart, N., and J. Austin, On the relationship between the quasi-biennial oscillation, total chlorine, and the Antarctic ozone hole, *Quart. J. Roy. Meteorol. Soc.*, *122*, 183-217, 1996.
- Butchart, N., and J. Austin, Middle atmosphere climatologies from the troposphere-stratosphere configuration of the UKMO's unified model, *J. Atmos. Sci.*, *55*, 2782-2809, 1998.
- Callis, L.B., J.C. Alpert, and M.A. Geller, An assessment of thermal, wind, and planetary wave changes in the middle and lower atmosphere due to 11-year UV flux variations, *J. Geophys. Res.*, *90*, 2273-2282, 1985.
- Callis, L.B., M. Natarajan, J.D. Lambeth, and R.E. Boughner, On the origin of midlatitude ozone changes: Data analysis and simulations for 1979-1993, *J. Geophys. Res.*, *102*, 1215-1228, 1997.
- Cariolle, D., and M. Deque, Southern Hemisphere medium-scale waves and total ozone disturbances in a spectral general circulation model, *J. Geophys. Res.*, *91*, 10825-10846, 1986.
- Cariolle, D., A. Lassere-Bigory, and J.-F. Royerand, A general circulation model simulation of the springtime Antarctic ozone decrease and its impact on midlatitudes, *J. Geophys. Res.*, *95*, 1883-1898, 1990.
- Chandra, S., and R.D. McPeters, The solar cycle variation of ozone in the stratosphere inferred from Nimbus 7 and NOAA 11 satellites, *J. Geophys. Res.*, *99*, 20665-20671, 1994.
- Chipperfield, M.P., and J.A. Pyle, Model sensitivity studies of Arctic ozone depletion, *J. Geophys. Res.*, in press, 1998.
- Chipperfield, M.P., A.M. Lee, and J.A. Pyle, Model calculations of ozone depletion in the Arctic polar vortex for 1991/92 to 1994/95, *Geophys. Res. Lett.*, *23*, 559-562, 1996.
- Crutzen, P.J., I.S.A. Isaksen, and G.C. Reid, Solar proton events: Stratospheric sources of nitric oxide, *Science*, *189*, 457-458, 1975.
- Cubasch, U., K. Hasselmann, H. Hock, E. Maier-Reimer, U. Mikalajewicz, B. Santer, and R. Sausen, Time-dependent greenhouse warming computations with a coupled ocean-atmosphere model, *Clim. Dyn.*, *8*, 55-69, 1992.
- Dameris, M., V. Grewe, R. Hein, C. Schnadt, C. Brühl, and B. Steil, Assessment of the future development of the ozone layer, *Geophys. Res. Lett.*, *25*, 3579-3582, 1998.
- Danilin, M.Y., N.-D. Sze, M.K.W. Ko, J.M. Rodriguez, and M.J. Prather, Bromine-chlorine coupling in the Antarctic ozone hole, *Geophys. Res. Lett.*, *23*, 153-156, 1996.
- Danilin, M.Y., N.-D. Sze, M.K.W. Ko, J.M. Rodriguez, and A. Tabazadeh, Stratospheric cooling and Arctic ozone recovery, *Geophys. Res. Lett.*, *25*, 2141-2144, 1998.
- DeMore, W.B., S.P. Sander, D.M. Golden, R.F. Hampson, M.J. Kurylo, C.J. Howard, A.R. Ravishankara, C.E. Kolb, and M.J. Molina, *Chemical Kinetics and Photochemical Data for Use in Stratospheric Modeling*, Evaluation No. 12, JPL Publ. 97-4, Jet Propulsion Laboratory, Pasadena, Calif., 1997.
- Déqué, M., and J.P. Piedelievre, High resolution climate simulation over Europe, *Clim. Dyn.*, *11*, 321-339, 1995.
- Donovan, D.P., H. Fast, Y. Makino, J.C. Bird, A.I. Carswell, J. Davies, T.J. Duck, J.W. Kaminski, C.T. McElroy, R.L. Mittermeier, S.R. Pal, V. Savastiouk, D. Velkov, and J.A. Whiteway, Ozone, column ClO, and PSC measurements made at the NDSC Eureka Observatory (80°N, 86°W) during the spring of 1997, *Geophys. Res. Lett.*, *24*, 2709-2712, 1997.
- Douville, H., S. Planton, J.-F. Royer, and S. Tyteca, Climatic impact of CO₂ doubling: Part I, Radiative effects on global and regional climates, *J. Geophys. Res.*, submitted, 1998.
- Elkins, J.W., T.M. Thompson, T.H. Swanson, J.H. Butler, B.D. Hall, S.O. Cummings, D.A. Fisher, and A.G. Raffo, Decrease in the growth rates of atmospheric chlorofluorocarbons 11 and 12, *Nature*, *364*, 780-783, 1993.
- Farman, J.C., B.G. Gardiner, and J.D. Shanklin, Large losses of total ozone in Antarctica reveal seasonal ClO_x/NO_x interaction, *Nature*, *315*, 207-210, 1985.

PREDICTING THE FUTURE OZONE LAYER

- Fels, S.B., J.D. Mahlman, M.D. Schwarzkopf, and R.W. Sinclair, Stratospheric sensitivity to perturbations in ozone and carbon dioxide: Radiative and dynamical response, *J. Atmos. Sci.*, 37, 2265-2297, 1980.
- Fleming, E.L., S. Chandra, C.H. Jackman, D.B. Conditine, and A.R. Douglass, The middle atmospheric response to short and long term solar UV variations: Analysis of observations and 2D model results, *J. Atmos. Terr. Phys.*, 57, 333-365, 1995.
- Friedl, R.R., B.E. Anderson, S.L. Baughcum, J. Hallett, K.-N. Liou, P.J. Rasch, D.H. Rind, K. Sassen, H.B. Singh, L.R. Williams, and D.J. Wuebbles, *Atmospheric Effects of Subsonic Aircraft: Interim Assessment Report of the Advanced Subsonic Technology Program*, NASA Ref. Publ. 1400, National Aeronautics and Space Administration, Washington, D.C., 1997.
- Garcia, R.R., and S. Solomon, A possible relationship between interannual variability in Antarctic ozone and the quasi-biennial oscillation, *Geophys. Res. Lett.*, 14, 848-851, 1987.
- Garcia, R.R., S. Solomon, R.G. Roble, and D.W. Rusch, A numerical response of the middle atmosphere to the 11-year solar cycle, *Planet. Space Sci.*, 32, 411-423, 1984.
- Golombek, A., and R.G. Prinn, A global three-dimensional model of the circulation and chemistry of CFCl_3 , CF_2Cl_2 , CH_3CCl_3 , CCl_4 , and N_2O , *J. Geophys. Res.*, 91, 3985-4002, 1986.
- Goutail, F., J.-P. Pommereau, C. Phillips, C. Deniel, A. Sarkissian, F. Lefèvre, E. Kyrö, M. Rummukainen, P. Ericksen, S.B. Andersen, B.-A. Kaastad-Hoiskar, G.O. Braathen, V. Dorokhov, and V.U. Khattatov, Total ozone depletion in the Arctic during the winters 1993-94 and 1994-95, *J. Atmos. Chem.*, in press, 1998.
- Granier, C., and G. Brasseur, Ozone and other trace gases in the Arctic and Antarctic regions: Three-dimensional model simulations, *J. Geophys. Res.*, 96, 2995-3011, 1991.
- Grewe, V., M. Dameris, and R. Sausen, The impact of stratospheric dynamics and chemistry on Northern Hemisphere mid-latitude ozone loss, *J. Geophys. Res.*, in press, 1998.
- Groß, J.-U., C. Brühl, and T. Peter, Impact of aircraft emissions on tropospheric and stratospheric ozone: Part I, Chemistry and 2-D model results, *Atmos. Environ.*, 32, 3173-3184, 1998.
- Hadjinicolaou, P., J.A. Pyle, M.P. Chipperfield, and J.A. Kettleborough, Effect of interannual meteorological variability on mid-latitude O_3 , *Geophys. Res. Lett.*, 24, 2993-2996, 1997.
- Haigh, J.D., The impact of solar variability on climate, *Science*, 272, 981-984, 1996.
- Hamilton, K., Comprehensive meteorological modeling of the middle atmosphere: A tutorial review, *J. Atmos. Terr. Phys.*, 58, 1591-1627, 1996.
- Hansen, G., T. Svenoe, M.P. Chipperfield, A. Dahlback, and U.-P. Hoppe, Evidence of substantial ozone depletion in winter 1995/96 over northern Norway, *Geophys. Res. Lett.*, 24, 799-802, 1997.
- Hanson, D.R., and E.R. Lovejoy, Heterogeneous reaction in liquid sulfuric acid: $\text{HOCl} + \text{HCl}$ as a model system, *J. Phys. Chem.*, 100, 6397-6405, 1996.
- Hanson, D.R., and A.R. Ravishankara, Reactive uptake of ClONO_2 onto sulfuric acid due to reaction with HCl and H_2O , *J. Phys. Chem.*, 98, 5728-5735, 1994.
- Hanson, D.R., and A.R. Ravishankara, Heterogeneous chemistry of bromine species in sulfuric acid under stratospheric conditions, *Geophys. Res. Lett.*, 22, 385-388, 1995.
- Hanson, D.R., A.R. Ravishankara, and S. Solomon, Heterogeneous reactions in sulfuric acid under stratospheric conditions, *J. Geophys. Res.*, 99, 3615-3629, 1994.
- Hanson, D.R., A.R. Ravishankara, and E.R. Lovejoy, Reaction of BrONO_2 with H_2O on submicron sulfuric acid aerosol, and the implication for the lower stratosphere, *J. Geophys. Res.*, 101, 9063-9069, 1996.
- Hofmann, D.J., Recovery of Antarctic ozone hole, *Nature*, 384, 222, 1996.
- Hofmann, D.J., and T. Deshler, Evidence from balloon measurements for chemical depletion of stratospheric ozone in the Arctic winter of 1989-90, *Nature*, 349, 300-305, 1991.
- Hofmann, D.J., J.W. Harder, S.R. Rolf, and J.M. Rosen, Balloon-borne observations of the development and vertical structure of the Antarctic ozone hole in 1986, *Nature*, 326, 59-62, 1987.
- Hofmann, D.J., T. Deshler, P. Amedieu, W.A. Matthews, P.V. Johnston, Y. Kondo, W.R. Sheldon, G.J. Byrne, and J.R. Benbrook, Stratospheric clouds and ozone depletion in the Arctic during January 1989, *Nature*, 340, 117-121, 1989.

- Hofmann, D.J., S.J. Oltmans, J.A. Lathrop, J.M. Harris, and H. Vömel, Record low ozone at the South Pole in the spring of 1993, *Geophys. Res. Lett.*, *21*, 421-424, 1994.
- Hofmann, D.J., S.J. Oltmans, B.J. Johnson, J.A. Lathrop, J.M. Harris, and H. Vömel, Recovery of ozone in the lower stratosphere at the South Pole during the spring of 1994, *Geophys. Res. Lett.*, *22*, 2493-2496, 1995.
- Hofmann, D.J., S.J. Oltmans, J.M. Harris, B.J. Johnson, and J.A. Lathrop, Ten years of ozonesonde measurements at the south pole: Implications for recovery of springtime Antarctic ozone, *J. Geophys. Res.*, *102*, 8931-8943, 1997.
- Hollandsworth, S.M., R.D. McPeters, L.E. Flynn, W. Planet, A.J. Miller, and S. Chandra, Ozone trends derived from combined Nimbus 7 SBUV and NOAA SBUV/2 data, *Geophys. Res. Lett.*, *22*, 905-908, 1995.
- Hood, L.L., J.L. Jirikowic, and J.P. McCormack, Quasi-decadal variability of the stratosphere: Influence of long term solar ultraviolet variations, *J. Atmos. Sci.*, *50*, 3941-3958, 1993.
- Huang, T.Y.W., and G.P. Brasseur, Effect of long-term solar variability in a two-dimensional interactive model of the middle atmosphere, *J. Geophys. Res.*, *98*, 20413-20427, 1993.
- IPCC (Intergovernmental Panel on Climate Change), *Climate Change 1995: The Science of Climate Change*, edited by J.T. Houghton, L.G. Meira Filho, B.A. Callander, N. Harris, A. Kattenberg, and K. Maskell, Cambridge University Press, Cambridge, U.K., 1996.
- IPCC (Intergovernmental Panel on Climate Change), *Aviation and the Global Atmosphere: A Special Report of IPCC Working Groups I and III*, edited by J.T. Houghton, D. Lister, J. Penner, M. McFarland, D. Griggs, and D. Dokken, Cambridge University Press, Cambridge, U.K., in preparation, 1999.
- Jackman, C.H., Energetic particle influences on NO_y and ozone in the middle atmosphere, in *Interactions Between Global Climate Subsystems: The Legacy of Hann*, edited by G.A. McBean and M. Hantel, pp. 131-139, *Geophys. Monogr.* *75*, IUGG, vol. 15, American Geophysical Union, Washington, D.C., 1993.
- Jackman, C.H., The impact of emissions from space transport systems on the state of the atmosphere, in *Proceedings of an International Scientific Colloquium on Impact of Emissions from Aircraft and Spacecraft upon the Atmosphere*, April 18-20, 1994, Cologne, Germany, edited by U. Schumann and D. Wurzel, pp. 366-371, German Aerospace Research Establishment, 1994.
- Jackman, C.H., M.C. Cerniglia, J.E. Nielsen, D.J. Allen, J.M. Zawodny, R.D. McPeters, A.R. Douglass, J.E. Rosenfield, and R.B. Rood, Two-dimensional and three-dimensional model simulations, measurements, and interpretation of the influence of the October 1989 solar proton events on the middle atmosphere, *J. Geophys. Res.*, *100*, 11641-11660, 1995.
- Jackman, C.H., E.L. Fleming, S. Chandra, D.B. Considine, and J.E. Rosenfield, Past, present and future modeled ozone trends with comparisons to observed trends, *J. Geophys. Res.*, *101*, 28753-28767, 1996a.
- Jackman, C.H., D.B. Considine, and E.L. Fleming, Space Shuttle's impact on the stratosphere: An update, *J. Geophys. Res.*, *101*, 12523-12529, 1996b.
- Jackman, C.H., D.B. Considine, and E.L. Fleming, A global modeling study of solid rocket aluminum oxide emission effects on stratospheric ozone, *Geophys. Res. Lett.*, *25*, 907-910, 1998.
- Johns, T.C., R.E. Carnell, J.F. Crossley, J.M. Gregory, J.F.B. Mitchell, C.A. Senior, S.F.B. Tett, and R.A. Wood, The second Hadley Centre coupled ocean-atmosphere GCM: Model description, spinup and validation, *Clim. Dyn.*, *13*, 103-134, 1997.
- Jones, A.E., S. Bekki, and J.A. Pyle, On the atmospheric impact of launching the Ariane 5 rocket, *J. Geophys. Res.*, *100*, 16651-16660, 1995.
- Kinne, S., O.B. Toon, and M.J. Prather, Buffering of stratospheric circulation by changing amounts of tropical ozone: A Pinatubo case study, *Geophys. Res. Lett.*, *19*, 1927-1930, 1992.
- Kinnison, D.E., K.E. Grant, P.S. Connell, D.A. Rotman, and D.J. Wuebbles, The chemical and radiative effects of the Mt. Pinatubo eruption, *J. Geophys. Res.*, *99*, 25705-25731, 1994.
- Knight, J.R., J. Austin, R.G. Grainger, and A. Lambert, A three-dimensional model simulation of the impact of Mt. Pinatubo aerosol on the Antarctic ozone hole, *Quart. J. Roy. Meteorol. Soc.*, *124*, 1527-1558, 1998.

PREDICTING THE FUTURE OZONE LAYER

- Knudsen, B.M., N. Larsen, I. St. Mikkelsen, J.-J. Morcrette, G.O. Braathen, E. Kyrö, H. Fast, H. Gernandt, H. Kanzawa, H. Nakane, V. Dorokhov, V. Yushkov, G. Hansen, M. Gil, and R.J. Shearman, Ozone depletion in and below the Arctic vortex for 1997, *Geophys. Res. Lett.*, 25, 627-630, 1998.
- Kodera, K., and H. Koide, Spatial and seasonal characteristics of recent decadal trends in the northern hemispheric troposphere and stratosphere, *J. Geophys. Res.*, 102, 19433-19447, 1997.
- Koike, M., Y. Kondo, M. Hayashi, Y. Iwasaka, P.A. Newman, M. Helten, and P. Aimeidieu, Depletion of Arctic ozone in the winter 1990, *Geophys. Res. Lett.*, 18, 791-794, 1991.
- Kyrö, E., P. Taalas, T.S. Jorgensen, B. Knudsen, F. Stordal, G. Braathen, A. Dahlback, R. Neuber, B.C. Krüger, V. Dorokhov, V.A. Yushkov, V.V. Rudakov, and A. Torres, Analysis of the ozone soundings made during the first quarter of 1989 in the Arctic, *J. Geophys. Res.*, 97, 8083-8091, 1992.
- Lait, L.R., M.R. Schoeberl, and P.A. Newman, Quasi-biennial modulation of the Antarctic ozone depletion, *J. Geophys. Res.*, 94, 11559-11571, 1989.
- Larsen, N., B. Knudsen, I. St. Mikkelsen, T.S. Jorgensen, and P. Eriksen, Ozone depletion in the Arctic stratosphere in early 1993, *Geophys. Res. Lett.*, 21, 1611-1614, 1994.
- Law, K.S., and J.A. Pyle, Modeling trace gas budgets in the troposphere: 1, Ozone and odd nitrogen, *J. Geophys. Res.*, 98, 18377-18400, 1993.
- Lefèvre, F., G.P. Brasseur, I. Folkins, A.K. Smith, and P. Simon, Chemistry of the 1991-92 stratospheric winter: Three-dimensional model simulations, *J. Geophys. Res.*, 99, 8183-8195, 1994.
- Lefèvre, F., F. Figarol, K. Carslaw, and T. Peter, The 1997 Arctic ozone depletion quantified from three-dimensional model simulations, *Geophys. Res. Lett.*, 25, 2425-2428, 1998.
- Lipson, J.B., M.J. Elrod, T.W. Beiderhase, L.T. Molina, and M.J. Molina, Temperature dependence of the rate constant and branching ratio for the OH + ClO reaction, *J. Chem. Soc., Faraday Trans.*, 93, 2665-2673, 1997.
- Mahfouf, J.F., D. Cariolle, J.-F. Royer, J.-F. Geleyn, and B. Timbal, Response of the Météo-France climate model to changes in CO₂ and sea surface temperature, *Clim. Dyn.*, 9, 345-362, 1993.
- Manney, G.L., L. Froidevaux, J.W. Waters, R.W. Zurek, W.G. Read, L.S. Elson, J.B. Kumer, J.L. Mergenthaler, A.E. Roche, A.O'Neill, R.S. Harwood, I. MacKenzie, and R. Swinbank, Chemical ozone depletion of ozone in the Arctic lower stratosphere during winter 1992-93, *Nature*, 370, 429-434, 1994.
- Manney, G.L., R.W. Zurek, L. Froidevaux, and J.W. Waters, Evidence for Arctic ozone depletion in late February and early March 1994, *Geophys. Res. Lett.*, 22, 2941-2944, 1995.
- Manney, G.L., M.L. Santee, L. Froidevaux, J.W. Waters, and R.W. Zurek, Polar vortex conditions during the 1995-96 Arctic winter: Meteorology and MLS ozone, *Geophys. Res. Lett.*, 23, 3203-3206, 1996.
- Manney, G.L., L. Froidevaux, M.L. Santee, R.W. Zurek, and J.W. Waters, MLS observations of Arctic ozone loss in 1996-1997, *Geophys. Res. Lett.*, 24, 2697-2700, 1997.
- McCormack, J.P., and L.L. Hood, Apparent solar cycle variations of upper stratospheric ozone and temperature: Latitude and seasonal dependencies, *J. Geophys. Res.*, 101, 20933-20944, 1996.
- McKenna, D.S., R.L. Jones, L.R. Poole, S. Solomon, D.W. Fahey, K.K. Kelly, M.H. Proffitt, W.H. Brune, M. Loewenstein, and K.R. Chan, Calculations of ozone destruction during the 1988/89 Arctic winter, *Geophys. Res. Lett.*, 17, 553-556, 1990.
- McPeters, R.D., S.M. Hollandsworth, L.E. Flynn, J.R. Herman, and C.J. Seftor, Long-term ozone trends derived from the 16-year combined Nimbus 7/Meteor 3 TOMS Version 7 record, *Geophys. Res. Lett.*, 23, 3699-3702, 1996.
- Michelangeli, D.V., M. Allen, and Y.L. Yung, Chichón volcanic aerosols: Impact of radiative, thermal, and chemical perturbations, *J. Geophys. Res.*, 94, 18429-18443, 1989.
- Mitchell, J.F.B., T.C. Johns, J.M. Gregory, and S.F.B. Tett, Climate response to increasing levels of greenhouse gases and sulphate aerosols, *Nature*, 376, 501-504, 1995.
- Molina, M.J., L.T. Molina, R. Zhang, R.F. Meads, and D.D. Spencer, The reaction of ClONO₂ with HCl on aluminum oxide, *Geophys. Res. Lett.*, 24, 1619-1622, 1997.

- Montzka, S.A., J.H. Butler, R.C. Myers, T.M. Thompson, T.H. Swanson, A.D. Clarke, L.T. Lock, and J.W. Elkins, Decline in the tropospheric abundance of halogen from halocarbons: Implications for stratospheric ozone depletion, *Science*, 272, 1318-1322, 1996.
- Müller, R., P.J. Crutzen, J.-U. Groöf, C. Brühl, J.M. Russell III, and A.F. Tuck, Chlorine activation and ozone depletion in the Arctic vortex: Observations by the Halogen Occultation Experiment on the Upper Atmosphere Research Satellite, *J. Geophys. Res.*, 101, 12531-12554, 1996.
- Müller, R., P.J. Crutzen, J.-U. Groöf, C. Brühl, J.M. Russell III, H. Gernandt, D.S. McKenna, and A.F. Tuck, Severe chemical ozone loss in the Arctic during the winter of 1995-96, *Nature*, 389, 709-712, 1997a.
- Müller, R., J.-U. Groöf, D.S. McKenna, P.J. Crutzen, C. Brühl, J.M. Russell III, and A.F. Tuck, HALOE observations of the vertical structure of chemical ozone depletion in the Arctic vortex during winter and early spring 1996-1997, *Geophys. Res. Lett.*, 24, 2717-2720, 1997b.
- Newman, P.A., J.F. Gleason, R.D. McPeters, and R.S. Stolarski, Anomalous low ozone over the Arctic, *Geophys. Res. Lett.*, 24, 2689-2692, 1997.
- Park, J.H., M.K.W. Ko, C.H. Jackman, and R.A. Plumb (eds.), *Report of the 1997 Models and Measurements Workshop*, November 3-5, 1997, Williamsburg, Virginia, NASA Ref. Publ., National Aeronautics and Space Administration, Washington, D.C., in press, 1998.
- Pawson, S., and B. Naujokat, Trends in daily wintertime temperatures in the northern stratosphere, *Geophys. Res. Lett.*, 24, 575-578, 1997.
- Payan, S., C. Camy-Peyret, P. Jeseck, T. Hawat, G. Durry, and F. Lefèvre, First direct simultaneous HCl and ClONO₂ profiles in the Arctic vortex, *Geophys. Res. Lett.*, submitted, 1998.
- Pitari, G., A numerical study of the possible perturbation of stratospheric dynamics due to Pinatubo aerosols: Implications for tracer transport, *J. Atmos. Sci.*, 50, 2443-2461, 1993.
- Pitari, G., and V. Rizi, An estimate of the chemical and radiative perturbation of stratospheric ozone following the eruption of Mt. Pinatubo, *J. Atmos. Sci.*, 50, 3260-3276, 1993.
- Pitari, G., and G. Visconti, Possible effects of CO₂ increase on the high-speed civil transport impact on ozone, *J. Geophys. Res.*, 99, 16879-16896, 1994.
- Pitari, G., S. Palermi, G. Visconti, and R.G. Prinn, Ozone response to a CO₂ doubling: Results from a stratospheric circulation model with heterogeneous chemistry, *J. Geophys. Res.*, 97, 5953-5962, 1992.
- Pitari, G., V. Rizi, L. Ricciardulli, and G. Visconti, High-speed civil transport impact: The role of sulfate, nitric acid trihydrate, and ice aerosols studied with a two-dimensional model including aerosol physics, *J. Geophys. Res.*, 98, 23141-23164, 1993.
- Proffitt, M.H., K. Aikin, J.J. Margitan, M. Loewenstein, J.R. Podolske, A. Weaver, K.R. Chan, H. Fast, and J.W. Elkins, Ozone loss inside the northern polar vortex during the 1991-1992 winter, *Science*, 261, 1150-1154, 1993.
- Randel, W.J., F. Wu, J.M. Russell III, J.W. Waters, and L. Froidevaux, Ozone and temperature changes in the stratosphere following the eruption of Mount Pinatubo, *J. Geophys. Res.*, 100, 16753-16764, 1995.
- Randeniya, L.K., P.F. Vohralik, I.C. Plumb, and K.R. Ryan, Heterogeneous BrONO₂ hydrolysis: Effect on NO₂ columns and ozone at high latitudes in summer, *J. Geophys. Res.*, 102, 23543-23557, 1997.
- Rasch, P.J., B.A. Boville, and G.P. Brasseur, A three-dimensional circulation model with coupled chemistry for the middle atmosphere, *J. Geophys. Res.*, 100, 9041-9071, 1995.
- Reinsel, G.C., G.C. Tiao, A.J. Miller, D.J. Wuebbles, P.S. Connell, C.L. Mateer, and J.J. DeLuisi, Statistical analysis of total ozone and stratospheric Umkehr data for trends and solar cycle relationship, *J. Geophys. Res.*, 92, 2201-2209, 1987.
- Renard, J.B., F. Lefèvre, M. Pirre, C. Robert, and D. Huguenin, Vertical profile of the nighttime stratospheric OClO, *J. Atmos. Chem.*, 26, 65-76, 1997.
- Rex, M., N.R.P. Harris, P. von der Gathen, R. Lehmann, G.O. Braathen, E. Reimer, A. Beck, M.P. Chipperfield, R. Alfier, M. Allaart, F. O'Connor, H. Dier, V. Dorokhov, H. Fast, M. Gil, E. Kyrö, Z. Litynska, I. St. Mikkelsen, M.G. Molyneux, H. Nakane, J. Notholt, M. Rummukainen, P. Viatte, and J. Wenger, Prolonged stratospheric ozone loss in the 1995-96 Arctic winter, *Nature*, 389, 835-838, 1997.

PREDICTING THE FUTURE OZONE LAYER

- Rex, M., P. von der Gathen, N.R.P. Harris, D. Lucic, B.M. Knudsen, G.O. Braathen, S.J. Reid, H. De Backer, H. Claude, R. Fabian, H. Fast, M. Gil, E. Kyrö, I. St. Mikkelsen, M. Rummukainen, H.G. Smit, J. Stähelin, C. Varotsos, and I. Zaitcev, In situ measurements of stratospheric ozone depletion rates in the Arctic winter 1991/92: A Lagrangian approach, *J. Geophys. Res.*, *103*, 5843-5853, 1998a.
- Rex, M., P. von der Gathen, G.O. Braathen, S.J. Reid, N.R.P. Harris, M. Chipperfield, E. Reimer, A. Beck, R. Alfier, R. Krüger-Carstensen, H. De Backer, D. Balis, C. Zerefos, F. O'Connor, H. Dier, V. Dorokhov, H. Fast, A. Gamma, M. Gil, E. Kyrö, M. Rummukainen, Z. Litynska, I. St. Mikkelsen, M. Molyneux, and G. Murphy, Chemical ozone loss in the Arctic winter 1994/95 as determined by the Match technique, *J. Atmos. Chem.*, in press, 1998b.
- Rind, D., R. Suozzo, N.K. Balachandran, and M.J. Prather, Climate change and the middle atmosphere: Part I, the doubled CO₂ climate, *J. Atmos. Sci.*, *47*, 475-494, 1990.
- Rind, D., D. Shindell, P. Lonergan, and N.K. Balachandran, Climate change and the middle atmosphere: Part III, The doubled CO₂ climate revisited, *J. Clim.*, *11*, 876-894, 1998.
- Roeckner, E., K. Arpe, L. Bengtsson, S. Brinkop, L. Dumenil, M. Esch, E. Kirk, F. Lunkheit, M. Ponater, B. Rockel, R. Sausen, U. Schlese, S. Schubert, and M. Windelband, *Simulation of the Present-Day Climate with the ECHAM Model: Impact of Model Physics and Resolution*, Max-Planck-Institut für Meteorologie Report 93, Max-Planck-Institut für Meteorologie, Hamburg, 1992.
- Rosenfield, J.E., D.B. Considine, P.E. Meade, J.T. Bacmeister, C.H. Jackman, and M.R. Schoeberl, Stratospheric effects of Mount Pinatubo aerosol studied with a coupled two-dimensional model, *J. Geophys. Res.*, *102*, 3649-3670, 1997.
- Ross, M., Local effects of solid rocket motor exhaust on stratospheric ozone, *J. Spacecr. Rockets*, *33*, 144-153, 1996.
- Ross, M.N., J.O. Ballenthin, R.B. Gosselin, R.F. Meads, P.F. Zittel, J.R. Benbrook, and W.R. Sheldon, In situ measurement of Cl₂ and O₃ in a stratospheric solid rocket motor exhaust plume, *Geophys. Res. Lett.*, *24*, 1755-1758, 1997a.
- Ross, M.N., J.R. Benbrook, W.R. Sheldon, P.F. Zittel, and D.L. McKenzie, Observation of stratospheric ozone depletion in rocket exhaust plumes, *Nature*, *390*, 62-64, 1997b.
- Russell, J.M. III, M. Luo, R.J. Cicerone, and L.E. Deaver, Satellite confirmation of the dominance of chlorofluorocarbons in the global stratospheric chlorine budget, *Nature*, *379*, 526-529, 1996.
- Schoeberl, M.R., M.H. Proffitt, K.K. Kelly, L.R. Lait, P.A. Newman, J.E. Rosenfield, M. Loewenstein, J.R. Podolske, S.E. Strahan, and K.R. Chan, Stratospheric constituent trends from ER-2 profile data, *Geophys. Res. Lett.*, *17*, 469-477, 1990.
- Shindell, D.T., S. Wong, and D. Rind, Interannual variability of the Antarctic ozone hole in a GCM: Part I, The influence of tropospheric wave variability, *J. Atmos. Sci.*, *54*, 2308-2319, 1997.
- Shindell, D.T., D. Rind, and P. Lonergan, Climate change and the middle atmosphere: Part IV, Ozone photochemical response to doubled CO₂, *J. Clim.*, *11*, 895-918, 1998a.
- Shindell, D.T., D. Rind, and P. Lonergan, Increased polar stratospheric ozone losses and delayed eventual recovery due to increasing greenhouse gas concentrations, *Nature*, *392*, 589-592, 1998b.
- Siskind, D.E., J.T. Bacmeister, M.E. Summers, and J.M. Russell III, Two-dimensional model calculations of nitric oxide transport in the middle atmosphere and comparison with Halogen Occultation Experiment data, *J. Geophys. Res.*, *102*, 3527-3545, 1997.
- Smyshlyayev, S.P., and V.A. Yudin, Numerical simulation of the aviation release impact on the ozone layer, *Izv. Atmos. Oceanic Phys.*, *31*, 116-125, 1995.
- Solomon, S., R.W. Portmann, R.R. Garcia, L.W. Thomason, L.R. Poole, and M.P. McCormick, The role of aerosol variations in anthropogenic ozone depletion at northern midlatitudes, *J. Geophys. Res.*, *101*, 6713-6727, 1996.
- Solomon, S., R.W. Portmann, R.R. Garcia, W. Randel, F. Wu, R. Nagatani, J. Gleason, L. Thomason, L.R. Poole, and M.P. McCormick, Ozone depletion at mid-latitudes: Coupling of volcanic aerosols and temperature variability to anthropogenic chlorine, *Geophys. Res. Lett.*, *25*, 1871-1874, 1998.
- Steil, B., M. Dameris, C. Brühl, P.J. Crutzen, V. Grewe, M. Ponater, and R. Sausen, Development of a chemistry module for GCMs: First results of a multi-annual integration, *Ann. Geophys.*, *16*, 205-228, 1998.

- Syage, J.A., and M.N. Ross, An assessment of the total ozone mapping spectrometer for measuring ozone levels in a solid rocket plume, *Geophys. Res. Lett.*, *23*, 3227-3230, 1996.
- Tie, X.X., G.P. Brasseur, B. Briegleb, and C. Granier, Two-dimensional simulation of Pinatubo aerosol and its effects on stratospheric ozone, *J. Geophys. Res.*, *99*, 20545-20562, 1994.
- Timbal, B., J.F. Mahfouf, J.-F. Royer, U. Cubasch, and J.M. Murphy, Comparison between doubled CO₂ time-slice and coupled experiments, *J. Clim.*, *10*, 1463-1469, 1997.
- Velders, G.J.M., *Scenario Study of the Effects of CFC, HCFC, and HFC Emissions on Stratospheric Ozone*, Report No. 722201 006, National Institute of Public Health and the Environment, The Netherlands, 1995.
- Velders, G.J.M., *Effect of Greenhouse Gas Emissions on Stratospheric Ozone Depletion*, Report No. 722201 011, National Institute of Public Health and the Environment, The Netherlands, 1997.
- von Clarmann, T., G. Wetzel, H. Oelhaf, F. Fried-Vallon, A. Linden, G. Maucher, M. Seefeldner, O. Trieschmann, and F. Lefèvre, ClONO₂ vertical profile and estimated mixing ratios of ClO and HOCl in the winter Arctic stratosphere from MIPAS limb emission spectra, *J. Geophys. Res.*, *102*, 16157-16168, 1997.
- von der Gathen, P., M. Rex, N.R.P. Harris, D. Lucic, B.M. Knudsen, G.O. Braathen, H. De Backer, R. Fabian, H. Fast, M. Gil, E. Kyrö, I. St. Mikkelsen, M. Rummukainen, J. Stähelin, and C. Varotsos, Observational evidence for chemical ozone depletion over the Arctic in winter 1991-92, *Nature*, *375*, 131-134, 1995.
- Waters, J.W., W.G. Read, L. Froidevaux, T.A. Lungu, V.S. Perun, R.A. Stachnik, R.F. Jarmot, R.E. Cofield, E.F. Fishbein, D.A. Flower, J.R. Burke, J.C. Hardy, L.L. Nakamura, B.P. Ridenoure, Z. Shippany, R.P. Thurstans, L.M. Avallone, D.W. Toohey, R.L. DeZafra, and D.T. Shindell, Validation of UARS Microwave Limb Sounder ClO measurements, *J. Geophys.*, *101*, 10091-10127, 1996.
- Weissenstein, D.K., M.K.W. Ko, I.G. Dyominov, G. Pitari, L. Ricciardulli, G. Visconti, and S. Bekki, The effects of sulfur emissions from HSCT aircraft: A 2-D model intercomparison, *J. Geophys. Res.*, *103*, 1527-1547, 1998.
- Wetzel, G., T. von Clarmann, H. Oelhaf, F. Fried-Vallon, A. Linden, G. Maucher, M. Seefeldner, O. Trieschmann, and F. Lefèvre, HNO₃ and N₂O₅ vertical profiles in the winter arctic stratosphere from MIPAS limb emission spectra, *J. Geophys. Res.*, *102*, 19177-19186, 1997.
- WMO (World Meteorological Organization), *Atmospheric Ozone 1985, Assessment of Our Understanding of the Processes Controlling Its Present Distribution and Change*, Global Ozone Research and Monitoring Project—Report No. 16, Geneva, 1986.
- WMO (World Meteorological Organization), *Scientific Assessment of Ozone Depletion: 1991*, Global Ozone Research and Monitoring Project—Report No. 25, Geneva, 1992.
- WMO (World Meteorological Organization), *Scientific Assessment of Ozone Depletion: 1994*, Global Ozone Research and Monitoring Project—Report No. 37, Geneva, 1995.
- Zerefos, C.S., K. Tourpali, B.R. Bojkov, D.S. Balis, B. Rognerud, and I.S.A. Isaksen, Solar activity-total column ozone relationships, observations and model studies with heterogeneous chemistry, *J. Geophys. Res.*, *102*, 1561-1569, 1997.
- Zurek, R.W., G.L. Manney, A.J. Miller, M.E. Gelman, and R.M. Nagatani, Interannual variability of the north polar vortex in the lower stratosphere during the UARS mission, *Geophys. Res. Lett.*, *23*, 289-292, 1996.